La pyrolyse solaire de biomasse agricoles, forestières et contaminées par des métaux

Rui Li

THÈSE

Pour obtenir le grade de

Docteur

Délivré par

UNIVERSITE DE PERPIGNAN VIA DOMITIA

Préparée au sein de l'école doctorale ED305

Et de l'unité de recherche CNRS-PROMES

Spécialité: SCIENCES DE L'INGENIEUR

Présentée par Rui LI

Solar pyrolysis of agricultural, forest and metal-contaminated biomass

Soutenue le 2 Décembre 2020 devant le jury composé de

M. Frédéric MARIAS, Professeur, Université de Pau	Rapporteur
M. Laurent VAN DE STEENE, HDR, CIRAD Montpellier	Rapporteur
Mme. Marion DUCOUSSO, Dr, Université de Pau	Examinateur
M. Kuo ZENG, Associate Professor, Huazhong University of Science and Technology, Wuhan, China	Examinateur
M. Gilles FLAMANT, DR CNRS émérite, CNRS-PROMES	Co-Directeur de thèse
M. Ange NZIHOU, Professeur, IMT-Mines Albi	Co-Directeur de thèse

Table of content

Abstract

Biomass, as a renewable energy source, can contribute to relieving the energy crisis and environmental pollutions. Pyrolysis is an attractive thermochemical process to convert biomass into biofuels. Solar energy processes improve the heat and mass balance of the biomass pyrolysis to produce transportable fuels, chemicals, and biomaterials. In the present study, solar pyrolysis of agricultural and forestry by-product biomass and metal-polluted wood has been examined. Pine sawdust, peach pit, grape stalk, and grape marc, were used as the raw materials as the agricultural and forestry by-products in a series of solar pyrolysis experiments in a lab-scale reactor. We studied the impacts of operating conditions (i.e., temperature from 800 to 2000°C, heating rate from 10 to 150°C/s, and lignocellulose composition) on the product yields (i.e., gas, tar, and char) and syngas composition. The gas yield of different biomass residues generally increases with the temperature and heating rate, while the liquid yield shows an opposite trend. Lignin, hemicellulose, and cellulose contents, as well as pellet size, of the by-products studied have an impact on the product profile under fast solar pyrolysis. Lignin content is associated with greater char and tar yields, but less gas yields. Hemicellulose pyrolysis produces more volatiles, but less char and tar yields than cellulose pyrolysis.

Solar pyrolysis of chicken-litter waste and rice husk of different particle sizes (280 and 500 μm) was performed at different solar conditions aiming at investigating optimal operating parameters, such as temperature, particle size, and heating rate, to produce pyrolysis gasses with high calorific value. Temperature was found to have the highest effect on the gas yield during pyrolysis. Gases produced from solar assisted biomass pyrolysis have high concentration of combustible products which can be directly used as fuels.

Biomass can be contaminated by heavy metals. Experiments were carried out to study the effects of heavy metals (copper and nickel), in combination with heating temperature

and heating rate, on solar pyrolysis products of impregnated willow. Results of the investigation indicate that solar pyrolysis of heavy metal contaminated biomass is promising to produce valuable syngas such as hydrogen and carbon monoxide. Additionally, the effects of these heavy metals on the chemical composition, structure, and morphology of pyrolysis char from the impregnated willow were studied. Results prove that heavy metal and solar pyrolysis temperature affect the char properties. A conduction model was developed to describe the behavior of temperature inside the pellets. A kinetic scheme from literature involving the primary and the secondary reactions is adopted to carry out the simulations of temperature. A finite difference method was used for solving the heat transfer equation with an explicit scheme. The model is solved for two dimensions (i.e., time and axial position) in order to make it simpler and save computational time.

Keywords: solar pyrolysis, biomass, metal-polluted biomass, particle size, heating parameters; products' yield, syngas, char characterization

Résumé

La biomasse est une source d'énergie renouvelable qui peut contribuer à résoudre la crise énergétique et les problèmes environnementaux. La pyrolyse est un procédé thermochimique de conversion la biomasse en biocarburants. L'énergie solaire permet d'améliorer le bilan matière et énergie de la pyrolyse de la biomasse pour produire des carburants, des produits chimiques et des biomatériaux transportables. Dans cette étude, nous avons étudié expérimentalement la pyrolyse solaire de sous-produits agricoles, forestiers et de bois contaminé par des métaux lourds. Dans le cas de la biomasse de sous-produits agricoles et forestiers, la sciure de pin, les noyaux de pêche, les tiges et marcs de raisin, a été utilisée comme matières premières dans un réacteur de laboratoire. Nous avons étudié l'influence des conditions opératoires (c.-à-d. la température de 800 à 2000°C, la vitesse de chauffage de 10 à 150°C/s et la composition de lignocellulose) sur les rendements de production des produits de la réaction (c.-à-d. gaz, tar (liquide) et char (solide)) et la composition du gaz de synthèse. Généralement le rendement en gaz augmente avec la température et la vitesse de chauffe pour les divers types de résidus de biomasse, tandis que le rendement en liquide progresse de façon opposée. Les teneurs en lignine, hémicellulose et cellulose, ainsi que la taille des pastilles d'échantillon, des sous-produits étudiés ont un impact sur la distribution des produits de pyrolyse solaire rapide. La teneur en lignine est associée à des rendements plus élevés en char et en liquide, mais moins en gaz. La pyrolyse de l'hémicellulose produit plus de composés volatils, mais moins de char et de tar que la pyrolyse de la cellulose.

La pyrolyse solaire des déchets de litière de poulet et des pailles de riz de différentes tailles de particules (280 et 500 μm) a été effectuée dans différentes conditions solaires afin d'étudier les paramètres de fonctionnement optimaux, tels que la température, la taille des particules et la vitesse de chauffe, pour produire des gaz de pyrolyse à haute valeur calorifique. La température a l'effet le plus important sur le rendement en gaz pendant la

pyrolyse. Les produits gazeux à partir de la pyrolyse de la biomasse assistée par l'énergie solaire contiennent une forte concentration de produits combustibles.

La biomasse peut être contaminée par des métaux lourds. Des expériences ont été conçues pour étudier les effets des métaux lourds (cuivre et nickel) sur les produits de pyrolyse solaire du saule imprégné. Les résultats de cette étude indiquent que la pyrolyse solaire de la biomasse contaminée par des métaux lourds permet de produire du gaz de synthèse riche en hydrogène et monoxyde de carbone. De plus, les effets de ces métaux lourds sur la composition chimique, la structure et la morphologie du charbon de pyrolyse du saule imprégné ont été étudiés. Les résultats prouvent que la température de pyrolyse affecte les propriétés du charbon.

Un modèle de conduction a été développé pour décrire le phénomène de pyrolyse à partir de l'évolution du profil de température à l'intérieur des pastilles. Un schéma cinétique de la littérature impliquant les réactions primaires et secondaires est adopté pour effectuer les simulations des transferts couplés. Une méthode aux différences finies est utilisée pour résoudre l'équation de transfert de chaleur avec un schéma explicite. Le modèle est résolu pour deux dimensions (c'est-à-dire le temps et la position axiale) afin de le rendre plus simple et de gagner du temps de calcul.

Mots-clés: pyrolyse solaire, biomasse, biomasse polluée par les métaux, taille des particules, paramètres de chauffage; rendement des produits, gaz de synthèse, caractérisation des chars

Résumé long en français

Introduction Générale

L'énergie est essentielle à la production industrielle et agricole, ainsi qu'à la vie courante de la population mondiale. Selon l'Agence Internationale de l'Energie (AIE), la demande mondiale d'énergie doit augmenter de 2,3% en 2018, soit environ le double du taux de croissance moyen depuis 2010 en raison de la croissance de l'économie mondiale et du besoin de chauffage et de refroidissement de certaines régions du monde causé par les conditions météorologiques (AIE 2019). De ce point de vue, les combustibles fossiles répondent pour l'essentiel à l'augmentation de la demande énergétique totale.

La consommation d'énergie fossile, comme le gaz naturel, le charbon, l'essence, etc., devrait augmenter sans cesse. Cependant, ces formes d'énergie ne sont pas renouvelables et leur consommation se traduit par l'émission de gaz à effet de serre dans l'atmosphère, ce qui aggrave encore le réchauffement climatique. Un niveau élevé de consommation d'énergie augmente inévitablement les émissions de CO_2. En 2019, l'estimation des émissions mondiales de CO_2 associées à la consommation d'énergie était de 33 Gt (AIE 2020).

Les énergies renouvelables, y compris l'hydraulique, la biomasse, l'énergie géothermique, l'énergie éolienne et solaire, sont l'une des solutions prometteuses pour résoudre les problèmes causés par la consommation d'énergie conventionnelle, garantissant une consommation durable des ressources énergétiques. Les énergies renouvelables progressent de plus de 4% en moyenne, avec un rythme à deux chiffres au cours de l'année 2018. Il y a une augmentation de 6% pour la production mondiale de biocarburants en 2018. Cependant, pour assurer un air plus propre et un développement

durable, l'utilisation de sources d'énergie modernes et renouvelables doit se développer plus rapidement.

La bioénergie est définie comme un produit biologique ou de la biomasse utilisée spécifiquement à des fins énergétiques. La biomasse est consommée pour produire de l'électricité et de la chaleur et convertie en produits secondaires tels que les biocarburants qui peuvent être utilisés dans le secteur des transports. Actuellement, la bioénergie est la source d'énergie renouvelables la plus importante dans le monde, représentant plus de deux tiers des formes d'énergie renouvelable. La bioénergie représente 13 à 14% de la consommation d'énergie totale (Global Energy Statistics 2019, World Bioenergy Association). La conversion de la biomasse en énergie est influencée par différentes conditions, telles que la disponibilité en masse des matières premières, leurs compositions et les procédés de conversion.

La pyrolyse est considérée comme l'un des processus les plus attractifs pour convertir la biomasse en biogaz, bio-huile et bio-char. L'opération de pyrolyse nécessite un apport d'énergie comme le chauffage électrique ou la combustion d'une fraction de la biomasse initiale ce qui réduit l'efficacité de conversion énergétique et cause des problèmes environnementaux. Ce défaut peut être corrigé en utilisant l'énergie solaire concentrée comme apport de chaleur pour convertir la biomasse en combustibles solaires. La mise en œuvre de l'énergie solaire concentrée comme source de chaleur pour les réactions de pyrolyse permet d'augmenter l'efficacité de conversion énergétique et massique du processus de pyrolyse et réduire les rejets polluants.

Enfin, on peut noter un manque de données fiables et actualisées sur la bioénergie aux niveaux mondial et local, en raison de la nature informelle et locale de la plupart des matières premières et des technologies utilisées pour la production de bioénergie.

L'objectif de cette thèse est de valoriser les déchets de bois et agricoles à travers la pyrolyse solaire. Par conséquent, différentes études paramétriques ont été réalisées pour optimiser la distribution des produits. Des analyses quantitatives et qualitatives des produits de pyrolyse ont également été réalisées dans le même but.

Une brève introduction de chaque chapitre est décrite ci-dessous.

- **Chapitre 1** décrit le contexte et les progrès récents de la recherche sur la pyrolyse solaire de la biomasse. Des informations générales sur la biomasse, y compris les avantages et l'importance de la bioénergie, sont introduites. Les déchets agricoles et forestiers sont une classe importante de biomasses. L'accent est mis sur le type, la distribution mondiale, la composition et les propriétés de ces biomasses. La contamination en métaux lourds des produits agricoles et forestiers est également décrite. La pyrolyse de la biomasse est une autre partie de ce chapitre. Les paramètres qui déterminent le fonctionnement de la pyrolyse sont discutés. La caractérisation des produits de pyrolyse constitue la dernière partie de cette revue bibliographique.

- **Chapitre 2** présente les matériaux agricoles et forestiers ainsi que les paramètres et les procédures qui sont adoptés pour les pyrolyser. Les méthodes de caractérisation des produits sont décrites en détail. Le traitement des données et la méthode d'analyse, y compris les équations utilisées, sont également présentées dans ce chapitre.

- **Chapitre 3** présente les résultats de la pyrolyse du bois de pin et des déchets en trois sous-sections. Il a été démontré que la température finale, la vitesse de chauffe et la composition lignocellulosique impactent la pyrolyse du bois de pin et des déchets agricoles (y compris la litière de poulet et la balle de riz). L'effet de la taille des pastilles de bois de pin sur les produits de pyrolyse, en termes de rendement en charbon, en gaz et en huile et en compositions de gaz est également étudié.

- **Chapitre 4** se concentre sur les biomasses polluées par les métaux en utilisant du saule imprégné par le cuivre et le nickel comme échantillons. À cet égard, les effets combinés des paramètres opératoires de la pyrolyse (température et vitesse de chauffage) et des métaux lourds (cuivre et nickel) sont étudiés.

- **Chapitre 5** rapporte la modélisation de la pyrolyse de la biomasse. Les propriétés thermo-physiques, la cinétique de pyrolyse, la puissance et l'évolution caractéristique sont considérées comme des variables d'entrée lors de cette modélisation. Le bois de pin est utilisé comme matériau.

À la fin de la thèse, les conclusions principales dérivées des études présentées ci-dessus sont énoncés, et les perspectives pour les recherches futures sont proposées.

Chapitre 1: Revue Bibliographique

La demande d'énergie augmente au cours des dernières décennies. En conséquence, la consommation de combustibles fossiles augmente également, ce qui, à son tour, entraîne des émissions importantes de gaz à effet de serre dans l'atmosphère et aggrave le problème du réchauffement climatique. La biomasse est une source d'énergie renouvelable qui peut être utilisée pour contribuer à remédier à ce problème. La pyrolyse solaire est prometteuse pour libérer l'énergie contenue dans la biomasse en la convertissant en biocarburants. L'objectif de ce chapitre est de décrire les contextes et les études actuelles sur la pyrolyse de la biomasse par l'énergie solaire pour la conversion en biocarburants. Ce chapitre de revue jette les bases pour déterminer les orientations des recherches actuelles. La structure de ce chapitre comprend les trois sections suivantes.

- La **Section 1.1** Décrit les informations de base sur l'énergie de la biomasse.

- La **Section 1.2** résume le type, la distribution et la composition des déchets agricoles et forestiers. Cette section décrit également la contamination des déchets agricoles et forestiers.

- La **Section 1.3** discute le processus de pyrolyse solaire de la biomasse. Les paramètres qui influencent le processus de pyrolyse et la caractérisation des produits sont résumés.

Chapitre 2: Matériaux et méthodes

Ce chapitre présente les informations et la caractérisation des matériaux, la configuration et les procédures expérimentales, l'analyse des produits et la méthode de

traitement des données. Par conséquent, trois sections constituent ce chapitre.

- La **Section 2.1** présente la caractérisation des biomasses utilisées dans cette étude, y compris le bois de pin, les déchets agricoles, la litière de poulet et la balle de riz, ainsi que le bois de saule pollué par les métaux lourds (Cu et Ni).

- La **Section 2.2** décrit les configurations expérimentales et les procédures de pyrolyse solaire des biomasses décrites ci-dessus.

- La **Section 2.3** discute des méthodes de traitement des données.

Chapitre 3: La pyrolyse du bois de pin et des déchets

Comme il a été indiqué au chapitre 1, aucun des réacteurs solaires existants pour la conversion thermochimique des matériaux carbonés ne permet de contrôler correctement la composition et la pression de l'atmosphère. De plus, les vitesses de chauffe et de refroidissement des échantillons ainsi que le niveau et la durée du plateau de température pendant la transformation chimique sont mal contrôlés. Normalement, la pyrolyse conventionnelle est effectuée en dessous de 1000°C dans des réacteurs manquant de flexibilité. Les réacteurs solaires ont des caractéristiques supérieures aux conventionnels car ils offrent une température de chauffage flexible allant de 600°C à 2000°C et plus, et une vitesse de chauffe allant de 5°C/s à plus de 450°C/s, avec un coût d'énergie minimal. Par conséquent, une étude sur l'effet des conditions opératoires très particulières produites par l'énergie solaire concentrée sur les compositions et les propriétés du produit est nécessaire. Trois études constituent ce chapitre, elles sont décrites dans les sections suivantes.

- La **Section 3.2** présente la pyrolyse du bois de pin et des déchets agricoles. Dans cette section, les effets de la température finale, de la vitesse de chauffe et de la composition lignocellulosique sur les produits de pyrolyse sont discutés.

- La **Section 3.3** décrit la pyrolyse du bois de pin de différentes tailles de pastille. Elle met en évidence le rôle des réactions secondaires de l'huile sur les rendements du char, du gaz et de l'huile, ainsi que sur la composition du gaz.

- La **Section 3.4** discute des effets des différentes vitesses de chauffe, températures et types de biomasse sur la distribution des produits de pyrolyse et la composition des gaz pendant la pyrolyse solaire de la litière de poulet et de balle de riz.

Chapitre 4: Pyrolyse de la biomasse polluée par les métaux

La phyto-extraction est efficace pour résoudre les problèmes de pollution des métaux lourds (HM), et la pyrolyse est une technologie efficace et économique pour convertir la biomasse contaminée en char, gaz et huile. Ce chapitre étudie le comportement et les effets combinés des métaux lourds pendant la réaction de pyrolyse et analyse les chars contaminés résultants. À cet égard, le cuivre (Cu) et le nickel (Ni) ont été choisis pour l'imprégnation du bois de saule afin de simuler les hyperaccumulateurs, car ces métaux lourds sont couramment détectés dans les plantes contaminées. De plus, les deux métaux pourraient agir comme catalyseurs in-situ dans les réactions de pyrolyse de la biomasse contaminée. Le cuivre et le nickel représentent des contenus métalliques volatiles et non volatiles dans la plage de température des réactions de pyrolyse solaire. Afin de comprendre le rôle et le comportement des métaux lourds pendant les réactions de pyrolyse solaire, ce chapitre est organisée suivant les deux sections suivantes.

- La **Section 4.2** présente la pyrolyse des saules bruts et les saules pollués par les métaux lourds. Dans cette section, les effets combinés des métaux lourds et des paramètres de chauffage (c.-à-d. La température et la vitesse de chauffe) sur les produits de pyrolyse solaire sont étudiés.

- La **Section 4.3** étudie les effets de la température et de la contamination des métaux lourds sur la composition chimique, la structure et la morphologie du charbon produit par la pyrolyse solaire des saules pollués par les métaux lourds.

Chapitre 5: Modélisation de la Pyrolyse Solaire

En plus des travaux expérimentaux, des simulations tentent de prédire l'influence des différents paramètres affectant les performances de la pyrolyse. Cette étape de simulation vise à prédire l'évolution de la température en fonction du temps et de la position axiale pendant les premières minutes de la pyrolyse solaire de pastilles de biomasse par simulation à l'aide de MATLAB et Excel.

Un modèle de conduction a été développé pour décrire le comportement de la température à l'intérieur des pastilles. Un schéma cinétique issu de la littérature impliquant les réactions primaires et secondaires est adopté pour tenir compte des réactions de pyrolyse dans les simulations. Une méthode de différence finie est utilisée pour résoudre l'équation de conservation de l'énergie avec un schéma explicite. Une équation analytique tirée du schéma cinétique est utilisée pour modéliser la disparition de la biomasse. Le modèle est dynamique et 1D..

- La **Section 5.2** décrit les modèles de l'étape de simulation et les méthodes de résolution.

- La **Section 5.3** décrit la valeur des paramètres, tels que les propriétés thermo-physiques des pastilles, la cinétique de disparition de la biomasse, l'évolution de la puissance solaire incidente afin de simuler l'évolution des caractéristiques pendant la pyrolyse solaire.

- La **Section 5.4** présente les résultats. La consommation de biomasse et la distribution de la température sont présentés en fonction du temps et à la position axiale. Ce modèle simple peut décrire l'évolution globale d'un ensemble complexe de processus de pyrolyse. Cependant, une validation expérimentale est nécessaire.

Chapitre 6: Conclusions et Perspectives

La biomasse, y compris les déchets de sous-produits agricoles et forestiers, représente une classe de source d'énergie renouvelable, une solution intéressante pour la substitution des combustibles fossiles. La pyrolyse solaire promet de convertir la biomasse en une forme d'énergie stockable, comme le gaz de synthèse. Ce travail vise à étudier expérimentalement l'influence les paramètres de la pyrolyse solaire influençant la libération de l'énergie stockée dans les déchets agricoles et forestiers. Les résultats sont présentés sous la forme de l'évolution des rendements des différents produits et de la composition du gaz de synthèse. D'autre part, les effets de la taille de pastille ont été étudiés en utilisant le modèle développé par nos collègues argentins (PROBIEN, CONICET - UNCo.). Des caractérisations de char provenant de la pyrolyse du saule pollué par les métaux lourds ont été effectuées pour étudier les effets de la température et de la contamination des métaux lourds sur les propriétés du char. Enfin, un modèle simple de conduction-réaction a été développé pour décrire la distribution de température à l'intérieur de la pastille de biomasse. Ainsi, les résultats de cette étude peuvent se résumer en les cinq principales conclusions suivantes:

(1) Les produits de pyrolyse sont influencés à la fois par les conditions opératoires du réacteur (la température en premier lieu puis la vitesse de chauffe) et par la composition lignocellulosique de la biomasse.

(2) La taille de pastille, la température et la vitesse de chauffe ont un impact conjoint sur la distribution des produits de pyrolyse.

(3) Le type de biomasse influence la composition des produits générés par la pyrolyse solaire dans différentes conditions opératoires.

(4) Les métaux lourds, Ni et Cu, ont un effet sur les produits de pyrolyse en quantité et en propriété.

(5) La simulation numérique permet de prédire l'évolution de la température et de la consommation de la biomasse durant la pyrolyse. La comparaison avec les données expérimentales reste néanmoins un défi.

Les conclusions principales de cette étude sont présentées ci-dessus. Les résultats obtenus de l'étude actuelle jettent les bases des recherches futures. Les perspectives

peuvent être formulées autour de cinq aspects principaux

(1) Amélioration technique du système solaire expérimental existant

Bien que la précision des expériences solaires ait été largement améliorée depuis le début de cette étude, l'amélioration du processus expérimental ou de la technologie de mesure est encore nécessaire en ce qui concerne les problèmes expérimentaux qui n'ont pas été totalement résolus. La mesure de la température de surface de l'échantillon par pyrométrie en présence de vapeur doit être améliorée. La synchronisation du système de contrôle PID avec l'obturateur et la minuterie doit nécessairement être également améliorée. De plus, l'installation d'un système de collecte de l'huile pratique se ferait particulièrement intéressante. L'analyse de la qualité de l'huile et la mesure de sa contamination en métaux lourds pourra contribuer à orienter le choix des conditions optimales de pyrolyse.

(2) Validation des résultats de simulation et amélioration du modèle

La confrontation des résultats obtenus à partir de la simulation et des expériences est nécessaire pour produire des résultats plus cohérents. La caractérisation des propriétés de la biomasse, telles que la densité, la conductivité thermique et la chaleur spécifique, est nécessaire avant le début de la pyrolyse. La calorimétrie doit être effectuée pour obtenir la densité du flux solaire en fonction de l'ouverture des volets de l'obturateur. La vérification des données du modèle dynamique est très importante pour confirmer les résultats de la simulation. Le modèle présente plusieurs simplifications, telles que l'hypothèse que la porosité de l'échantillon constante pendant la réaction. En fait, la porosité de l'échantillon évolue avec la température et la conversion chimique, ce qui doit être amélioré pour produire des résultats plus précis.

(3) Installation du système de spectroscopie induite par laser (LIBS)

Afin d'effectuer une mesure in situ de l'évolution de la concentration des métaux (tels que Na, K, Ca, Cu et Ni) dans le résidu solide pendant la pyrolyse solaire de la biomasse, il est nécessaire d'intégrer une mesure LIBS avec les réacteurs solaires existants. Le couplage des

mesures LIBS relatives à la vaporisation des métaux à haute température avec les données de gaz de synthèse et les propriétés char est nécessaire pour comprendre le comportement des métaux lors des réactions de pyrolyse.

(4) Mise à l'échelle du réacteur solaire à partir des résultats de mesure à l'échelle du laboratoire

L'objectif de la technologie de pyrolyse solaire est de développer une unité commerciale à l'échelle du mégawatt fonctionnant en mode continu. Cette unité peut utiliser soit le concept de front de réaction mobile (le réactif est poussé en continu au point focal et le charbon est séparé par gravité), soit un lit fluidisé ou un réacteur à sel fondu. Le réacteur à sel fondu permet à la chaleur d'être rapidement transférée aux matières premières et de fonctionner de manière stable même sous des transitoires d'énergie solaire. Par ailleurs, le sel retient les métaux lourds de la biomasse contaminée. Les caractéristiques uniques du réacteur solaire comprennent le contrôle direct de la température du réacteur, de la vitesse de chauffe et du temps de séjour des solides.

Acknowledgement

Thanks to LABEX-SOLSTICE, the French "Investments for the future" program managed by the National Agency for Research, for the financial support to my PhD project.

First of all, I sincerely thank my supervisors, Professors Gilles Flamant and Ange Nzihou, for all the knowledge, help, and opportunity they provided to me. Without their guidance and persistent help with patience, this dissertation would not be shown in its current form. I gratefully appreciate Dr. Daniel Gauthier for leading me to learn how to implement and improve our experimental setup before he retires. I also thank Professor Doan Pham Minh for his kind helps and arrangements during my stay in Ecole des Mines d'Albi.

This work is the result of many exchanges with people from different laboratories and different countries. Without their help, support and rich experience, it is impossible to complete this work. Thanks to the efficient collaborations with:

- The RAPSODEE Laboratory of IMT-Mines d'Albi; in particular, for the physicochemical analysis of the samples.

- The Institute for Research and Development in Process Engineering, Biotechnology and Alternative Energies (PROBIEN, CONICET - UNCo), Argentina, in particular for the modelling.

- The Department of Environmental Sciences, Faculty of Science Engineering, Macquarie University, Australia, for the work on solar pyrolysis of chicken litter and rice husk.

I am very grateful to the faculty at CNRS-PROMES and RAPSODEE. Thanks to the technicians for their great support in helping me carry out experiments and share their knowledge of analytical techniques with me. Thanks to Roger Garcia for the help of installation of solar reactor; to Christophe Escape for the help of calibration of pyrometer; to Emmanuel Guillot and Nicolas Boullet for the guide and assistance to carry out our experiments; to Yonko Gorand for the SEM&EDX analysis; to Beche Eric for the Raman analysis; to Céline Boachon and Sylvie Delconfetto for the BET analysis; to Jean Marie Sabathier for the CHNO-S and ICP-AES measurements; to Christine Rolland for the SEM

imaging. Of cause, I also appreciate all the colleagues from the two laboratories for the great atmosphere and helps during my studies as a PhD candidate.

The PhD program could not have been completed without the inspiration, friendship, and support of many colleagues and friends. I am grateful to all for your company and the joys we have shared. I would like to send a special thanks to Kuo Zeng for sharing me his working experiments and knowledge of the domain, to my fellow Thomas Fasquelle for saving me when I had Kidney stones! I appreciate Santiago Brun and José Soria for their help and support with the simulation.

Finally, I would like to extend my heartfelt thanks to my parents and my wife for your selfless dedication. Thank you all for always believing in me and support me to move forward in the real life.

Rui LI

July 2020

General Introduction

Energy is essential for industrial and agricultural production, as well as routine life of the global population. According to the International Energy Agency (IEA), the global energy demand was estimated to grow by 2.3% in 2018, which is approximately twice the average growth rate since 2010 due to growing of global economy and the need for heating and cooling certain regions of the world caused by weather conditions (IEA 2019). Today, fossil fuels meet most part of the increase in total energy demand.

Consumption of the fossil energy, such as natural gas, coal, gasoline, etc., is expected to endlessly increase if their contribution to the overall energy supply is not modified. However, these forms of energy are not renewable and their consumption results in the emission of greenhouse gas to the atmosphere that further worsens the global warming situation. High level of energy consumption inevitably increases CO_2 emission. In 2019, estimate of global CO_2 emissions associated with energy consumption was 33 Gt (IEA 2020).

Renewable energies include hydraulic, biomass, geothermal energy, wind and solar powers, are one of the promising solutions to solve the problems caused by consumption of conventional energy, and can ensure sustainable consumption of energy resources (Tsai et al. 2006; Asadullah 2013). Renewable energy grows by more than 4%, at a double-digit pace over the last year. There is an increase by 6% for the global biofuel production in 2018. However, to realize a cleaner air and sustainable development, the use of modern, renewable energy sources needs to expand more quickly.

Bioenergy refers to the biological commodity or biomass that is used specifically for energy purposes. Biomass is consumed for generating electricity and heat and converted to secondary products such as biofuels that can be used in the transportation sector. At

present, bioenergy occupies the largest proportion of renewable energy source globally, accounting for more than two-thirds of the renewable forms of energy. Bioenergy accounts for 13-14% of the total energy consumption (Global Energy Statistics 2019, World Bioenergy Association). Bioenergy represents a complex energy system. The conversion of biomass to energy is influenced by different conditions, such as mass availability of feedstock, technology pathways, and end products.

Pyrolysis is regarded as one of the most attractive processes to convert biomass into bio-gas, bio-oil, and bio-char (Di Blasi 1993). The operation of pyrolysis requires input of extra energy such as electrical heating source, combustion of some non-condensables or char (Van de Velden et al. 2010), which reduces the conversion efficiency (both mass and energy) and causes environmental problems. This can be overpassed using concentrated solar energy as the heat input for converting biomass into solar fuels (Zeng et al. 2015). The implementation of concentrated solar energy as the source of heat for the pyrolysis reactions can increase the energy conversion efficiency of the pyrolysis process and reduce the pollution discharge (Nizhou et al. 2012). It is important to notice that there is a lack of reliable and updated data on bioenergy in both global and local levels, due to the informal and local nature of most feedstock and technology used for production of bioenergy.

The objective of this thesis is to valorize the agriculture wastes and woods by going through the solar pyrolysis process. Therefore, different parametric studies have been carried out to optimize the product distribution. Quantity and quality analyses of the pyrolysis products have also been done for the same goal.

A brief introduction of each chapter is described below.

- **Chapter 1** describes the background and recent research progresses of solar pyrolysis of biomass. General information on biomass, including advantage and importance of biomass energy, is introduced. Agricultural and forestry wastes are an important class of biomasses. Focus is given to type, global distribution, composition, and property of these biomass. Heavy metal contamination of agricultural and forestry products is also described. Biomass pyrolysis is another part of this chapter. Parameters that determine pyrolysis

operation are discussed. Characterization of pyrolysis products is the last part of this literature review.

- **Chapter 2** provides the composition of agricultural and forestry materials, and parameters and procedures that are adopted to pyrolyze them. Methods of product characterization are described in details. Data processing and mathematical analysis method, including the equations used, are also well shown in this chapter.

- **Chapter 3** investigates the process of pine woods and wastes pyrolysis, which are included in three subsections. The final temperature, heating rate, and lignocellulose composition are proven to have an impact on pyrolysis of pine wood and agricultural wastes (including chicken litter and rice husk). Pellet size of pine wood also effects the pyrolysis products, in terms of char, gas and tar yields and gas compositions.

- **Chapter 4** focuses on the metal polluted biomasses using the copper and nickel contaminated willows as examples. In this regard, combined effects of pyrolysis operating parameters (temperature and heating rate) and heavy metals (copper and nickel) are studied.

- **Chapter 5** reports the modeling and verification of pyrolysis of biomass. Thermophysical properties, biomass consumption, power, and characteristic evolution are considered as variables during this modeling. Pine wood pyrolysis is simulated.

In the end of the thesis, the main conclusions derived from the studies shown above are presented, and the prospects for further researches are proposed.

Bibliography

Asadullah M. Technical challenges of utilizing biomass gasification gas for power generation: An overview. Journal of Energy Technology and Policy, 2013, 3: 137–143.

Di Blasi C. Modeling and simulation of combustion processes of charring and non-charring solid fuels. Progress in Energy and Combustion Science, 1993, 19: 71–104.

IEA. Global Energy & CO_2 Status Report 2019, IEA, Paris, 2019. https://www.iea.org/reports/global-energy-co2-status-report-2019

IEA. Global CO_2 emissions in 2019, IEA, Paris, 2020. https://www.iea.org/articles/global-co2-emissions-in-2019

Nzihou A, Flamant G, Stanmore B. Synthetic fuels from biomass using concentrated solar energy - A review. Energy, 2012, 42: 121–131.

Tsai CR, Chen F, Ruo AC, Chang MH, Chu HS, Soong CY, Yan WM, Cheng CH. An analytical solution for transport of oxygen in cathode gas diffusion layer of PEMFC. International Journal of Hydrogen Energy, 2006, 31: 2179–2192.

Van de Velden M, Baeyens J, Brems A, Janssens B, Dewil R. Fundamentals, kinetics and endothermicity of the biomass pyrolysis reaction. Renewable Energy, 2010, 35: 232–242.

Zeng K, Minh DP, Gauthier D, Weiss-Hortala E, Nzihou A, Flamant G. The effect of temperature and heating rate on char properties obtained from solar pyrolysis of beech wood. Bioresource Technology, 2015, 182: 114–119.

Chapter 1

Literature Review

The demand for energy is increasing over the past several decades. As a result, fossil fuel consumption is expected to grow, which, in turn, results in emission of a large amount of greenhouse gases into the atmosphere and further worsens the global warming problem. Biomass is attractive as a source of renewable energy that can contribute to remedy this problem. Solar pyrolysis is promising in releasing energy hidden in biomass by converting it into biofuels. The objective of this chapter is to describe the backgrounds and current studies on pyrolysis of biomass by solar energy for converting into biofuels. This review chapter will set a stage in determining the directions of the present researches. The structure of this chapter includes the following three sections.

- **Section 1.1** describes basic information on biomass energy, including advantages of biomass energy.

- **Section 1.2** summarizes the type, distribution, and composition of agricultural and forestry waste. Also in this section, the contamination of agricultural and forestry wastes is described.

- **Section 1.3** discusses the process of solar pyrolysis of biomass. The parameters that

influence pyrolysis process and product characterization are summarized.

1.1 Biomass energy

1.1.1 Biomass

Biomass is termed as all organic materials produced by plants, animals, and microorganisms; it also includes the organic substances that originate from excretion and metabolisms of those organisms, including agricultural and forestry wastes, aquatic plants, and organic wastes from urban life and industrial production (Cao et al. 2017). In general, biomass covers a variety of biogenic materials, excluding those mineralized in geological formations. Globally, biomass is the fourth most consumed source of energy after the conventional energies, such as fossil oil, coal, and natural gas. Biomass accounts for 14% of the primary energy consumption of the world (Haarlemmer et al. 2016).

The world's total biomass is estimated to be ~400 Gt C (Pan et al. 2013). Approximately 16.3 Pg C are removed annually by human for food and wood products, land-use change, and fires caused by human (Haberl et al. 2007). Considering the huge areas of 4.03 billion hectares, about 30% of the Earth's total land area, forest accounts for 80% of the total plant biomass (Kindermann et al. 2008), or even higher (92%) (Cao et al. 2017). Because of the natural conditions and resources that can be used by plants, the biomass production is not evenly distributed throughout the world. Due to the plenty of light and heat resources, tropical forest across the equator accounts for about two-thirds of the biomass in only about 15% of areas (**Table 1.1**). Temperate forests and boreal forests are important, but only produce about 10% of the total biomass due to limitation of the light and heat resources. Although the other land excluding crop land covers 60% of the area, it is insignificant (only 5.1%) to contribute to the total global biomass production. Wood is the largest source of biomass energy. It is widely used as raw materials in the pyrolysis due to its global richness.

Crops produce only a small proportion of total biomass (2.7%) in about 10% of land. Nevertheless, this part is essential for feeding the humans. Estimate of the global total live

forest biomass was 363 Pg C, mostly contributed by aboveground tissues (80%) and less (20%) by belowground tissues (Cairns et al. 1997; Jackson et al. 1996, 1997). Global necromass, including organic matter in soils, litter, and deadwood, is even more than live biomass in terms of carbon, accounting for 58% of total ecosystem (Pan et al. 2013).

Table 1.1. Area and current total biomass estimates for the global terrestrial biomes.

	Area (10^6 ha)	%	Current biomass (Pg C)	%
Tropical forest	1949.4	14.9	262.1	66.6
Temperate forest	766.7	5.9	46.6	11.8
Boreal forest	1135.2	8.7	53.9	13.7
Other land except crop land	7870.0	60.2	20.0	5.1
Crop land	1350.0	10.3	10.8	2.7
Total	13071.3		393.4	

Data source : Pan et al. (2013).

1.1.2 Advantages of biomass energy

The most attractive property of biomass is its capacity to be renewed. It can directly replace fossil resources in many applications, such as production of heat, chemicals and biomaterials, and production of power and transportation fuels through the pyrolysis process (Bridgwater 2003). Biomass energy has the advantages over conventional fossil energy in the following aspects. Biomass produced by plants stores solar energy through photosynthesis in the chloroplasts in green plant tissues. Such lignocelluloic biomass is renewable, because large quantity of plants grow and die every year on the planet, offering enormous quantity of biomasses. The environmental friendship is another attractive property of lignocellulosic biomass energy. Because it contains low sulfur and nitrogen, biomass generates less Sox and Nox when combusting as energy fuel by comparison with

fossil fuels. Also, the equivalence of carbon dioxide amount consumed during biomass production to the released amount during biomass combustion makes zero emission of carbon dioxide which is the largest greenhouse gas emitted by human activity (Doren et al. 2017). The third advantage of biomass is its availability from almost everywhere on the earth. Because of these properties, biomass energy is even more attractive than not only the non-renewable forms of energies (i.e., fossil oil, coal, and natural gas), but also the other forms of renewable energies (i.e., solar, wind, geothermal, and tidal energy) (Durak and Aysu 2016). Moreover, the advantages of biomass as energy source also include lower cost with higher conversion efficiency than the conventional forms of energy. Biomass production creates job opportunities, benefits recovery of degraded land and increase of biodiversity, and reduces damage to environment by consuming agricultural residues (Gercel 2002; McKendry 2002).

1.1.3 Importance of biomass energy

The demand of energy to support economic and human living activities has been increasing over the last several decades and is expected to grow in the foreseeable future. Global consumption of energy has increased from 269 EJ in 2000 to 370 MJ in 2017 (International Energy Agency 2019), causing growing consumption of fossil fuels. This results in emission of mass of greenhouse gases into the atmosphere and serious concern of air pollution. From the environmental protection point of view, biomass sheds a light to resolve the environmental problem caused by over consuming conventional forms of energy. So, biomass energy is receiving much attention as an alternative of fossil energy. Consumption of biomass energy does not contribute to increase greenhouse gas emission, mostly CO_2. Carbon dioxide produced by plant-based biomass is regenerated through photosynthesis of plant green tissues, so the amount of CO_2 in the atmosphere is balanced.

Because of its huge amount produced annually in the globe, biomass can serve as a source of environmental-friendly energy instead of fossil fuels. The increasing demand of energy along with the need of diminishing greenhouse gas emissions has led to the attention

towards renewable fuels. In this regard, biomass, as a renewable energy source, can partly relieve the energy crisis and environmental pollutions, since it represents a carbon neutral fuel with extra benefits such as low content of nitrogen and sulphur. It can be converted to a large diversity of gaseous, liquid, and solid fuels using thermochemical conversion processes. **Figure 1.1** illustrates the production of biofuels from biomass.

Figure 1.1. Production of biofuels from biomass (Swain 2016)

1.2 Agricultural and forestry wastes

1.2.1 Types and distribution of agricultural and forestry wastes

Agricultural and forestry wastes had little interest for centuries. However, they started being considered as valuable feedstock for energy transformation with the concern of the energy community for their valorization in the last decades. Typical agricultural and forestry biomasses include agricultural residues, hardwood, softwood, herbaceous, paper waste, and industrial by-products etc. (**Table 1.2**) (Cao et al. 2017). They are produced during crop harvest in the fields, lumbering wasters, and food processing vegetal wastes (Treinyte et al.

2018). In a recent review by Guedes et al. (2018), 165 types of agricultural and forestry biomasses have been studied, and rice husk, palm shell, *Jatropha curcas* cake, rapeseed, and pine wood are the top biomasses that have been more frequently studied than the other types of biomasses.

It was seen that biofuel production has exerted a significant impact on the increase of crop demand during the period of 2000 to 2015 (FAO and OECD 2019a). In the USA, it was estimated that about 700 million tons of dry non-grain biomass feedstock could be produced annually based on a renewable manner, and about 241 million tons of agricultural resources and 103 million tons on a dry mass basis could be used in biofuel production (Langholtz et al. 2016). The annual production of agricultural straws in China is estimated to be 740 million tons (Zhang et al. 2016). During the past 5 decades, agricultural production has increased by over three folds, which mainly resulted from the expansion of land used for agricultural application, improvement of productivity due to technical improvement of 'Green Revolution', and increasing growth of population (FAO 2017; FAO and OECD 2019b). Increasing attention has been paid and numerous studies have been conducted to explore the alternative application of agricultural wastes (Duque-Acevedo et al. 2020).

It is necessary to consider the sources of biomass for the purpose of energy. Grains from cereal crops, such as wheat, rice, corn, etc., and oil crops, such as soybean and rapeseed, grown to feed people on arable lands, are not regarded as sustainable and renewable sources of energy. However, non-edible residues of these crops, such as straws, husks, and cobs, as well as organic residues from food processing etc., are suitable as biomass energy sources. Jatropha, camelina, miscanthus, and short-rotation tree crops are purposely grown as bioenergy crops. Feedstock serving as biomass energy source include non-marketable wood residues, for example, branches, barks, dead wood, etc. (Whalen et al. 2017). There is a risk that the demand of biofuel may compete with food production consumed by human (FAO 2009). So, biomass feedstock specific for biofuels are mostly grown on marginal agricultural lands.

Table 1.2. Compositions of different classes of typical agricultural and forestry biomass.

Class of raw materials	Type of materials	Cellulose (wt.%)	Hemicellulose (wt.%)	Lignin (wt.%)
Agricultural residues	Rice straw	36.1	24.7	16.4
	Rice husk	34.7	17.4	25.5
	Wheat straw	41.2	27.7	18.5
	Corn stover	38.8	23.5	20.2
	Corn cobs	44.0	36.4	18.0
	Rapeseed straw	33.9	18.2	15.3
	Sugar cane bagasse	56.0	4.6	26.4
	Sunflower stalks	34.1	26.2	26.8
	Sweet sorghum bagasse	36.2	24.6	13.1
Hardwood	White poplar	42.3	20.7	21.0
	Hybrid poplar	51.3	20.2	17.6
	Aspen	47.1	19.6	22.1
	Eucalyptus globulus	39.8	21.4	25.7
	Eucalyptus	40.2	18.9	25.1
Softwood	Spruce	43.8	20.8	28.8
	Pinus radiata	51.5	11.7	34.5
Herbaceous	Switchgrass	32.8	23.7	18.2
	Alfalfa	24.7	14.7	14.9
	Bermuda	25.6	19.3	19.3
Paper waste	Newspapers	44.2	17.8	26.8
	Recycled paper	60.8	14.2	8.4
Industrial by-products	Distiller's grains	12.6	16.9	-
	Brewer's spent grain	18.5	26.5	19.3

Source of the data: Cao et al. (2017).

1.2.2 Composition and property of agricultural and forestry wastes

Agricultural and forestry biomass, consisting of plants and plant-based materials, is typical lignocellulosic biomass. In contrast to animal cell, plant cell has a unique structure, cell wall, which encloses the organelles and makes independence between cells. The major components of cell walls include carbohydrate polymers (i.e., microfibrils of cellulose, hemicellulose, and pectin) and non-carbohydrate polymers (i.e., lignin and protein). So, cellulose, hemicellulose, and lignin, macromolecules made up of carbon, hydrogen, and oxygen atoms, are the largest proportion of lignocellulosic biomass components (Barta and Ford 2014). As such, agricultural and forestry biomass comprises of these organic polymers with varying concentrations among different types of materials (**Table 1.2**) (Cao et al. 2017).

1.2.3 Contamination of agricultural and forestry wastes

Soil and water pollution by heavy metals (HMs), including lead (Pb), cadmium (Cd), mercury (Hg), arsenic (As), chromium (Cr), zinc (Zn), copper (Cu), and nickel (Ni), is identified as a serious problem worldwide (Li et al. 2019). Phytoextraction by certain plants that have high HM enrichment capacity is one of the effective solution to decontaminate the soil and waste (He et al. 2019). This kind of plants known as hyperaccumulators can absorb HMs from polluted soil or water by roots and accumulate them in roots, stems, and leaves (Liu et al. 2017a). Contents of HMs in hyperaccumulators after phytoextraction are hundreds of times higher than the surroundings (Nizhou et al. 2013). For example, the contents of copper and nickel in hyperaccumulators grown on polluted soil can reach 4 g/kg and 10 g/kg, thousands of times higher than contents in polluted soil (Lievens et al. 2009; Zhang et al. 2016). It means that the used biomass for phytoextraction is contaminated by HMs. How to dispose of HM contaminated biomass in the right way becomes a critical issue. Pyrolysis is proposed as a feasible, economical, and environmentally post-treatment method, which can recycle HM contaminated biomass into valuable products (i.e., gas, oil, and char) (Chen et al. 2014). Heavy metal contaminated biomass volume is reduced a lot with minimized pollution

discharge (Zeng et al. 2019).

1.3 Pyrolysis of biomass

Biomass is a renewable energy solution that can be directly replace fossil resources in many applications, such as reproduction of heat, chemicals and biomaterials, production of power, and transportation fuels through pyrolysis process. The prerequisite of application of biomass as energy source is conversion of raw materials through thermal, biological or mechanical means. Pyrolysis and gasification are the most attractive thermochemical processes to convert biomass into biofuels due to feedstock flexibility and conversion efficiency (Çaglar and Demirbas 2002; Bridgwater 2003). Pyrolysis represents the first (main) chemical step in gasification, and combustion, among other processes. It can also be a stand-alone process.

1.3.1 Biomass pyrolysis

Pyrolysis is a thermal-based decomposition process in the absence of oxygen. It is regarded as a costly and simple method for biomass conversion (Bridgwater 2002). Products of biomass pyrolysis include bio-oil, incondensable gas, and char (**Figure 1.2.**). Three types of pyrolysis, i.e., slow, fast, and flash pyrolysis, can be distinguished depending on the operating conditions, such as temperature, heating rate, and residence time. Slow pyrolysis requires lower temperature (about 400°C), lower heating rate, and longer residence time. Under these conditions, biomass is heated slowly, favoring the char production. Fast pyrolysis, which occurs at a moderate temperature, high heating rate, and short residence time of vapor, promotes liquid or bio-oil formation. Biomass is rapidly heated to the final temperature prior to degradation. To produce more bio-oil, the maximum temperature should not exceed 600°C; while the final temperature can be high at 1000°C, or even up to 2000°C (Zeng et al. 2016), if the product of interest is gas. Flash pyrolysis occurs at a very

high heating rate and reacts within only a few seconds (Goyal et al. 2008).

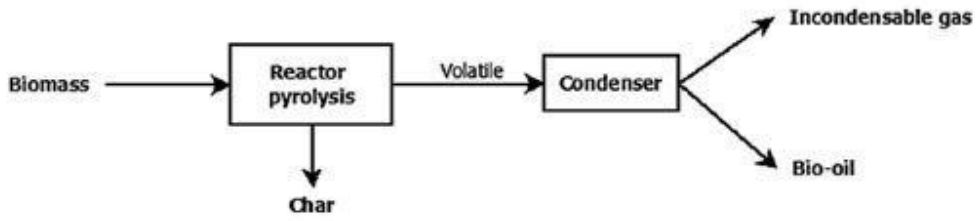

Figure 1.2. Diagram of biomass pyrolysis process (Guedes et al. 2018)

Pyrolysis requires extra energy input such as electrical heating source, combustion of some non-condensables or of the char (Van de Velden et al. 2010), thus reducing the energy conversion efficiency and causing environmental problems. This can be overpassed using concentrated solar energy as the heat input for processing biomass into solar fuels (Zeng et al. 2015b). Indeed, implementing of concentrated solar energy as heat source for the pyrolysis reactions can increase the energy conversion efficiency of the process and reduce its pollution discharge (Nzihou et al. 2012). In this objective, a few researchers have used image furnace for simulating solar-driven carbonaceous material pyrolysis (Hopkins et al. et al. 1984; Authier et al. 2009). In previous studies, the liquid products were the target or main products. However, in spite of the interest of using real solar furnace for biomass pyrolysis, published works related to such type of pyrolysis are scarce (Zeng et al. 2014, 2015a; Zeaiter et al. 2015).

Traditional pyrolysis is normally conducted below 1000°C in flexibility-lacking reactors. Compared to such reactors, solar driven reactors are very interesting since they provide both a flexible heating temperature that ranges from 600°C up to 2000°C and more, and a flexible heating rate ranging from 5°C/s to more than 450°C/s, with a minimal energy cost. Therefore, more combustible gas products can be produced due to the advantages of direct solar pyrolysis (high temperature and fast heating rate). The pyrolysis gas products have a higher heating value than conventionally gasified gases (Abnisa and Wan Daud 2014), and therefore, they can be utilized as fuel gas for power generation, heat or transportable fuel

production.

There is another advantage of the solar furnace, flexible heating rates. Traditional reactors, such as thermogravimetry (TGA) or tubular reactors, present a slow heating rate (10-100 K/min), whereas solar furnaces allow a flexible heating rate up to 450 K/s. Therefore, with the high heating rate range, kinetic/thermal effects of solar furnace are very representative of fast pyrolysis.

1.3.2 Solar thermochemical pyrolysis of biomass

Pyrolysis produces three main products: char, condensable gases (tar and water), and non-condensable gases (H_2, CO, CO_2, and CH_4). Depending on the operating conditions and feedstock properties, pyrolysis will produce different distributions and yields and, consequently, will affect the behavior of the succeeding steps.

Studies on solar pyrolysis and gasification of carbonaceous biomass were pioneered in the 1980s in the USA and Europe. In the studies conducted by Gregg et al. (1980) and Taylor et al. (1983), direct solar irradiation packed bed reactor, coal, activated carbon, coke, coal, and biomass mixture, as well as charcoal, wood, and paper, were subjected to solar pyrolysis to study the solar steam gasification using similar solar furnace with different powers. Different gasification efficiencies were obtained and different syngases were produced. Since then, different reactors have been developed for flash pyrolysis (Antal et al. 1983) and particle-type reactor (Lédé et al. 1986). A lot of researches on biomass pyrolysis have been carried to develop reactors heated by combustion of pyrolysis products. Typical slow and fast pyrolysis reactors have been reviewed by Bridgwater et al. (2012). The contribution of these devices to the chemical transformation of carbonaceous materials at medium and high temperatures is poorly understood. New reactors have been developed in the last decades, for example, directly irradiated particulate solar reactor, vortex flow reactor (Haueter et al. 1999), fluidized bed reactor (Bridgwater and Peacocke 2000; Stiles and Kandiyoti 2003; Van de Veldena et al. 2008; Kodama et al. 2010), indirectly heated particulate reactor (Perkins et

al. 2009; Lichty et al. 2010), and indirectly heated packed bed reactor (Piatkowski et al. 2009). A rotary kiln (Li et al. 1999) and a free fall reactors (Zanzi et al. 1999) have been developed. However, none of these solar reactors for thermochemically converting carbonaceous biomass permits controlling atmosphere composition and pressure, heating, and cooling rates of the samples, and level and duration of the temperature plateau during the chemical transformation in the temperatures ranging from 1100 K to 2300 K.

Figure 1.3 diagrams three steps of pyrolysis process of wet carbonaceous, i.e., drying, primary pyrolysis, and secondary pyrolysis (Neves et al. 2011). Briefly, the carbonaceous biomass is dried at 100-200°C. Certain internal rearrangements, bond breakages, free radical and carbonyl group formation, accompanying small amount of release of moisture, carbon monoxide and carbon dioxide occur during this initial step. The primary pyrolysis is the second step, which occurs at a temperature range of 250-500°C. The decomposition of sample results in the production of the primary products, which can be involved in different secondary reactions to produce the final products at higher temperatures.

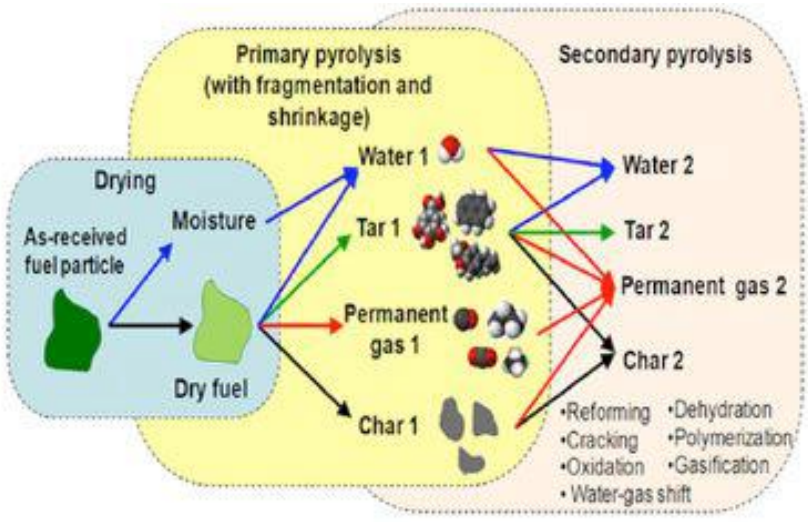

Figure 1.3. Three steps of pyrolysis of wet carbonaceous feedstock (Neves et al. 2011)

Usually, a carbonaceous sample experiences three stages during the primary vapor secondary reactions, the primary, secondary, and tertiary processes, at different

temperature ranges (**Figure 1.4**) (Evans and Milne 1987). During the primary stage at temperatures ranging from 500°C to 600°C, products with higher molecular weight slightly break to form lighter aromatics and oxygenate within a second. When temperature is raised to about 700°C during the second stage, monocarbon oxide, light olefins, and aromatics are formed from carbohydrates. The third stage occurs at higher temperatures, resulting in the formation of the tertiary products, such as aromatics.

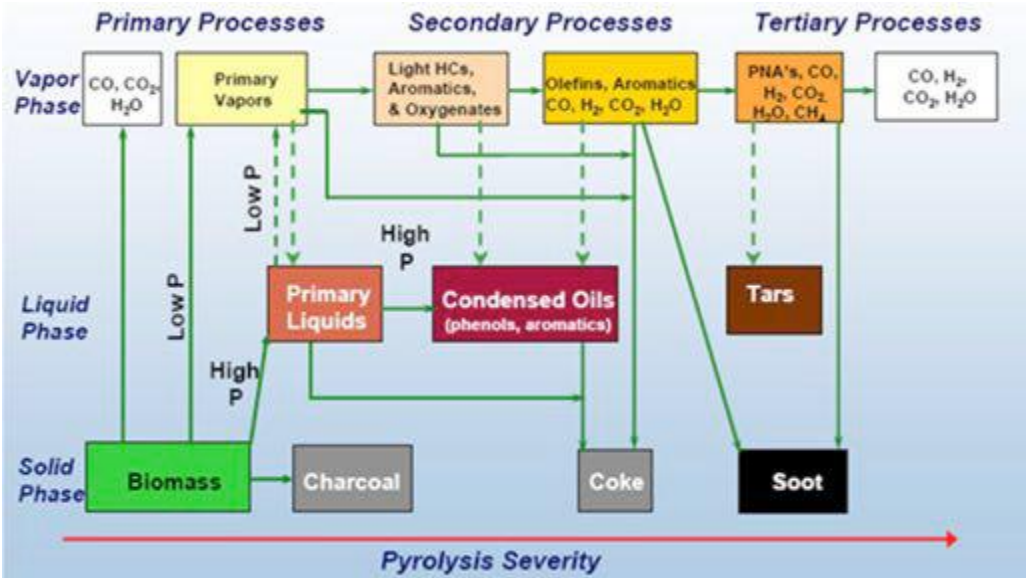

Figure 1.4. Pyrolysis pathways of carbonaceous feedstock (Evans and Milne 1987)

1.3.3 Operation parameters determining pyrolysis process

Biomass pyrolysis involves extremely complex chemical and physical processes, such as transient heat transfer, mass transfer, chemical reactions, and their interactions. These processes are influenced by temperature, heating rate, biomass particle size and density, physical and chemical pretreatments of the process and others (Guedes et al. 2018). Numerous studies have investigated the effects of different processing parameters on the distribution, yield, and composition of the pyrolysis products.

Solar assisted biomass pyrolysis is currently an emerging technology attracting

considerable research interest (Yadav and Banerjee 2016; Zeng et al. 2017a; Weldekidan et al. 2018a). Parameters that influence conventional pyrolysis of biomass impact also on solar pyrolysis of biomass (Zeng et al. 2017a). Fuels with higher calorific values and chemicals of different quality and quantity can be achieved from the solar pyrolysis of biomass by varying the operating parameters. Solar pyrolysis is different from conventional pyrolysis by providing fast heating rate and achieving flexible temperatures that can range up to 3000°C. With only limited studies investigating solar assisted biomass pyrolysis, the distribution of solar pyrolysis products at different solar conditions are still not sufficiently investigated.

1.3.3.1 Temperature

Biomass pyrolysis requires heat to initiate and perform the whole process. During pyrolysis process, the temperature increase results in decomposing biomass bonds. The increment of biomass conversion efficiency is associated with increase of temperature. Heat can be supplied by partially combusting some of the evolved volatiles, thereby reducing the overall amount of produced pyrolysis products, or through external solar heat. Heat can significantly improve the efficiency of the pyrolysis process. Integration of solar energy to drive the thermochemical processing of biomass offers opportunities for developing new and sustainable biomass-solar technologies (Wu et al. 2018).

Raise in temperature promotes production of liquids at a mild temperature range; however, at extremely high temperatures, liquid yield declines and gas yield increases due to secondary cracking of the volatiles (Isahak et al. 2012). Temperatures in the range of 400-650°C at different heating rates (5 to 700°C/min) were investigated for different types of biomass. Bio-oil yields from rice husk and waste palms were found to increase with temperature and reached maximum values of 70% at 450°C and 72.4% at 500°C, respectively. However, a further increase in the temperature favors formation of gas and bio-chars. Lower ranges of pyrolysis temperatures (>500°C) for processing of wood chip produces CO_2, CO, and small amount of CH_4 from primary decomposition, and at temperatures higher than 650°C the CO, CH_4, and H_2 concentrations increase due to secondary tar cracking (Morf et al. 2002). The gas product especially H_2 and CO yield significantly increased with temperature

(from 600 to 1600°C) and heating rate (from 5 to 50°C/s) mainly due to the enhanced secondary tar reactions (Zeng et al. 2017b).

Temperature has an impact on not only yield, but also quality of the liquid products of pyrolysis. Higher temperature promotes cracking of the aliphatic species and aromatics formation, which influences the H/C ratio and organonitrogen content of bio-oil product (Huang et al. 2014). The impacts of temperatures during pyrolysis on compositions of bio-oil, such as contents of carbon, hydrogen, and oxygen, have been reported in different types of biomass, but contents of water, nitrogenous matters, ethers, and aldehydes are less affected by temperatures during pyrolysis (Ates and Işıkdağ 2008; Pütün et al. 2008; Alvarez et al. 2014; Ly et al. 2016).

1.3.3.2 Heating rate

Heating rate is another important parameter in biomass pyrolysis. Heating rate does not impact on the pyrolysis process independently, rather, it exerts its effect on pyrolysis process depending on other pyrolysis parameters, such as type of biomass. There is not a linear relationship between heating rate and the bio-oil yield. It was reported that at a lower range of heating rate from 7 to 50°C/min, the bio-oil yield from the pyrolysis of hornbeam shell does not vary indicating negligible effect of heating rate for the conditions tested (Morali and Sensoz 2015). In the pyrolysis of olive bagasse experiment at lower range of heating rates, the bio-oil production at 10°C/min was even less than at 50°C/min (Şensöz et al. 2006). However, a parabolic change of bio-oil production occurs in several biomass pyrolysis at higher heating rates. In the study of sesame stalk pyrolysis experiment, the bio-oil yield increased by 58% when the heating rate raised from 100°C/min to 300°C/min, but it did not increase further at high heating rate of 800°C/min (Ateş et al. 2004). Fast heating may reduce water content in the bio-oil by inhibiting the secondary dehydration reactions. Higher heating rates favor the production of oxygen-containing gases, i.e., CO_2 and/or CO, thus reducing the oxygen content in the pyrolysis liquid product (Akhtar et al. 2012). Heating rates up to 100°C/s can create heat and mass transfer limitations in samples during pyrolysis, hence bringing substantial variations to

the yield and composition of pyrolysis gases, possibly due to non-homogenous heating of the samples. Yields of CO, H_2, CH_4, and C_2H_6 were observed to increase when the heating rate raised from 5 to 50°C/s in the solar pyrolysis of beech wood (Zeng et al. 2015c).

1.3.3.3 Biomass feedstock

Biomass feedstock differs in their contents of lignin, cellulose, and hemicellulose, as well as proteins, fats, and lipids (Weldekidan et al. 2019). Variation in these biomass components may vary even in the same type of biomass produced in different soils, grown in different conditions, and harvested at different growth stages. The volatile matter, ash, and moisture contents are also some of the typical variations in biomass which can affect the distribution of pyrolysis products (Guedes et al. 2018). Biomass with a higher lignin content tends to produce more char than cellulose and hemicellulose, which favors the production of tar and non-condensable volatiles; while biomass having higher cellulose and hemicellulose contents may produce higher yield of bio-oil than that with high lignin content (Akhtar and Saidina Amin 2012). High heating rate and temperature are useful to degrade lignin because it has a great structural stability, thus facilitating the production of bio-oil. The amount of volatile matter in feedstock also plays a significant role in determining the quantity of each pyrolysis product. High percentage of volatile materials, such as cellulose, results in high volatility and reactivity, which favors production of bio-oil. So, pyrolysis of biomass with high volatile material content can yield more bio-oil (Jung et al. 2008; Omar et al. 2011; Casoni et al. 2015). Pyrolysis of cellulose and hemicellulose produces more liquid than lignin (Qu et al. 2011; Kim et al. 2013; Quan et al. 2016). Also, a high tar yield can be obtained from feedstock with high content of volatile matter due to improved volatility and reactivity advantages (Omar et al. 2011). Pre-treatment of biomass has an impact on the liquid yield. Casoni et al. (2015) reported that the mushroom fungus treatment of sunflower hulls increased bio-oil production from pyrolysis, which resulted from the enzymatic activity of mushroom that promoted the degradation of the lignin structure, making the biomass more vulnerable to thermal attack. However, the acid treatment prevents cellulose fibers

from thermal attack and reduces the liquid yield.

Many studies have demonstrated that ash is negatively correlated with bio-oil yield produced by biomass pyrolysis, but positively correlated with char and gas production (Abdullah and Gerhauser 2008; Razuan et al. 2010; Pattiya and Suttibak 2012; Pattiya et al. 2012; Abnisa et al. 2013; Lee et al. 2013). The elements, such as sodium, potassium, sulfur, and phosphorus, in ash, have an effect on liquid production (Venderbosh and Prins 2010).

Moisture content of the biomass is important in the pyrolysis process. Water in the final liquid product originates from two sources, one is the moisture from the raw materials, and the other is from the dehydration reactions during the process of pyrolysis (Abnisa et al. 2013; Cardoso et al. 2016). The moisture content impacts on the quality of bio-oil, and high moisture content decreases the viscosity of bio-oil, which is important in the fuel injection system, the atomization quality, and combustion properties of the fuel (Lu et al. 2008). The moisture also improves the stability and reduces the calorific value of bio-oil. To ensure the quality of bio-oil product, a maximum of moisture in the biomass allowed is 10%.

1.3.3.4 Particle size

Particle size affects the yield and composition of the pyrolysis products. As biomass has low thermal conductivity, very large particle size can limit heat transfer to adjacent particles, resulting in an inefficient pyrolysis process. Shen et al. (2009) investigated the effects of different particle sizes (0.18 to 5.6 mm) of mallee wood on pyrolysis at 500°C and found a decrease of the liquid yield by around 14%, while the gas and char yields increased by around 14% and 4% when the particle size increased from 0.3 to 1.5 mm, respectively. However, a further increase up to 5.6 mm could not bring any significant variations to the results. Small particle sizes enhance the formation of H_2 and CO contents. The relative increments of 18.3% and 17.0% were recorded in the H_2 and CO yields, respectively, as the particle sizes changed from 10 to 5 mm in the pyrolysis of municipal solid waste at 900°C. However, it was reported that the particle size <2 mm of grape bagasse, *Cynara cardunculus*, and soybean cake in the fixed bed reactor does not impact on the product yields (Encinar et

al. 1998, 2000; Uzun et al. 2006). Similar conclusion was drawn in the pyrolysis experiments using rice straw, soybean cake, and sugarcane bagasse as the raw materials (Pütün et al. 2004; Şensöz and Kaynar 2006; Varma and Mondal 2017). It is difficult to specify a range of particle size that optimizes the yield of bio-oil, because the efficiency of biomass pyrolysis may vary depending on the types of biomass and pyrolysis reactors, as well as the processing parameters. Flash pyrolysis generally requires smaller particle size for complete decomposition of biomass. The cost of further processing biomass must be considered.

Conventional gasifiers (fixed or fluidized beds) usually treat centimeter sized biomass particles, since they cannot be economically processed into very fine sizes due to its high volatile content and moisture level. These large biomass particles may provide sufficient residence time for tar to decompose homogeneously and heterogeneously inside the particle to give secondary gas, tar, and char, which can also affect the product yields. Moreover, the average thermal conductivity of biomass is very low. Then, both biomass size and effective thermal conductivity (λ_{eff}) along with the high operating values of temperature and heating rates encountered in these units could make intra-particle heat transfer mechanism to play an important role in product distribution from pyrolysis.

Most of the experimental and modelling researches regarding tar intra-particle secondary reactions were performed under slow heating rate and low temperature. Nonetheless, no results have ever been reported concerning pyrolysis of thermally thick particles at both high heating rate and final temperature. Pozzobon et al. (2014) studied experimentally (by macro TGA) and numerically the effect of biomass aspect ratio in tar cracking. The final reactor temperature was 700°C and the heating rate was 30°C/s. Tar yield was shown to decrease with increasing biomass length, while the particle diameter was held constant. They stated that the optimum aspect ratio for achieving intra-particle tar decomposition is 1.1 according to the numerical analysis. In a macro TGA experimental essay to study intra-particle secondary reactions of tar during biomass pyrolysis of a centimeter wood cylinder, Pattanotai et al. (2013) compared the product yields of sawdust and wood cylinder at 0.5°C/s (low heating rate, kinetic controlled regime), revealing the occurrence of intra-particle secondary reactions. They concluded that tar intra-particle decomposition is

important when slowly pyrolyzing “thermally thick” particles. Bennadji et al. (2014) conducted an experimental study and compared the pyrolysis behavior of two different sizes of wood spheres. Pyrolysis was run at atmospheric pressure in a bench-scale tubular reactor which was designed to pyrolyze solids at a maximum temperature of 482°C. A numerical model was also formulated and validated against the experimental data. Kenarsari and Zheng (2014) formulated a model validated by comparing experimental data found in bibliography. A 3D particle model was formulated accounting for transport phenomena along with primary pyrolysis and homogeneous and heterogeneous tar decomposition. The model was validated with experimental data from literature (Shi et al. 2016).

A majority of studies have been conducted to examine the effect of parameters individually while maintaining the other parameters constant, and very few researches have considered the joint effects of the pyrolysis processing parameters (Abnisa et al. 2011; Isa et al. 2011; Ellens and Brown 2012; Arazo et al. 2017). This requires a special experimental design and plan to involve multiple variables within a study. The central composite design was employed in the studies to analyze different processing parameters (Isa et al. 2011; Arazo et al. 2017). The weight of each variable and interactions between the variables should also be considered when analyzing the effects of different processing parameters on the yield and quality of pyrolysis products.

1.3.4 Characterization of pyrolysis products

Studies have demonstrated that the properties and distribution of products generated by solar pyrolysis, i.e., bio-oil, char, tar, and gas, are dependent of temperature and heating rate (Neves et al. 2011; Akhtar et al. 2012). Because primary tars easily crack into low molecular weight gases at above approximately 500°C (Balat et al. 2009), the liquid yield decreases and gas yield generally increases over this temperature (Pütün 2010). The char yield initially decreases with rising temperature and then remains at a plateau above 600°C (Akhtar and Amin 2012). Fast heating rates reduce the heat and mass transfer limitations for small particles, thus it favors bond-scission reactions and enhances the yield of primary

volatiles (tar and gases) at cost of char yield (Salehi et al. 2009). The yields of liquid and gases (CO, CO_2, H_2, CH_4, and C_2H_6) markedly increase when increasing the heating rate from 5°C/min to 80°C/min at the final pyrolysis temperature of 720°C (Williams and Besler 1996). However, the liquid and gas yields do not improve with further heating rate increase, once heat and mass transfer limitations are overcome (Akhtar and Amin 2012). Various studies confirmed the obvious influence of biomass characteristics on the pyrolysis reactions and product yields. The compositional structures, which are mainly cellulose, hemicellulose, and lignin, vary among the biomass feedstock (Mahmoudi et al. 2010), and they have different pyrolysis characteristics (Yang et al. 2007). Cellulose relates to the wood strength and decomposes in the temperature range of 240-350°C and hemicellulose decomposes in the range 200-260°C. Lignin is more difficult to dehydrate due to its physical and chemical properties, it decomposes in the temperature range of 280-500°C. Cellulose turns generally into condensable vapor during pyrolysis. In contrast, hemicellulose produces more non-condensable gas and less tar. Lignin degrades slowly and forms char.

Besides, temperature and heating rate are known to affect HM transformation during conventional pyrolysis of contaminated biomass (Liu et al. 2017a). Many heavy metals such as Cu and Ni have catalytic effect on biomass pyrolysis reactions (Nzihou et al. 2019). In HM contaminated biomass, HMs can work as *in situ* catalysts during pyrolysis for enhancing quality and value of products (Eibner et al. 2015). Copper promoted hemicellulose pyrolysis at low temperature (around 270°C) and restricted the final degradation of cellulose and lignin, which enhanced primary oil (levoglucosan) production (Xing et al. 2016). Copper effectively catalyzed the chain-breaking of lignin at 450-600°C for producing more C7-C10 compounds (Liu et al. 2012). At high pyrolysis temperature of 750°C, Cu(II) was fully turned into Cu^0 (Li et al. 2019). Similarly, Ni^0 could be produced by the pyrolysis of Ni(II) polluted wood at temperatures below 500°C (Richardson et al. 2010). The newly formed Ni^0 could catalyze the tar conversion into H_2 production in the pyrolysis process (Richardson et al. 2013). Bru et al. (2007) found that gas yield obtained from Ni impregnated biomass at 700°C increased from 20.0% to 33.1% with H_2 yield rising by 260% compared to those from the raw biomass. Nickel catalyzed the carboxyl and carbonyl broken for more CO_2 formation, while it

restricted CH_4 release (Liu et al. 2017b). The catalytic activities of HMs are greatly affected by their different chemical states, which interacts with other pyrolysis factors (temperature and heating rate). However, the effect of heavy medal on product distribution during solar pyrolysis is still a question.

1.4 Bibliography

Abdullah N, Gerhauser H. Bio-oil derived from empty fruit bunches. Fuel, 2008, 87: 2606–2613.

Abnisa F, Arami-Niya A, Wan Daud WMA, Sahu JN, Noor IM. Utilization of oil palm tree residues to produce bio-oil and biochar via pyrolysis. Energy Conversion and Management, 2013, 76: 1073–1082.

Abnisa F, Wan Daud WMA. A review on co-pyrolysis of biomass: An optional technique to obtain a high-grade pyrolysis oil. Energy Conversion and Management, 2014, 87: 71–85.

Abnisa F, Wan Daud WMA, Sahu JN. Optimization and characterization studies on bio-oil production from palm shell by pyrolysis using response surface methodology. Biomass Bioenergy, 2011, 35: 3604–3616.

Akhtar J, Amin NS. A review on operating parameters for optimum liquid. Renewable and Sustainable Energy Reviews, 2012, 16: 5101–5109.

Alvarez J, Lopez G, Amutio M, Bilbao J, Olazar M. Bio-oil production from rice husk fast pyrolysis in a conical spouted bed reactor. Fuel, 2014, 128: 162–169.

Antal MJ, Hofmann L, Moreira MJ, Brown CT, Steenblik R. Design and operation of a solar fired biomass flash pyrolysis reactor. Solar Energy, 1983, 30: 299–312.

Arazo RO, Angela D, Genuino D, Daniel M, De Luna G, Capareda SC. Bio-oil production from dry sewage sludge by fast pyrolysis in an electrically-heated fluidized bed reactor. Sustainable Environment Research, 2017, 27: 7–14.

Ateş F, Işıkdağ MA. Evaluation of the role of the pyrolysis temperature in straw biomass samples and characterization of the oils by GC/MS. Energy & Fuels, 2008, 22: 1936–1943.

Ateş F, Pütün E, Pütün AE. Fast pyrolysis of sesame stalk: Yields and structural analysis of bio-oil. Journal of Analytical and Applied Pyrolysis, 2004, 71: 779–790.

Authier O, Ferrer M, Mauviel G, Khalfi A-E, Lédé J. Wood fast pyrolysis: Comparison of lagrangian and eulerian modeling approaches with experimental measurements. Industrial & Engineering Chemistry Research, 2009, 48: 4796–4809.

Balat M, Balat M, Kırtay E, Balat H. Main routes for the thermo-conversion of biomass into fuels and chemicals. Part 1: Pyrolysis systems. Energy Conversion and Management, 2009, 50: 3147–3157.

Barta K, Ford PC. Catalytic conversion of nonfood woody biomass solids to organic liquids. Accounts of Chemical Research, 2014, 47: 1503–1512.

Bennadji H, Smith K, Serapiglia MJ, Fisher EM. Effect of particle size on low-temperature pyrolysis of woody biomass. Energy & Fuels, 2014, 28: 7527–7537.

Bridgwater AV. Renewable fuels and chemicals by thermal processing of biomass. Chemical Engineering Journal, 2003, 91: 87–102.

Bridgwater AV, Peacocke GVC. Fast pyrolysis processes for biomass. Renewable and Sustainable Energy Reviews, 2000, 4: 1–73.

Bridgwater AV. Review of fast pyrolysis of biomass and product upgrading. Biomass and Bioenergy, 2012, 38: 68–94.

Bru K, Blin J, Julbe A, Volle G. Pyrolysis of metal impregnated biomass: An innovative catalytic way to produce gas fuel. Journal of Analytical and Applied Pyrolysis, 2007, 78: 291–300.

Çaglar A, Demirbas A. Conversion of cotton cocoon shell to hydrogen rich gaseous products by pyrolysis. Energy Conversion and Management, 2000, 43: 489–497.

Cairns MA, Brown S, Helmer EH, Baumgardner GA. Root biomass allocation in the world's upland forests. Oecologia, 1997, 111: 1–11.

Cao LC, Zhang C, Chen HH, Tsang DCW, Luo G, Zhang SC, Chen JM. Hydrothermal liquefaction of agricultural and forestry wastes: state-of-theart review and future prospects. Bioresource Technology, 2017, 245: 1184–1193.

Cardoso CAL, Machado ME, Caramão EB. Characterization of bio-oils obtained from pyrolysis of bocaiuva residues. Renewable Energy, 2016, 91: 21–31.

Casoni AI, Bidegain M, Cubitto MA, Curvetto N, Volpe MA. Pyrolysis of sunflower seed hulls for obtaining bio-oils. Bioresource Technology, 2015, 177: 406–409.

Chen T, Zhang YX, Wang HT, Lu WJ, Zhou ZY, Zhang YC, Ren LL. Influence of pyrolysis temperature on characteristics and heavy metal adsorptive performance of biochar derived from municipal sewage sludge. Bioresource Technology, 2014, 164: 47–54.

Doren LGV, Posmanik R, Bicalho FA, Tester JW, Sills DL. Prospects for energy recovery during hydrothermal and biological processing of waste biomass. Bioresource Technology 2017, 225: 67–74.

Duque-Acevedo M, Belmonte-Ureña LJ, Cortés-García FJ, Camacho-Ferre F. Agricultural waste: Review of the evolution, approaches and perspectives on alternative uses. Global Ecology and Conservation, 2020, 22: e00902.

Durak H, Aysu T. Structural analysis of bio-oils from subcritical and supercritical hydrothermal liquefaction of *Datura stramonium* L. Journal of Supercritical Fluids, 2016, 108: 123–135.

Eibner S, Broust F, Blin J, Julbe A. Catalytic effect of metal nitrate salts during pyrolysis of impregnated biomass. Journal of Analytical and Applied Pyrolysis, 2015, 113: 143–152.

Ellens CJ, Brown RC. Optimization of a free-fall reactor for the production of fast pyrolysis bio-oil. Bioresource Technology, 2012, 103: 374–380.

Encinar J, Beltrán F, Ramiro A, González J. Pyrolysis/gasification of agricultural residues by carbon dioxide in the presence of different additives: Influence of variables. Fuel Processing Technology, 1998, 55: 219–233.

Encinar JM, González JF, González J. Fixed-bed pyrolysis of *Cynara cardunculus* L. Product yields and compositions. Fuel Processing Technology, 2000, 68: 209–222.

Evans RJ, Milne TA. Molecular characterization of the pyrolysis of biomass. 1. Fundamentals. Energy Fuels, 1987, 1: 123–137.

Food and Agriculture Organization of the United Nations (FAO), Organization for Economic Co-operation and Development (OECD). Background Notes on Sustainable, Productive and Resilient Agro-Food Systems: Value Chains, Human Capital, and the 2030 Agenda. A Report to the G20 Agriculture Deputies July 2019. https://www.oecd-ilibrary.org/docserver/dca82200-en.pdf?expires¼1563959111&id¼id&accname¼guest&checksum¼5BD0A7A51327DB165936B4AE57A0E5CE. 2019b. (Accessed 20 Jue 2020).

Food and Agriculture Organization of the United Nations (FAO), Organization for Economic Co-operation and Development (OECD). OECD-FAO Agricultural Outlook 2019-2028. http://www.fao.org/3/ca5308en/ca5308en.pdf. 2019a. (Accessed 20 June 2020)

Food and Agriculture Organization of the United Nations (FAO). Report of the FAO Expert Meeting on How to Feed the World in 2050. http://www. fao.org/3/ak542e/ak542e19.pdf. 2009. (Accessed 20 June 2020).

Food and Agriculture Organization of the United Nations (FAO). Strategic Work of FAO for Sustainable Food and Agriculture. http://www.fao.org/3/ai6488e.pdf. 2017. (Accessed 20 Jun 2020).

Gercel HF. The production and evaluation of bio-oils from the pyrolysis of sun ower-oil cake. Biomass Bioenergy, 2002, 23: 307–314.

Goyal HB, Seal D, Saxena RC. Bio-fuels from thermochemical conversion of renewable resources: A review. Renewable & Sustainable Energy Reviews, 2008, 12: 504–517.

Gregg DW, Taylor RW, Campbell JH, Taylor JR, Cotton A. Solar gasification of coal, activated carbon, code and coal and biomass mixtures. Solar Energy, 1980, 25: 353–364.

Guedes RE, Luna AS, Torres AR. Operating parameters for bio-oil production in biomass pyrolysis: A review. Journal of Analytical and Applied Pyrolysis, 2018, 129: 134–149.

Haarlemmer G, Guizani C, Anouti S, Deniel M, Roubaud A, Valin S. Analysis and comparison of bio-oils obtained by hydrothermal liquefaction and fast pyrolysis of beech wood. Fuel, 2016, 174: 180–188.

Haberl H, Erb KH, Krausmann F, Gaube V, Bondeau A, Plutzar C, Ginrich S, Lucht W, Fischer-Kowalski M. Quantifying and mapping the human appropriation of net primary production in earth's terrestrial ecosystems. Proceedings of the National Academy of Sciences of the United States of America, 2007, 104: 12942–12947.

Haueter P, Seitz T, Steinfeld A. A new high-flux solar furnace for high-temperature thermochemical research. Journal of Solar Energy Engineering, 1999, 121: 77–80.

Hazell P, Pachauri RK. Bioenergy and Agriculture: Promises and Challenges. 2006, https://doi.org/10.2499/2020focus14. (Accessed 20 June 2020).

He J, Strezov V, Kan T, Weldekidan H, Asumadu-Sarkodie S, Kumar R. Effect of temperature on heavy metal (loid) deportment during pyrolysis of *Avicennia marina* biomass obtained from phytoremediation. Bioresource Technology, 2019, 278: 214–222.

Hopkins MW, Dejenga C, Antal MJ. The flash pyrolysis of cellulosic materials using concentrated visible light. Solar Energy, 1984, 32: 547–551.

Huang X, Cao J, Shi P, Zhao X, Feng X. Influences of pyrolysis conditions in the production and chemical composition of the bio-oils from fast pyrolysis of sewage sludge. Journal of Analytical and Applied Pyrolysis, 2014, 110: 353–362.

Isa KM, Daud S, Hamidin N, Ismail K, Saad SA, Kasim FH. Thermogravimetric analysis and the optimisation of bio-oil yield from fixed-bed pyrolysis of rice husk using response surface methodology (RSM). Industrial Crops Production, 2011, 33: 481–487.

Isahak WNRW, Hisham MWM, Yarmo MA, Yun Hin TY. A review on bio-oil production from biomass by using pyrolysis method. Renewable and Sustainable Energy Reviews, 2012, 16: 5910–5923.

International Energy Agency. 2014 Key World Energy Statistics. 2015. (https://www.connaissancedesenergies.org/sites/default/files/pdf-actualites/keyworld_statistics_2015.pdf)

International Energy Agency. World Energy Outlook 2016. November 2016. (https://www.iea.org/reports/world-energy-outlook-2016)

Jackson RB, Canadell J, Ehleringer JR, Mooney HA, Sala OE, Schulze ED. A global analysis of root distributions for terrestrial biomes. Oecologia, 1996, 108: 389–411.

Jackson RB, Mooney HA, Schulze ED. A global budget for fine root biomass, surface area, and nutrient contents. Proceedings of the National Academy of Sciences of the United States of America, 1997, 94: 7362–7366.

Jung SH, Kang BS, Kim JS. Production of bio-oil from rice straw and bamboo sawdust under various reaction conditions in a fast pyrolysis plant equipped with a fluidized bed and a char separation system. Journal of Analytical and Applied Pyrolysis, 2008, 82: 240–247.

Kenarsari SD, Zheng Y. Fast pyrolysis of biomass pellets using concentrated solar radiation: A numerical study. Journal of Solar Energy Engineering, 136: 041004.

Kim SW, Koo BS, Ryu JW, Lee JS, Kim CJ, Lee DH, Kim GR, Choi S. Biooil from the pyrolysis of palm and Jatropha wastes in a fluidized bed. Fuel Processing Technology, 2013, 108: 18–124.

Kindermann GE, McCallum I, Fritz S, Obersteiner M. A global forest growing stock, biomass and carbon map based on FAO statistics. Silva Fennica, 2008, 42: 387–396

Kodama T, Gokon N, Enomoto S, Itoh S, Hatamachi T. Coal coke gasification in a windowed solar chemical reactor for beam-down optics. Journal of Solar Energy Engineering, 2010, 132: 041004.

Langholtz MH, Stokes BJ, Eaton LM. Billion-Ton Report: Advancing Domestic Resources for a Thriving Bioeconomy, Volume 1: Economic Availability of Feedstocks., ORNL/TM-2016/160. Oak Ridge National Laboratory, U.S. Department of Energy, Oak Ridge, TN. 2016.

Lédé J, Verzaro F, Antoine B, Villermaux J. Flash pyrolysis of wood in a cyclone reactor pyrolyse éclair du bois dans un réacteur cyclone. Chemical Engineering and Processing: Process Intensification, 1986, 20: 309–317.

Lee Y, Park J, Ryu C, Gang KS, Yang W, Park YK, Jung J, Hyun S. Comparison of biochar properties from biomass residues produced by slow pyrolysis at 500°C. Bioresource Technology, 2013, 148: 196–201.

Li AM, Li XD, Li SQ, Ren Y, Chi Y, Yan JH, Cen KF. Pyrolysis of solid waste in a rotary kiln: influence of final pyrolysis temperature on the pyrolysis products. Journal of Analytical and Applied Pyrolysis, 1999, 50: 149–162.

Li R, Huang H, Wang JJ, Liang W, Gao P, Zhang Z, Xiao R, Zhou B, Zhang X. Conversion of Cu(II)-polluted biomass into an environmentally benign Cu nanoparticles-embedded biochar composite and its potential use on cyanobacteria inhibition. Journal of Cleaner Production, 2019, 216: 25–32.

Lichty P, Perkins C, Woodruff B, Bingham C, Weimer AW. Rapid high temperature solar thermal biomass gasification in a prototype cavity reactor. Journal of Solar Energy Engineering, 2010, 132: 011012.

Lievens C, Carleer R, Cornelissen T, Yperman J. Fast pyrolysis of heavy metal contaminated willow: Influence of the plant part. Fuel, 2009, 88: 1417–1425.

Liu W, Li W, Jiang H, Yu H. Fates of chemical elements in biomass during its pyrolysis. Chemical Reviews, 2017a, 117: 6367–6398.

Liu W, Tian K, Jiang H, Zhang X, Ding H, Yu H. Selectively improving the bio-oil quality by catalytic fast pyrolysis of heavy-metal-polluted biomass: Take copper (Cu) as an example. Environmental Science & Technology, 2012, 46: 7849–7856.

Liu Y, Guo F, Li X, Li T, Peng K, Guo C, Chang J. Catalytic effect of iron and nickel on gas formation from fast biomass pyrolysis in a microfluidized bed reactor: A kinetic study. Energy & Fuels, 2017b, 31: 12278–12287.

Lu Q, Yang X, Zhu X. Analysis on chemical and physical properties of bio-oil pyrolyzed from rice husk. Journal of Analytical and Applied Pyrolysis, 2008, 82: 191–198.

Ly HV, Kim SS, Choi JH, Woo HC, Kim J. Fast pyrolysis of *Saccharina japonica* alga in a fixed-bed reactor for bio-oil production. Energy Conversion and Management, 2016, 122: 526–534.

Mahmoudi S, Baeyens J, Seville J. NOx formation and selective non-catalytic reduction (SNCR) in a fluidized bed combustor of biomass. Biomass and Bioenergy, 2010, 34: 1393–1409.

Maniatisl K, Baeyens J, Peeters H, Roggeman G. The EGEMIN flash pyrolysis process: commissioning and initial results. Advances in Thermochemical Biomass Conversion 1993. Springer Netherlands, 1993, pp. 1257–1264.

McKendry P. Energy production from biomass (part 1): Overview of biomass. Bioresource Technology, 2002, 83: 37–46.

Morali U, Şensöz S. Pyrolysis of hornbeam shell (*Carpinus betulus* L.) in a fixed bed reactor: Characterization of bio-oil and bio-char. Fuel, 2015, 150: 672–678.

Morf P, Hasler P, Nussbaumer T. Mechanisms and kinetics of homogeneous secondary reactions of tar from continuous pyrolysis of wood chips. Fuel, 2002, 81: 843–853.

Neves D, Thunman H, Matos A, Tarelho L, Gómez-Barea A. Characterization and prediction of biomass pyrolysis products. Progress in Energy and Combustion Science, 2011, 37: 611–630.

Nzihou A, Flamant G, Stanmore B. Synthetic fuels from biomass using concentrated solar energy - A review. Energy, 2012, 42: 121–131.

Nzihou A, Stanmore B. The fate of heavy metals during combustion and gasification of contaminated biomass-A brief review. Journal of Hazardous Materials, 2013, 256: 56–66.

Nzihou A, Stanmore B, Lyczko N, Minh DP. The catalytic effect of inherent and adsorbed metals on the fast/flash pyrolysis of biomass: A review. Energy, 2019, 170: 326–337.

Omar R, Idris A, Yunus R, Khalid K, Aida Isma MI. Characterization of empty fruit bunch for microwave-assisted pyrolysis. Fuel, 2011, 90: 1536–1544.

Pan Y, Birdsey RA, Phillips OL, Jackson RB. The structure, distribution., and biomass of the world's forests. The Annual Review of Ecology, Evolution, and Systematics, 2013, 44: 593–622.

Pattanotai T, Watanabe H, Okazaki K. Experimental investigation of intraparticle secondary reactions of tar during wood pyrolysis. Fuel, 2013, 104: 468–475.

Pattiya A, Sukkasi S, Goodwin V. Fast pyrolysis of sugarcane and cassava residues in a free-fall reactor. Energy, 2012, 44: 1067–1077.

Pattiya A, Suttibak S. Production of bio-oil via fast pyrolysis of agricultural residues from cassava plantations in a fluidised-bed reactor with a hot vapour filtration unit. Journal of Analytical and Applied Pyrolysis, 2012, 95: 227–235.

Perkins C, Weimer AW. Solar-thermal production of renewable hydrogen. AIChE Journal, 2009, 55: 286–293.

Piatkowski N, Wieckert C, Steinfeld A. Experimental investigation of a packed-bed solar reactor for the steam-gasification of carbonaceous feedstocks. Fuel Processing Technology, 2009, 90: 360–366.

Piatkowski N, Wieckert C, Weimer AW, Steinfeld A. Solar-driven gasification of carbonaceous feedstock – A review. Energy & Environmental Science, 2011, 4: 73–82.

Pozzobon V, Salvador S, Bezuan J-J, EL-Hafi M, Le Maoult Y, Flamant G. Radiative pyrolysis of wet wood under intermediate heat flux: Experiments and modeling. Fuel Processing Technology, 2014, 128: 319-330.

Pütün AE, Apaydm E, Pütün E. Rice straw as a bio-oil source via pyrolysis and steam pyrolysis. Energy, 2004, 29: 2171–2180.

Pütün E. Catalytic pyrolysis of biomass: Effects of pyrolysis temperature, sweeping gas flow rate and MgO catalyst. Energy, 2010, 35: 2761–2766.

Pütün E, Ateş F, Pütün AE. Catalytic pyrolysis of biomass in inert and steam atmospheres. Fuel, 2008, 87: 815–824.

Qu T, Guo W, Shen L, Xiao J, Zhao K. Experimental study of biomass pyrolysis based on three major components: Hemicellulose, cellulose, and lignin. Industrial & Engineering Chemistry Research, 2011, 50: 10424–10433.

Quan C, Gao N, Song Q. Pyrolysis of biomass components in a TGA and a fixedbed reactor: Thermochemical behaviors, kinetics, and product characterization. Journal of Analytical and Applied Pyrolysis, 2016, 121: 84–92.

Razuan R, Chen Q, Zhang X, Sharifi V, Swithenbank J. Pyrolysis and combustion of oil palm stone and palm kernel cake in fixed-bed reactors. Bioresource Technology, 2010, 101: 4622–4629.

Richardson Y, Blin J, Volle G, Motuzas J, Julbe A. *In situ* generation of Ni metal nanoparticles as catalyst for H_2-rich syngas production from biomass gasification. Applied Catalysis A: General, 2010, 382: 220–230.

Richardson Y, Motuzas J, Julbe A, Volle G, Blin J. Catalytic investigation of in situ generated Ni metal nanoparticles for tar conversion during biomass pyrolysis. Journal of Physical Chemistry C, 2013, 117: 23812–23831.

Salehi E, Abedi J, Harding T. Bio-oil from sawdust: Pyrolysis of sawdust in a fixed-bed system. Energy & Fuel, 2009, 23: 3767–3772.

Şensöz S, Demiral I, Gerçel HF. Olive bagasse (*Olea europea* L.) pyrolysis. Bioresource Technology, 2006, 97: 429–436.

Şensöz S, Kaynar I. Bio-oil production from soybean (*Glycine max* L.): Fuel properties of Bio-oil. Industrial Crops Production, 2006, 23: 99–105.

Shen J, Wang X-S, Garcia-Perez M, Mourant D, Rhodes MJ, Li C-Z. Effects of particle size on the fast pyrolysis of oil mallee woody biomass. Fuel, 2009, 88: 1810–1817.

Shi X, Ronsse F, Pieters JG. Finite element modeling of intraparticle heterogeneous tar conversion during pyrolysis of woody biomass particles. Fuel Processing Technology, 2016, 148: 302–316.

Stiles HN, Kandiyoti R. Secondary reactions of flash pyrolysis tars measured in a fluidized bed pyrolysis reactor with some novel design features. Fuel, 2003, 68: 275–282.

Swain PK. Utilisation of agriculture waste products for production of bio-fuels: A novel study. Materials Today: Proceedings, 2017, 4: 11959–11967.

Taylor RW, Berjoan R, Coutures JP. Solar gasification of carbonaceous materials. Solar Energy, 1983, 30: 513–525.

Treinyte J, Bridziuviene D, Fataraite-Urboniene E, Rainosalo E, Rajan R, Cesoniene L, Grazuleviciene V. Forestry wastes filled polymer composites for agricultural use. Journal of Cleaner Production, 2018, 205: 388–406.

Uzun BB, Pütün AE, Pütün E. Fast pyrolysis of soybean cake: Product yields and compositions. Bioresource Technology, 2006, 97: 569–576.

Van de Velden M, Baeyens J, Brems A, Janssens B, Dewil R. Fundamentals, kinetics and endothermicity of the biomass pyrolysis reaction. Renewable Energy, 2010, 35: 232–242.

Van de Veldena M, Baeyensa J, Boukisb I. Modeling CFB biomass pyrolysis reactors. Biomass and Bioenergy, 2008, 32: 128–139.

Varma AK, Mondal P. Pyrolysis of sugarcane bagasse in semi batch reactor: Effects of process parameters on product yields and characterization of products. Industrial Crops

Production, 2017, 95: 704–717.

Weldekidan H, Strezov V, He J, Kumar R, Asumadu-Sarkodie S, Doyi I, Jahan S, Kan T, Town G. Energy conversion efficiency of pyrolysis of chicken litter and rice husk biomass. Energy & Fuel, 2019, 33: 6509-6514.

Weldekidan H, Strezov V, Town G. Review of solar energy for biofuel extraction. Renewable and Sustainable Energy Reviews, 2018a, 88: 184–192.

Whelan J, Xu C, Shen F, Kumar A, Eklund M, Yan JY. Sustainable biofuel production from forestry, agricultural and waste biomass feedstocks. Applied Energy, 2017, 198: 281–283.

Williams PT, Besler S. The influence of temperature and heating rate on the slow pyrolysis of biomass. Renewable Energy, 1996, 7: 233–250.

Wu H, Gauthier D, Yu Y, Gao X, Flamant G. Solar-thermal pyrolysis of mallee wood at high temperatures. Energy & Fuels, 2018, 32: 4350–4356.

Xing S, Yuan H, Huhetaoli, Qi Y, Lv P, Yuan Z, Chen Y. Characterization of the decomposition behaviors of catalytic pyrolysis of wood using copper and potassium over thermogravimetric and Py-GC/MS analysis. Energy, 2016, 114: 634–646.

Yadav D, Banerjee R. A review of solar thermochemical processes. Renewable and Sustainable Energy Reviews, 2016, 54: 497–532.

Yang HP, Yan R, Chen HP, Lee DH, Zheng CG. Characteristics of hemicelluloses, cellulose and lignin pyrolysis. Fuel, 2007, 86: 1781–1788.

Zanzi R, Sjöström K, Björnbom E. Rapid high-temperature pyrolysis of biomass in a free-fall reactor. Fuel, 1999, 75: 545–550.

Zeaiter J, Ahmad MNM, Rooney D, Samneh B, Shammas E. Design of an automated solar concentrator for the pyrolysis of scrap rubber. Energy Conversion and Management, 2015, 101: 118–125.

Zeng K, Flamant G, Gauthier D, Guillot E. Solar pyrolysis of wood in a labscale solar reactor: Influence of temperature and sweep gas flow rate on products distribution. Energy Procedia, 2015a, 69: 1849–1858.

Zeng K, Gauthier D, Li R, Flamant G. Solar pyrolysis of beech wood: Effects of pyrolysis parameters on the product distribution and gas product composition. Energy, 2015c, 93: 1648–1657.

Zeng K, Gauthier D, Soria J, Mazza G, Flamant G. Solar pyrolysis of carbonaceous feedstocks: A review. Solar Energy, 2017a, 156: 73–92.

Zeng K, Gauthier D, Doan PM, Weiss-Hortala E, Nzihou A, Flamant G. Characterization of solar fuels obtained from beech wood solar pyrolysis. Fuel, 2017b, 188: 285–293.

Zeng K, Gauthier D, Flamant G. High temperature flash pyrolysis of wood in a lab-scale solar reactor. In: Proceedings of ASME 2014 8th International Conference on Energy Sustainability. Boston, USA (June 30–July 2, 2014).

Zeng K, Minh DP, Gauthier D, Weiss-Hortala E, Nzihou A, Flamant G. The effect of temperature and heating rate on char properties obtained from solar pyrolysis of beech wood. Bioresource Technology, 2015b, 182: 114–119.

Zeng K, Soria J, Gauthier D, Mazza G, Flamant G. Modeling of beech wood pellet pyrolysis under concentrated solar radiation. Renewable Energy, 2016, 99: 721–729.

Zhang D, Liu P, Lu X, Wang L, Pan T. Upgrading of low rank coal by hydrothermal treatment: Coal tar yield during pyrolysis. Fuel Processing Technology, 2016, 141: 117–122.

Zhang X, Laubie B, Houzelot V, Plasari E, Echevarria G, Simonnot M. Increasing purity of ammonium nickel sulfate hexahydrate and production sustainability in a nickel phytomining process. Chemical Engineering Research and Design, 2016, 106: 26–32.

Chapter 2

Materials and Methods

This chapter provides the characterization of materials, experimental setup and procedures, product analysis, and data processing method. Therefore, three sections are included in this chapter.

- **Section 2.1** presents the characterizations of biomass materials used in this study, including pine wood, agricultural wastes, chicken litter, and rice husk, as well as heavy metal (Cu and Ni) polluted willow wood.

- **Section 2.2** describes the experimental setups and procedures for solar pyrolysis of the above described biomasses.

- **Section 2.3** discusses the data processing methods. The mathematic formulas for calculation are provided in this section.

2.1 Sample characterization

2.1.1 Pine wood and agricultural wastes

The first set of raw materials used are four kinds of biomass particles issued from Northern Patagonia (Argentina – collaboration with PROBIEN, CONICET - UNCo) from both forestry (i.e., pine sawdust) and agricultural industries (i.e., peach pit, grape stalk, and grape marc in powder). The initial powder particles (100 µm in mean size) were compressed by a hydraulic compressor to form the pellets. The insulation is added around the crucible to avoid the internal temperature gradients. The feedstock analyses are shown in **Table 2.1**. It can be seen that the pine sawdust contains more cellulose than the agricultural wastes, ranging from 1.5 fold (peach pit) to almost 3 folds (grape marc and grape stalk). The hemicellulose is about 5 times more concentrated in pine sawdust and peach pit than in the other types of biomass, whereas the lignin content is almost identical in all biomass types. Finally, grape biomass contains a large amount of ash with respect to the other two feedstock: about 9 wt.% and 10 wt.% for marc and stalk, respectively. Experiments were run with cylindrical pellets (5 mm in height, 10 mm in diameter) made of compressed particles, corresponding to approximately 0.3 g. A very thin carbon layer was previously deposited on the pellet surface in order to increase its absorptivity of the concentrated solar radiation and to fix the surface emissivity. It helps keep the emissivity at approximately 0.95 for achieving a reliable pyrometer measurement accuracy. The carbon layer was removed before char mass measurement.

Table 2.1. Feedstock composition of pine wood and agricultural wastes.

Biomass	Volatile materials (wt.%)	Water-content (wt.%)	Elements (wt.%)					Ash (wt.%)	Lignocelluloses (wt.%)		
			C	H	N	S	O		Cellu-lose	Hemice-llulos	Lignin
Pine sawdust	82.4	7.2	50.9	6.0	0.1	0.05	42.9	0.5	43.0	20.0	26.8
Peach pit	79.1	7.2	53.0	5.9	0.3	0.05	39.1	1.6	31.6	21.0	27.5

Grape marc	68.5	10.9	52.9	5.9	1.9	0.03	30.4	8.8	15.3	5.0	38.0
Grape stalk	51.1	9.3	46.1	5.7	0.4	0	37.5	10.2	16.0	5.8	30.8

2.1.2 Chicken litter and rice husk

The second biomass materials are chicken-litter waste with a particle size of 280 µm and rice husk with two particle sizes of 280 and 500 µm (collaboration with the Department of Environmental Sciences, Faculty of Science Engineering, Macquarie University, Australia). The results of proximate and ultimate analysis of the two biomass samples are summarized in **Table 2.2**.

Table 2.2. Proximate and ultimate analysis results of chicken-litter waste and rice husk.

Biomass	Proximate analysis				Ultimate analysis				
	Ash	Volatile matter	Fixed carbon	Moisture	C	H	O*	N	S
Chicken-litter	27.1	62.6	10.3	9.9	46.9	5.4	4.2	5.4	0.3
Rice husk	25.3	54.5	14.1	6.0	34.3	5.0	60.1	0.4	0.2

* By difference

Note: Ash, volatile matter, fixed carbon, %mass, dry basis; moisture, %mass; ultimate parameters, %mass, ash free.

2.1.3 Heavy metal polluted willow wood

The copper or nickel impregnated willows were chosen to represent heavy metal contaminated biomass after phytoextraction. Raw and copper and nickel impregnated willow samples were prepared (Collaboration with RAPSODEE, IMT-Mines d'Albi). One hundred grams of willow wood particles (0.5-1 mm particle size) were impregnated with 1 L of 0.05% (w/v) nickel nitrate aqueous solution or 0.05% (w/v) copper nitrate aqueous solution prepared with $Cu(NO_3)_2 \cdot 6H_2O$ or $Ni(NO_3)_2 \cdot 6H_2O$ (Sigma-Aldrich, 99% purity). The prepared mixtures were stirred at ambient temperature for 24 h. The impregnated willow particles were then filtered and dried at 60°C for 24 h. The resulting Cu and Ni

concentrations in the impregnated willow were 0.29 mol/kg and 0.06 mol/kg, respectively. The dry wood particles are shown in **Figure 2.1**. Raw willow, willow with Cu, and willow with Ni correspond to the non-impregnated wood, Cu-impregnated wood, and Ni-impregnated wood as pyrolysis feedstock, respectively. Then, the raw and the impregnated willow woods were compressed into pellets. The pellets with 10 mm in diameter and 5 mm in height corresponding to about 0.3 g were used in the experiments. The characteristics of raw willow wood, Cu-contaminated willow wood, and Ni-contaminated willow wood measured by CHNS and ICP-OES are shown in **Table 2.3**.

Figure 2.1. Photo of the prepared willow wood particles

Table 2.3. Element concentrations in biomass feedstock.

Sample	%				Total element concentrations (mg/kg)						
	C	H	O	N	Ca	K	Mg	Na	Si	Cu	Ni
Raw willow	48.8	5.9	43.8	0.6	4255	847	275	168	218	25	3

Willow+Cu	48.6	6.0	44.0	0.6	4125	764	163	135	142	5156	3
Willow+Ni	48.7	5.8	43.9	0.7	4172	699	174	149	157	22	5632

The elemental compositions (C, H, N, and S) of the samples (raw willow, impregnated willow, raw willow char, and impregnate willow char) were determined using an elemental analyzer (Flash 2000). The oxygen content was determined by mass balance. Besides, all samples were mineralized following a specific mineralization protocol and analyzed by inductively coupled plasma optical emission spectroscopy (ICP-OES, HORIBA Jobin Yvon ULTIMA-2) for determining inorganics. Additionally, a scanning electron microscopy (SEM) together with an energy dispersive X-ray analyzer (SEM-EDX, Hitachi S4800, Japan) was used to investigate the microstructure and elemental distribution on char samples. A Raman spectroscopy (Confocal Raman-AFM WITEC Alpha 300AR microscope equipped with a CCD camera detector) was used to determine the carbon structure of the chars. The surface area of char was measured by N_2 adsorption with the Brunauer-Emmett-Teller method (BET Tristar II 3020 Micromeritics).

2.2 Experimental setups and procedures

2.2.1 Experimental setups

The experimental setup for solar pyrolysis of biomass is depicted in **Figure 2.2** and **Figure 2.3**. The maximum power and flux density are about 1.5 kW and 12000 kW/m^2, respectively. It consists in a 25 m^2 flat heliostat, a down-facing parabolic mirror (2 m in diameter and 0.85 m focal length), and a pyrolysis system. The parabolic mirror illuminated by the reflected beam of the heliostat concentrates the solar radiation to the wood pellet set in a graphite crucible. The graphite crucible is set at the focus of solar furnace holding the biomass pellet. The solar reactor is composed of two main parts, a metallic vessel and a transparent Pyrex window. A water-cooled sample holder is assembled with the metallic vessel. This sample holder is moved in and out of the vessel to insert and extract the sample pellets. The window is equipped with a porthole to measure the pellet temperature with a solar-blind optical pyrometer (KLEIBER monochromatic operating at 5.2 µm). The reactor is

swept with an argon flow controlled by a mass flowmeter (Bronkhorst, EL-FLOW®). A shutter located between the heliostat and the parabola can adjust the incident radiation of the reflected solar beam with a Proportional–Integral–Derivative (PID) controller based on the measured sample temperature for reaching the target heating rate and temperature. The final opening angle and speed of shutter opening correspond to the temperature and heating rate control. A 3100 SYNGAS analyzer is employed to on-line monitor the oxygen content in the reactor.

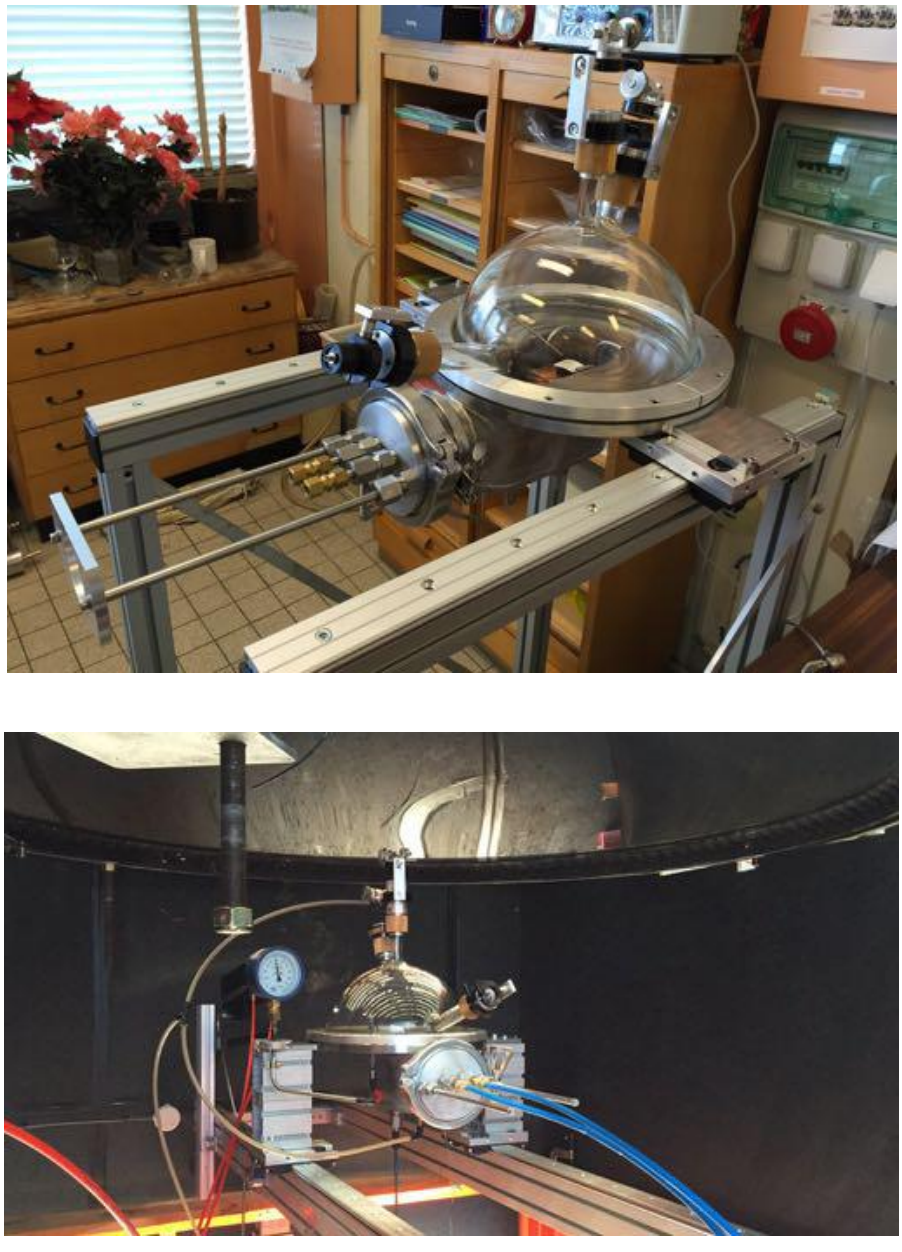

Figure 2.2. Photos of the solar pyrolysis reactor.

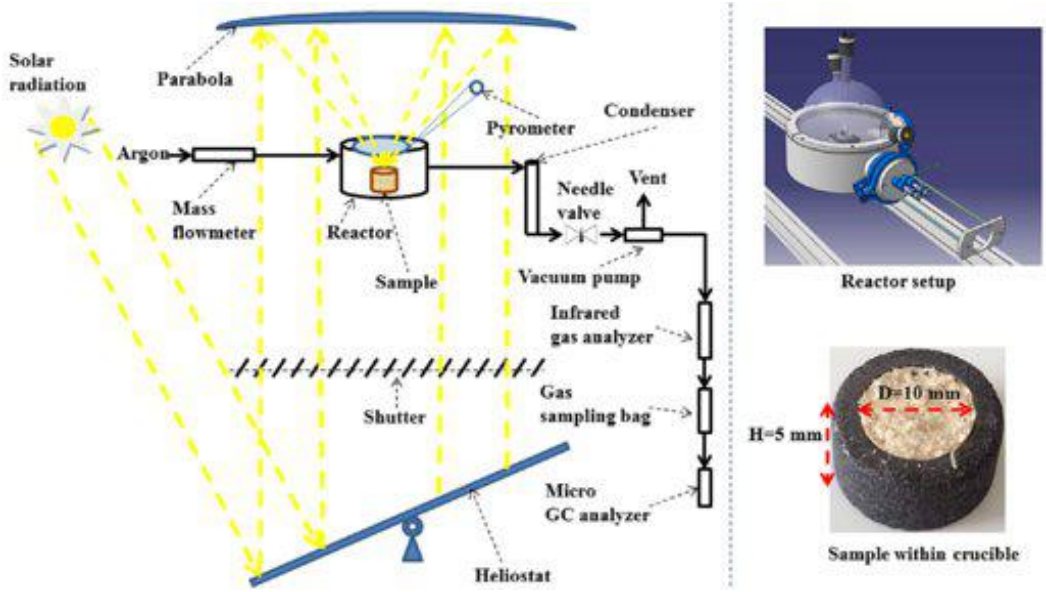

Figure 2.3. Schematic of the solar pyrolysis experimental setup

2.2.2 Experimental procedures

The reactor was swept by argon gas three times separated by a pumping step to eliminate all oxygen in the reactor. Then, the target temperature and heating rate were set on the PID controller for opening the shutter with the desired openness and speed. The shutter was open accordingly to start the pyrolysis. The solid residue resulting from solar pyrolysis regarded as char was cooled to the room temperature inside the crucible. The char was weighed for determining the yield and then stored in a desiccator for subsequent analyses. The pyrolysis gases were pumped out with a vacuum pump and passed through a condensation train for trapping liquid products. Finally, the gas products were collected in a sampling bag and then injected to gas chromatography (GC) (SRA Instruments MicroGC 3000) for further analysis.

Pyrolysis was performed for different temperatures (600, 800, 1000, 1200, 1400, 1600, 1800, and 2000°C) with different heating rates (10, 50, 150, and 450°C/s) under Argon (6, 7, or 9 NL/min flow rate). The duration of plateau temperature was around 4 min. Each

treatment was triplicated and the repeatability was satisfying. The difference between test data was always less than 5% relative.

2.3 Product analysis and calculation methods

For each experiment, the sample was weighted before and after pyrolysis to determine the mass of feedstock and char (the solid residue left in the crucible). The gas mass was calculated based on the Ideal Gas Law and the gas composition determined by micro-gas chromatography. Char and gas yields were calculated based on dry mass basis. The liquid yield was then obtained by difference from the mass balance. The lower heating value (LHV) of gas products was calculated based on the yield and LHVs of CO, H_2, CH_4, and C_2H_6. Finally, after each experiment, the reactor was cleaned by alcohol to eliminate any tar deposit on the walls. Each run was repeated at least 3 times for better accuracy, and the uncertainty on repeatability was always less than 5%.

2.3.1 Calculation of char yield

The mass of crucible and sample are measured before and after each experiment to improve the accuracy of the measurement. The char yields are calculated by **Equation 2.1**.

$$Y_{char} = \frac{m(cr+sp)' - m(cr)'}{m(cr+sp) - m(cr)} \times 100\% \qquad (2.1)$$

Where, Y_{char} is the char yield, $m(cr)$ and $m(cr)'$ are the masses of crucible before and after experiment, $m(cr+sp)$ is the mass of crucible filled with sample before experiment, and $m(cr+sp)'$ is the mass of crucible filled with produced char after experiment.

2.3.2 Calculation of gas yield

The syngas sampling is analyzed by a gas chromatography (SRA Instruments MicroGC

3000). The volume percentage of the syngas, including H_2, CO, CH_4, CO_2, and C_2H_6, is obtained. The gas yields are then calculated based on the Ideal Gas Law. The following demonstration shows the details to obtain **Equation 2.3**.

We assume that the collected syngas in the sampling bag has the same composition with the produced gas from the main exit.

According to the Ideal Gas Law,

$$PV = nRT$$

For example, if we are interested in H_2, we have,

$$P_{norm} \times v_{Ar} \times t \; = \; n(Ar) \times R \times T_{norm}$$

Where, P_{norm} is the normal pressure, v_{Ar} is the argon flow rate in Nm^3/min, t is the time of sampling collection in min, R is the Avogadro constant, T_{norm} is the normal temperature, and $n(Ar)$ is the argon content in mole.

In addition, according to the Ideal Gas Law, we have,

$$\frac{n(Ar)}{n(H_2)} = \frac{V(Ar)}{V(H_2)} = \frac{vp(Ar)}{vp(H_2)}$$

Where, $n(H_2)$ is the H_2 content in mole, $V(Ar)$ and $V(H_2)$ are the volume of argon and H_2, and $vp(Ar)$, and $vp(H_2)$ are the volume percentages measured by the GC.

From the above equations we can obtain,

$$n(H_2) = \frac{P_{norm} \times v_{Ar} \times t \times vp(H_2)}{R \times T_{norm} \times vp(Ar)} \qquad (2.2)$$

If we introduce,

$$m(H_2) = n(H_2) \times M(H_2)$$

Where, $m(H_2)$ is the mass of produced H_2, and $M(H_2)$ is the molecular weight of H_2.

We have,

$$m(H_2) = \frac{P_{norm} \times v_{Ar} \times t \times vp(H_2) \times M(H_2)}{R \times T_{norm} \times vp(Ar)}$$

With the same method, we can also obtain the masses of produced CO, CH_4, CO_2, and C_2H_6. The gas yield is then calculated by,

$$Y_{gas} = \frac{m(H_2) + m(CO) + m(CH_4) + m(CO_2) + m(C_2H_6)}{m_{sp}} \times 100\%$$

$$= \frac{P_{norm} \times v_{Ar} \times t \times [vp(H_2) \times M(H_2) + vp(CO) \times M(CO) + vp(CH_4) \times M(CH_4) + vp(CO_2) \times M(CO_2) + vp(C_2H_6) \times M(C_2H_6)]}{R \times T_{norm} \times s(Ar) \times m_{sp}}$$

(2.3)

Where, m_{sp} is the mass of biomass sample, $M(X)$ is the molecular weight, and $vp(X)$ is the volume percentage measured by the GC and,

$$vp(Ar) = 100\% - vp(H_2) - vp(CO) - vp(CH_4) - vp(CO_2) - vp(C_2H_6) - vp(O_2) - vp(N_2)$$

2.3.3 Calculation of specific gas composition

The specific gas composition (or volume fraction) is calculated with **Equation 2.2**, taking H_2 as an example.

$$s(H_2) = \frac{V(H_2)}{V(H_2) + V(CO) + V(CH_4) + V(CO_2) + V(C_2H_6)} \times 100\%$$

Where, $s(H_2)$ is the specific gas composition of H_2, and $V(X)$ is the volume of produced syngas.

According to the Ideal Gas law,

$$s(H_2) = \frac{n(H_2)}{n(H_2) + n(CO) + n(CH_4) + n(CO_2) + n(C_2H_6)}$$

If we introduce **Equation 2.2** for all the syngas, we can obtain,

$$s(H_2) = \frac{vp(H_2)}{vp(H_2) + vp(CO) + vp(CH_4) + vp(CO_2) + vp(C_2H_6)}$$

2.3.4 Calculation of tar yield

The tar yields in this study are obtained from mass balance,

$$Y_{Tar} = 100\% - Y_{char} - Y_{Gas}$$

Chapter 3

Pyrolysis of pine woods and wastes

3.1 Introduction

As it has been indicated in Chapter 1, none of the existing solar reactors for thermochemical conversion of carbonaceous materials permits the control of atmosphere composition and pressure. Moreover, the heating and cooling rates of the samples and the level and duration of the temperature plateau during the chemical transformation in a certain range of temperature are not well controlled in classical pyrolysis reactors. Normally, conventional pyrolysis is performed below 1000°C in flexibility-lacking reactors. Solar reactors have superior characteristics over the conventional ones because they offer a flexible heating temperature ranging from 600°C up to 2000°C and more, and a heating rate ranging from 5°C/s to more than 450°C/s, with a minimal energy cost. Therefore, a study on the effect of the very unique operating conditions produced by the concentrated solar

energy on the product compositions and properties is needed. In this chapter, the results of three pyrolysis campaigns are presented.

- Section 3.2 reports pyrolysis of pine wood and agricultural wastes. The effects of final temperature, heating rate, and lignocellulose composition on pyrolysis products are discussed.

Reference of the corresponding paper:

Li R, Zeng K, Soria J, Mazza G, Gauthier D, Rodriguez R, Flamant G. Product distribution from solar pyrolysis of agricultural and forestry biomass residues. Renewable Energy, 2016, 89: 27–35.

- **Section 3.3** describes pyrolysis of pine wood of different pellet sizes. It deals with the role of secondary tar reactions on the yields of char, gas, and tar, as well as gas compositions.

Reference of the corresponding paper:

Soria J, **Li R**, Flamant G, Mazza GD. Influence of pellet size on product yields and syngas composition during solar-driven high temperature fast pyrolysis of biomass. Journal of Analytical and Applied Pyrolysis, 2019, 140: 299–311.

- **Section 3.4** discusses the effects of different heating rates, temperatures, and biomass types on the pyrolysis product distribution and gas composition during the solar pyrolysis process of chicken litter and rice husk.

Reference of the corresponding paper:

Weldekidan H, Strezov V, **Li R**, Kan T, Town G, Kumar R, He J, Flamant G. Distribution of solar pyrolysis products and product gas composition produced from agricultural residues and animal wastes at different operating parameters. Renewable Energy, 2020, 151: 1102–1109.

3.2 Pyrolysis of pine wood and agricultural wastes

Four types of forestry and agricultural biomass by-products, i.e., pine sawdust, peach pit, grape stalk, and grape marc in powder, were subjected to fast pyrolysis in the lab-scale solar reactor presented in Chapter 2. The effect of final temperature (**Section 3.1.1.1**), heating rate (**Section 3.1.1.2**), and lignocellulose composition (**Section 3.1.1.3**) on the product yields and gas composition are discussed to address the pyrolysis of pine wood and agricultural wastes.

3.2.1 Effect of final temperature

Figure 3.1 presents the distribution of pyrolysis products as a function of the final temperature ranging from 800°C to 2000°C, with heating rate of 50°C/s, for the four types of biomass. At 50°C/s heating rate, higher final pyrolysis temperature results in higher gas yield and lower tar and char yields. For all types of biomass, the effect of temperature on the gas and tar yields is strong between 800°C and 1200°C, and then it levels. The decrease tendency is weaker for the tar yield. At 2000°C, the biomass composition has a little to no influence on the product distribution. The gas yields of pine sawdust and peach pit increase from 29.4% to 50.9% at temperatures between 800°C and 1200°C and slightly increase to 55.4% at 1600°C (**Figure 3.1a**). The highest gas yield of 63.5% is obtained from pine sawdust at the final temperature 2000°C, and gas yields for the other types of biomass are less than 10% lower only.

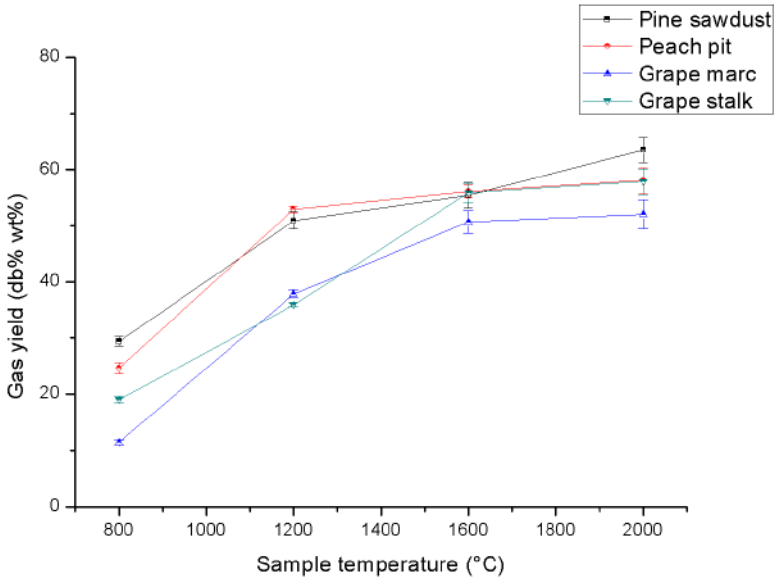
Pine sawdust
Peach pit
Grape marc
Grape stalk
Gas yield (db% wt%)
Sample temperature (°C)
0
20
40
60
80
800
1000
1200
1400
1600
1800
2000

(a)

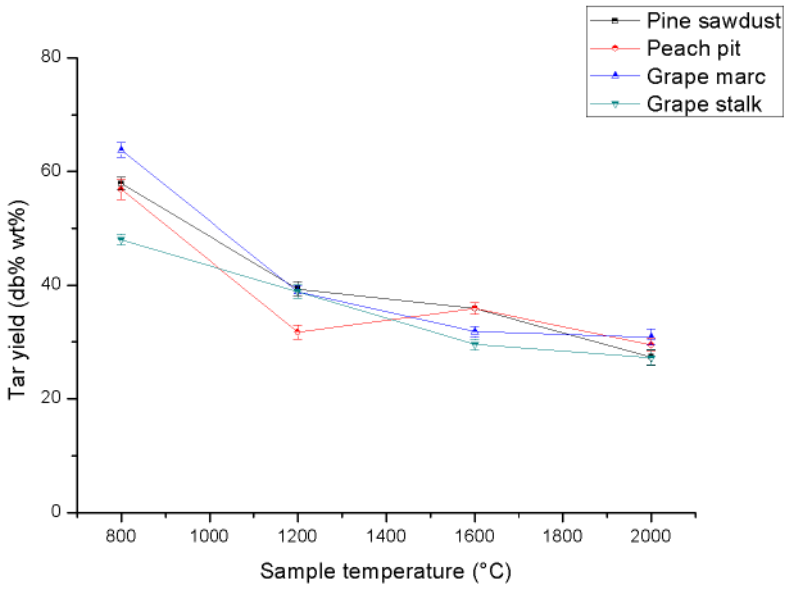
Pine sawdust
Peach pit
Grape marc
Grape stalk
Tar yield (db% wt%)
Sample temperature (°C)
0
20
40
60
80
800
1000
1200
1400
1600
1800
2000

(b)

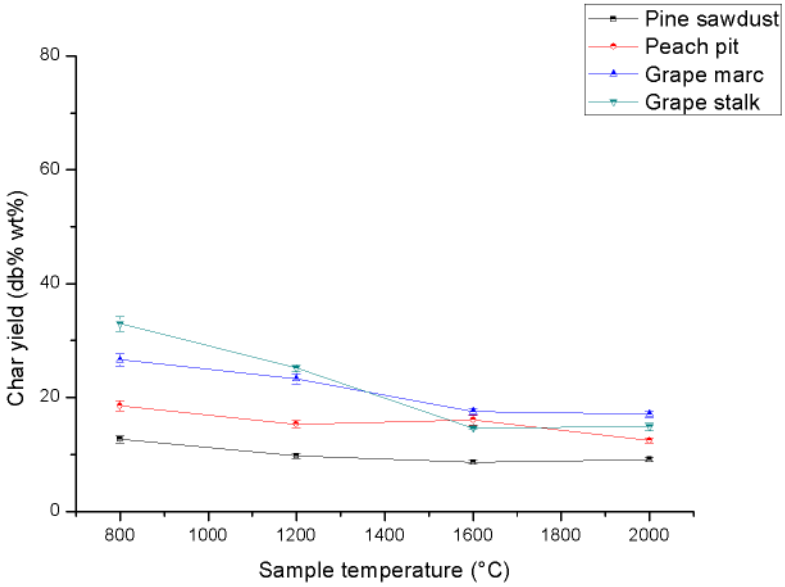

(c)

Figure 3.1. Effect of final temperature on product yields from biomass pyrolysis at heating rate 50°C/s. a: gas yield; b: tar yield; and c: char yield.

Figure 3.1b demonstrates that, at 50°C/s heating rate, the biomass composition has very little impact on the tar yield as soon as the biomass sample is pyrolyzed at temperature higher than 1200°C, and this impact is negligible at temperature above 1600°C. The increase in gas yield with temperature is due to the secondary tar cracking (Onay 2007). A high final temperature favors the tar secondary reactions into gas in the biomass pellet. Besides, a hot zone near the sample surface and considerable tar secondary reactions may occur. Numerous researches have investigated the effect of temperature on the product yields (Horne and Williams 1996; Williams and Besler 1996; Demirbas 2004a; Pütün et al. 2007; Garcia-Perez et al. 2008). At temperatures >800°C, the product distribution greatly depends on the tar secondary reactions. Tar secondary reactions are classified as homogeneous and heterogeneous, and they include such processes as cracking, partial oxidation, (re)polymerization etc. Condensation may also happen (Morf et al. 2002). These secondary reactions result in an extra tar decomposition and syngas formation. The pyrolysis reaction scheme is presented in **Figure 3.2** (Brigewater 2005). Fast pyrolysis proceeds through the primary and secondary reactions. The pellet increases intra-particle residence time of vapors.

High temperatures favor the gas production with the enhancing secondary reaction. This explains why the gas yields increase with the final temperature whereas the tar and char yields display an opposite trend (Brigewater 2005).

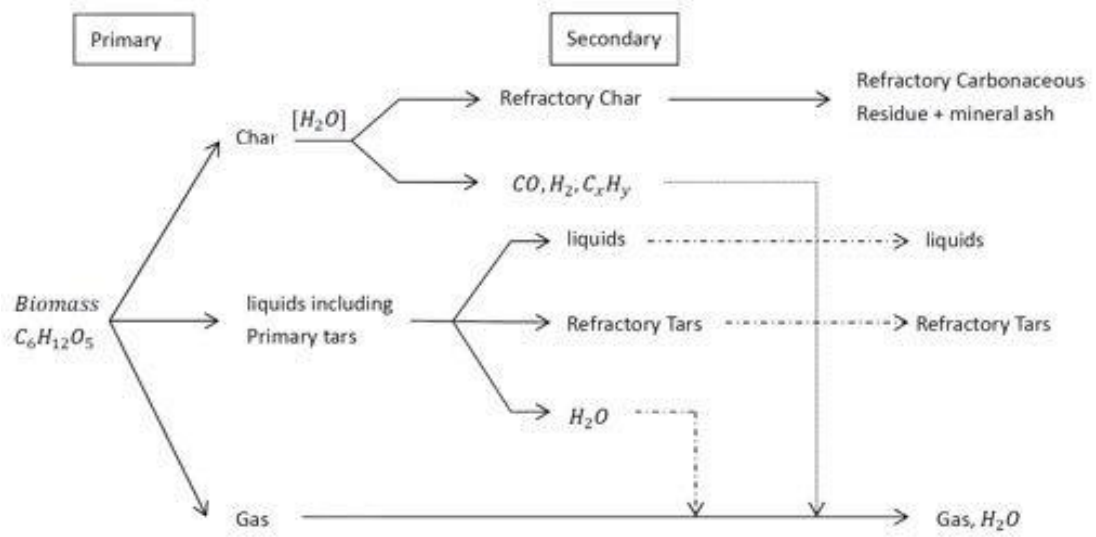

Figure 3.2. Pyrolysis reaction scheme (Brigewater 2005**)**

The effect of final temperature on the gas compositions issued from pyrolysis of the four types of biomass at the heating rate of 50°C/s is shown in **Figure 3.3**. Regardless the biomass type, CH_4, C_2H_6, and CO_2 contents decrease noticeably when the final pyrolysis temperature increase from 800 to 1200°C. Then, the trend is the same but the influence is weak. In all cases, the CO_2 plots confirm the occurrence of secondary reactions in gas phase. The contents of CH_4 and C_2H_6 decrease with temperature, since these molecules are not stable at temperature higher than 800°C and they are more and more cracked (Khan and Crynes 1970). For pine sawdust and peach pit, H_2 content increases deeply with temperature and CO content is almost not affected (**Figure 3.3a** and **3.3b**). Oppositely, CO content increases with the final temperature for grape marc and grape stalk, while H_2 content is not affected by the temperature (**Figure 3.3c** and **3.3d**). Finally, these two groups of biomass also differ strongly with respect to the H_2/CO ratio. For grape marc and grape stalk the H_2/CO ratio is always larger than 1 (1.3 and 1.2 at 1200°C, respectively), but less than 1 for

pine sawdust (almost equal to one at 1600°C only). It changes at about 1400°C for peach pit, less than one under 1400°C and almost equal to one above 1400°C. These opposite trends of the gaseous production (CO and H_2) of biomass solar pyrolysis are mainly due to the different lignocellulose contents (in particular cellulose) of the considered types of biomass.

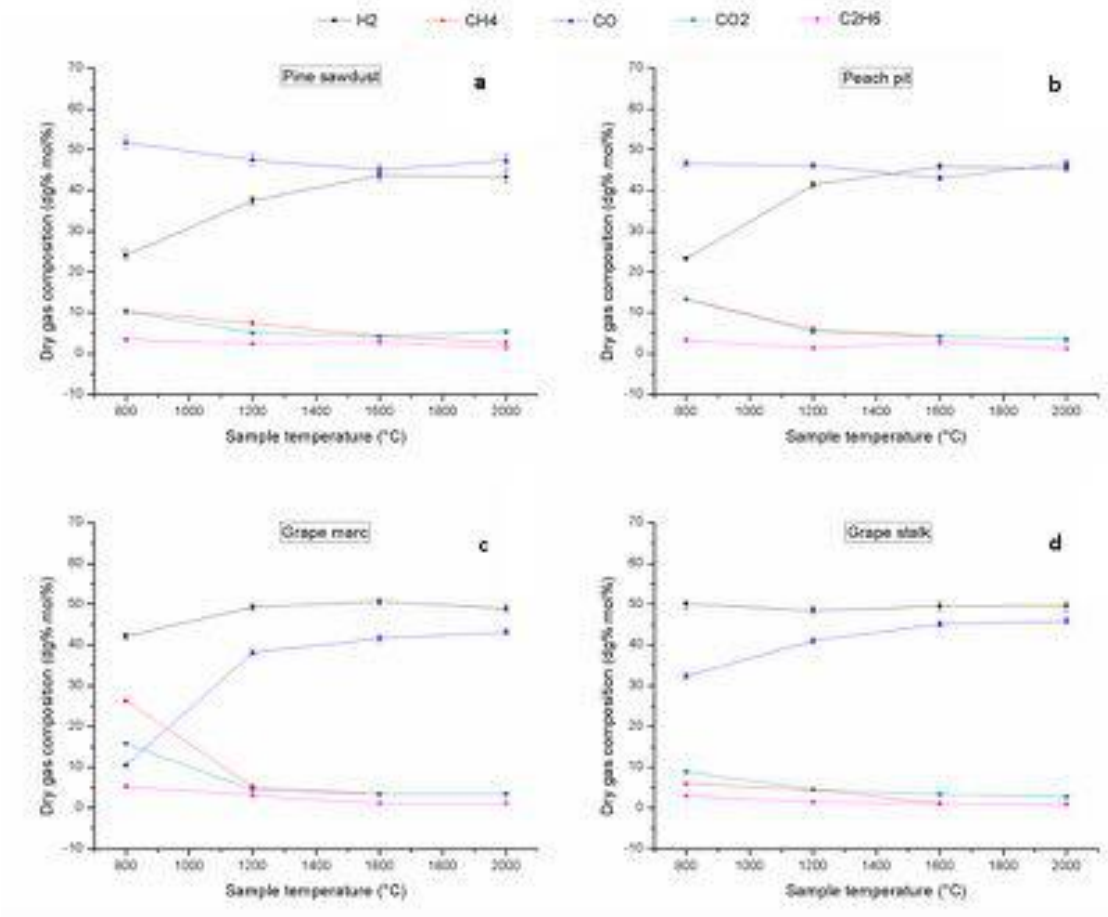

Figure 3.3. Effect of final temperature on dry gas composition from biomass pyrolysis at heating rate 50°C/s. a: pine sawdust; b: peach pit; c: grape marc; and d: grape stalk.

3.2.2 Effect of heating rate

Heating rate indicates the ability to heat the biomass particles, which influences the residence time of the volatiles in the hot zone. Earlier study has shown that higher heating rate is associated with shorter residence time (Gibbins-Mathame and Kandiyoti 1988). Since

the hot zone of this solar pyrolysis reactor is relatively small (Zeng et al. 2015a), the first effect induces the distribution of products. The gas yields increase with the heating rate (**Figure 3.4a**), while the tar yields decrease (**Figure 3.4b**), regardless of the biomass type. This is caused by the enhanced tar and char cracking reactions, resulting from the reduction in the heat and mass transfer limitations when the heating rate increases (Salehi et al. 2009). Once heat and mass transfer limitations are overcome, the liquid and gas yields stabilize with further increase in heating rate (Akhtar and Amin 2012), and the gas yield variation is not so strong when the heating rate is higher than 50°C/s. A relatively low heating rate can greatly favor the liquid production of solar pyrolysis (**Figure 3.4b**). The highest tar yield (65.3%) is obtained with pine sawdust pyrolyzed at the final temperature of 800°C and the heating rate of 10°C/s. For all biomass samples, the heating rate has very little influence and the char yield slightly reduces with the heating rate (**Figure 3.4c**). Nevertheless, the reduction of the tar residence time inside the sample with increasing heating rate may explain this decrease (Chhiti et al. 2012).

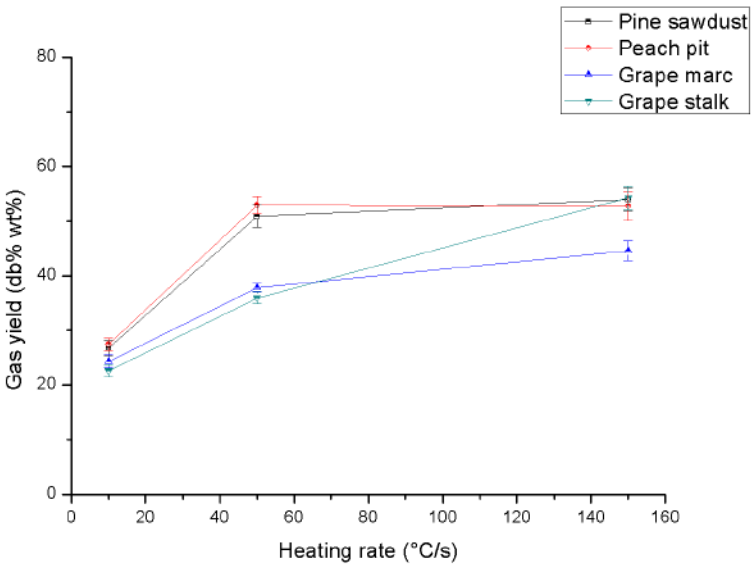

(a)

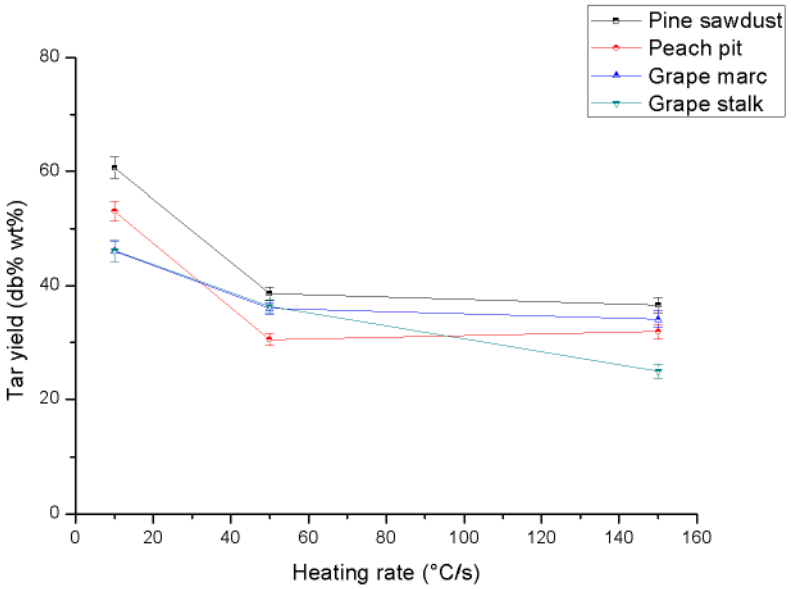

(b)

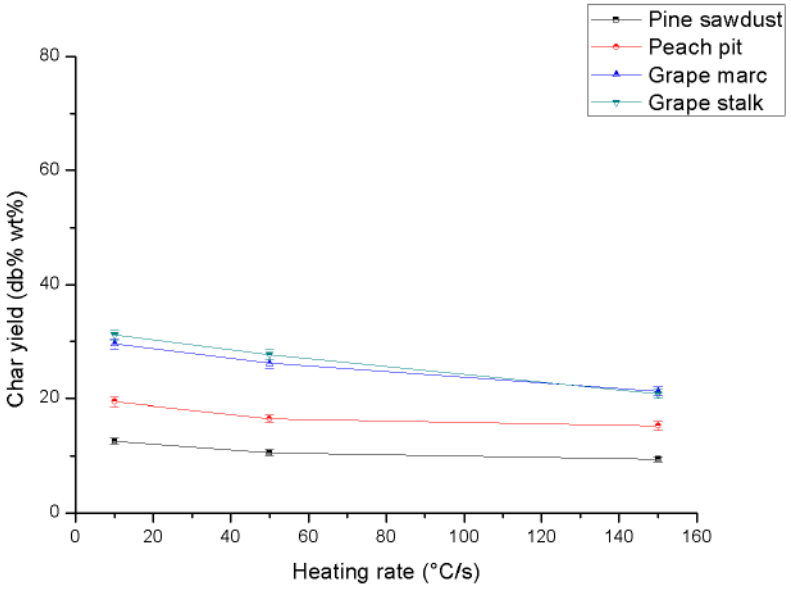

(c)

Figure 3.4. Effect of heating rate on product yields from biomass pyrolysis at final temperature 1200°C. a: gas yield; b: tar yield; and c: char yield.

Figure 3.5 demonstrates the influence of heating rate on the product gas composition. The gas composition clearly depends on the type of biomass and again the behavior of pine sawdust and peach pit differs from that of the grape by-products. Whereas the pyrolyzed grape by-products (both grape stalk and grape marc) produce about 50% H_2 and 35-42% CO regardless of the heating rate, the pine sawdust and peach pit pyrolysis produce more CO

(43-48%) than H_2 (30-40%). This means that the H_2/CO ratio is always greater than 1 for grape by-products but always smaller than 1 for pine sawdust and peach pit. For all types of biomass, the production of CO_2, CH_4, and C_2H_6 is much lower (0-10%) than that of H_2 and CO. It slightly decreases with increasing heating rate from 10°C/s to 50°C/s, and then, it remains stable. For all biomass wastes, the most obvious influence of heating rate on the gas composition is between 10 and 50°C/s. The gas composition remains relatively stable for higher heating rates. This result is in perfect agreement with previous results concerning the heating rate influence on the product yields.

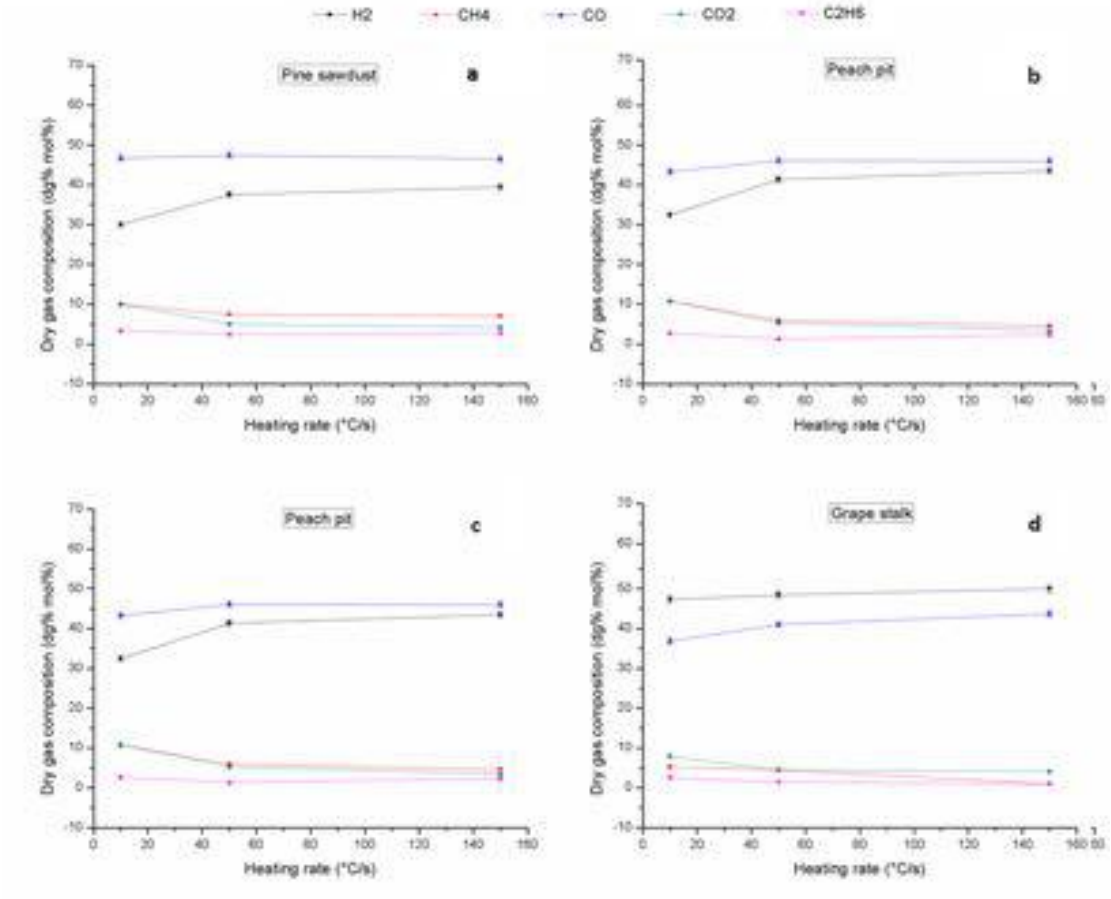

Figure 3.5. Effect of heating rate on dry gas composition from biomass pyrolysis at final temperature 1200°C. a: pine sawdust; b: peach pit; c: grape marc; and d: grape stalk.

3.2.3 Effect of lignocellulose composition

Taking the advantage of the various compositions in lignocelluloses for the four types of

waste biomass, the effect of lignin and cellulose contents on the pyrolysis product yields at final temperature of 1200°C and heating rate of 50°C/s was studied (**Figure 3.6**). The char and tar yields increase with the lignin content, whereas the gas yield decreases. Indeed, lignin pyrolysis produces more char than cellulose and hemicellulose pyrolysis. As shown before in **Figures 3. 1a** and **3. 1c**, both grape by-products, grape marc, and grape stalk, which contain more lignin than peach pit and pine sawdust, display higher char yields and lower gas yields when pyrolyzed. This result is in agreement with previous observation on the effect of lignin on liquid yields (Fahmi et al. 2008). Similarly, it was shown that higher hemicellulose content is associated with lower char and tar yields and higher gas yields: hemicellulose pyrolysis produces more volatiles, less char and tar than cellulose pyrolysis (Soltes et al. 1981).

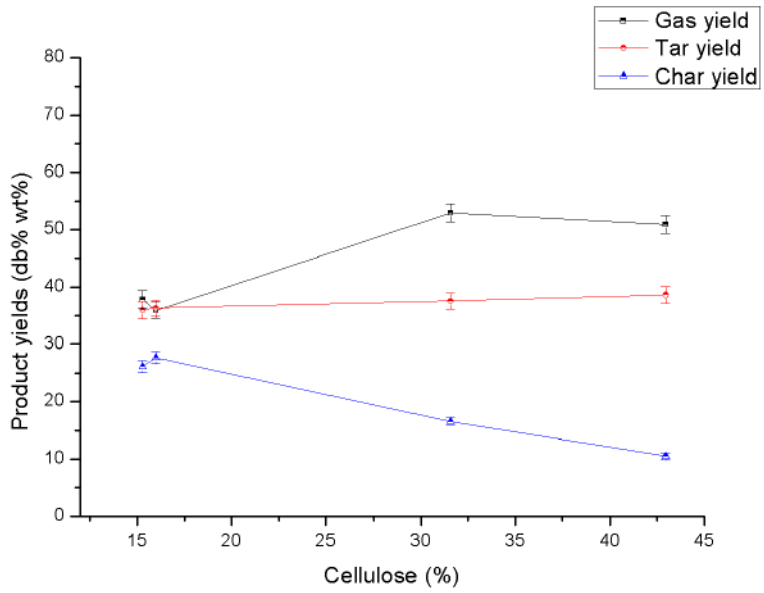

(a)

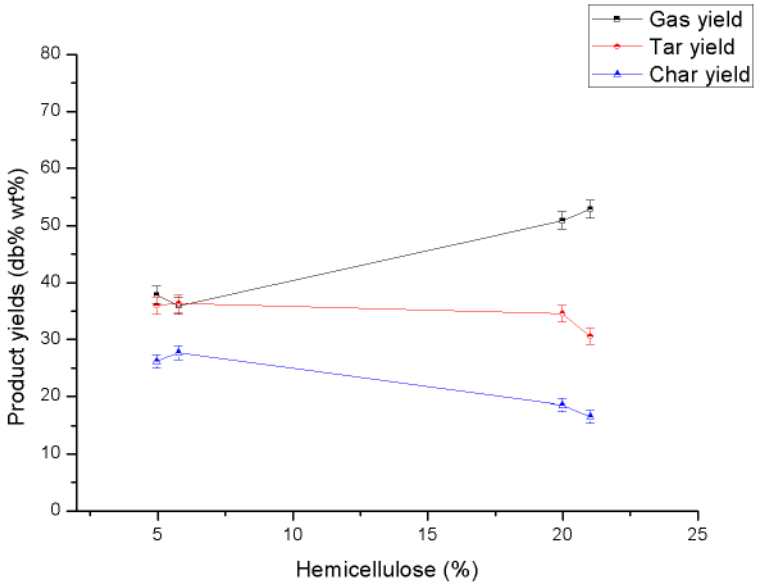

(b)

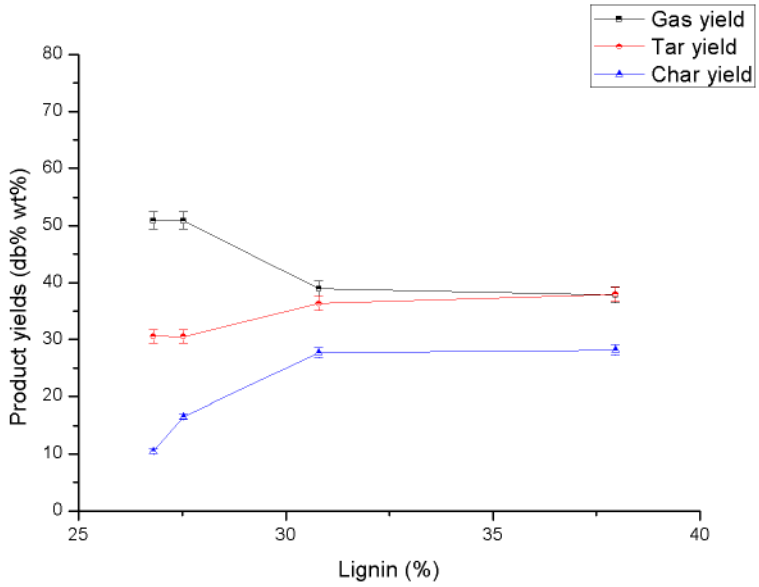

(c)

Figure 3.6. Effect of lignocelluloses on product yields from biomass pyrolysis at final temperature 1200°C and heating rate of 50°C/s. a: cellulose; b: hemicellulose; and c: lignin.

The effect of the biomass composition (lignocellulose components) on the pyrolysis produced gas composition is presented in **Figure 3.7**. It can be seen that CO production increases with the cellulose and hemicellulose contents, but decreases with the lignin

content. Oppositely, H_2 production decreases with the cellulose and hemicellulose contents, whilst increases with the lignin content. As a result, the H_2/CO ratio exceeds unity for the following composition: cellulose content smaller than 25 wt.%, hemicellulose content below 12% and lignin content in excess of 29%. This is mainly due to the lignin pyrolysis that forms more H_2 whereas cellulose and hemicellulose pyrolysis produces more CO and hydrocarbons.

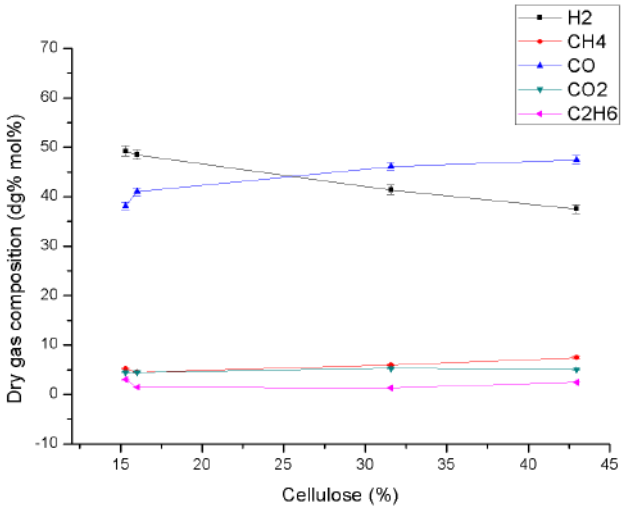

(a)

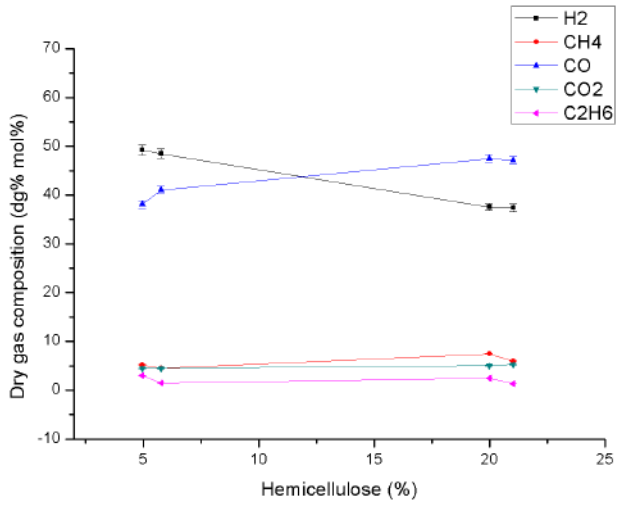

(b)

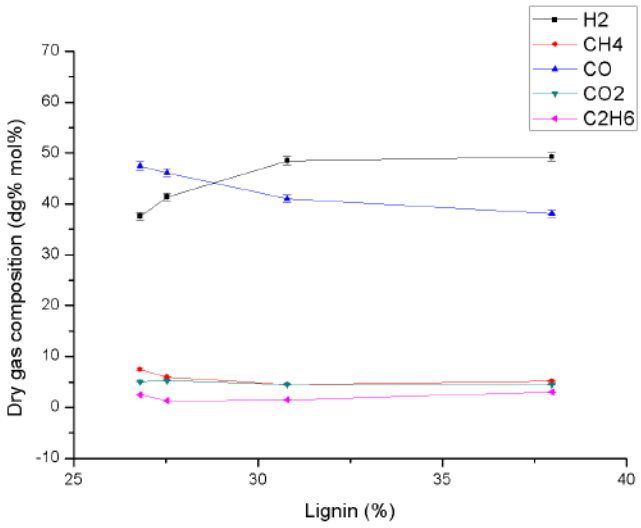

(c)

Figure 3.7. Effect of lignocelluloses on dry gas composition from biomass pyrolysis at final temperature 1200°C and heating rate of 50°C/s. a: cellulose; b: hemicellulose; and c: lignin.

3.2.4 Conclusion

Fast pyrolysis of the four types of agricultural and forestry biomass by-products was carried out in a lab-scale solar reactor to investigate the influences of final temperature, heating rate, and lignocellulose composition on the product yields and gas composition. It was shown that higher final temperature and heating rate favor the syngas production and the tar decomposition. The highest gas yield of 63.5 wt.% was obtained from pine sawdust at 2000°C and 50°C/s. Higher lignin content can enrich the char production, whereas higher cellulose and hemicellulose contents increase the gas yields. Contents of CO_2, CH_4, and C_2H_6 decrease with the pyrolysis final temperature. The CO content of the pyrolysis gas increases with the cellulose and hemicellulose contents, whereas the H_2 content increases with the lignin content. The H_2/CO ratio is always greater than one for both grape by-products, grape marc and grape stalk.

3.3 Pyrolysis of pine wood of different pellet sizes: the role of secondary tar reactions

Two types of pine sawdust pellets (5 and 10 mm in height, 10 mm in diameter) were used to study the effects of pellet sizes on pyrolysis products by determining characteristic times in **Section 3.3.1** and dimensionless numbers in **Section 3.3.2**. The effects of pellet sizes on yields of pyrolysis products, such as char, gas, and tar, are described in **Section 3.3.3**. In **Section 3.3.4**, the influences of pellet sizes on the main gaseous products are reported.

3.3.1. Characteristic times

The various characteristic times (in seconds) and dimensionless numbers, as well as the related data are shown in **Table 3.1**, where k_{py} is the pyrolysis kinetic constant, T is the temperature, R is the radius, ρ_p is the pellet density, C_p is the specific heat capacity, L_c is the characteristic length, L_0 is the initial pellet length, h is the global heat transfer coefficient, Φ is the incident flux, ΔT is the Characteristic temperature difference between the pellet surface and the surroundings, λ_{eff} is the effective thermal conductivity, μ is the volatiles viscosity, ΔP is the intra-particle over pressure, B is the permeability, and D_{eff} is the effective diffusivity.

Table 3.1. Thermo-physical properties for sawdust pellets, definition of the characteristic times and dimensionless numbers.

Properties	Reference
$\boldsymbol{k_{py} = 1 \cdot 10^8 \exp[-140000/RT]\ s^{-1}}$ (at 750K)	Chan et al. 1985
$\boldsymbol{\rho_p = 850\ kg/m^3}$	Measured
$\boldsymbol{C_p = 2300 - 1150exp(-0.0055T)\ J \cdot kg^{-1} \cdot K^{-1}}$	Blondeau et al. 2012
$\boldsymbol{L_c =}$ $\boldsymbol{L_0}$, m	Measured
$\boldsymbol{h = \Phi/\Delta T = 750 \sim 1100\ W \cdot m^{-2} \cdot K^{-1}}$	Estimated
$\boldsymbol{\lambda_{eff} = 0.255\ W \cdot m^{-1} \cdot K^{-1}}$	Okekunle et al. 2011
$\boldsymbol{\mu = 3 \cdot 10^{-5}\ kg \cdot m^{-1} \cdot s^{-1}}$	Shi et al. 2016
$\boldsymbol{\Delta P = 300}$ Pa	Shi et al. 2016, Soria et al. 2017
$\boldsymbol{B = 1 \cdot 10^{-12}\ m^2}$	Soria et al. 2017
$\boldsymbol{D_{eff} = 1 \cdot 10^{-5}\ m^2 s^{-1}}$	Shi et al. 2016
Phenomenon	**Characteristic time (s)**
Pyrolysis chemical kinetic, $\boldsymbol{t_{py}}$	$1/k_{py}$
External heat transfer, $\boldsymbol{t_{H,ext}}$	$\rho_p C_p L_c / h$
Internal heat transfer, $\boldsymbol{t_{H,int}}$	$\rho_p C_p L_C^2 / \lambda_{eff}$

Internal mass convection, $t_{M,conv}$	$\mu L_C^2/(\Delta P \cdot B)$
Internal mass diffusion, t_{diff}	L_C^2/D_{eff}
Dimensionless number	**Definition**
Pyrolysis number	$P_y = t_{py}/t_{H,int}$
Damköhler number	$D_a = t_{py}/t_{H,ext}$
Thermal Biot number	$Bi_T = t_{H,int}/t_{H,ext}$

The theory of characteristic time was adopted as the first approach to estimate the rate controlling mechanism. The characteristic time of a phenomenon is defined as the theoretical time needed for pyrolysis conversion when it is only controlled by the isolate individual phenomenon involved (Septien et al. 2012). It should be pointed out that during the pyrolysis process, the structure and thermo-physical properties of the solid (e.g., porosity, permeability, and density) will change. Therefore, these changes result in a certain variability and uncertainty in estimating the properties of the phases, particularly the solid properties, which influences the characteristic time scales (Authier et al. 2009). Consequently, only the order of magnitude of the characteristic time was taken into account. As the pellet is heated from the surface, the characteristic length corresponds to the initial pellet height ($L_c = L_0$). The global external heat transfer coefficient was estimated on the basis of calorimetric tests carried out, with the expression of $h = \Phi/\Delta T$, as proposed by previously (Christodoulou et al. 2013; Pozzobon et al. 2014; Pozzobon et al. 2018).

Table 3.2 shows the calculated characteristic times at 50°C/s heating rate. When the 5 mm pellet was pyrolyzed at the lowest temperature (800°C), the internal heat transfer time scale is around 3 times slower than t_{py}; while the external heat transfer time scale is approximately two orders of magnitude faster than the internal heat transfer time scale. An analysis from the Biot number (Bi) provides a better insight of the ratio between the corresponding time scales. The impact of internal heat transfer increases with the pellet height. When samples with both pellet heights were tested at temperature above 1200°C, the internal heat transfer ($t_{H,int}$) becomes the major limiting process, whereas the behavior can be considered as a thermal wave regime.

The 10 mm pellet presents a higher value of internal mass diffusion time than the 5 mm pellet (**Table 3.2**). Consequently, the intra-particle residence time of pyrolysis gas might be higher, leading to enhancement of tar secondary chemical reactions towards gas products.

Table 3.2. Characteristic time scales comparison for 50°C/s.

Phenomenon	800°C		1200°C		1600°C	
	5 mm	10 mm	5 mm	10 mm	5 mm	10 mm
t_{py}	$7{\cdot}10^{-2}$	$7{\cdot}10^{-2}$	$9{\cdot}10^{-4}$	$9{\cdot}10^{-4}$	$8{\cdot}10^{-5}$	$8{\cdot}10^{-5}$
$t_{H,ext}$	$4{\cdot}10^{1}$	$7{\cdot}10^{1}$	$1{\cdot}10^{1}$	$3{\cdot}10^{1}$	$1{\cdot}10^{1}$	$2{\cdot}10^{1}$
$t_{H,int}$	$2{\cdot}10^{2}$	$8{\cdot}10^{2}$	$2{\cdot}10^{2}$	$8{\cdot}10^{2}$	$2{\cdot}10^{2}$	$8{\cdot}10^{2}$
$t_{M,conv}$	$3{\cdot}10^{0}$	$8{\cdot}10^{0}$	$3{\cdot}10^{0}$	$8{\cdot}10^{0}$	$3{\cdot}10^{0}$	$8{\cdot}10^{0}$
t_{diff}	$3{\cdot}10^{0}$	$1{\cdot}10^{1}$	$3{\cdot}10^{0}$	$1{\cdot}10^{1}$	$3{\cdot}10^{0}$	$1{\cdot}10^{1}$

3.3.2. Dimensionless numbers

The definitions of the dimensionless numbers are presented in **Table 3.1**. The pyrolysis behavior is frequently described by means of the dimensionless numbers: the thermal Biot number (Bi_T), which relates the characteristic times for internal and external heat transfer processes; and the Pyrolysis number (P_y) that accounts for the ratio between kinetics and internal heat transfer characteristic times. The third relevant non-dimensional number is the Damköhler -*Da*- (or external Pyrolysis number, P_y'), which represents the ratio between the chemical kinetic mechanism and the external heat transfer process. Based on the values of Pyrolysis and thermal Biot numbers, four regimes can be defined (Bryden et al. 2002). The first one is known as *kinetically controlled pyrolysis*, where the rate of pyrolysis is determined exclusively by the chemical reactions. This regime is usually typical of very fine particles. Small particles (Bi_T< 0.2) are pyrolyzed under *thermally thin regime*. At this condition, the particle can be considered to have a uniform temperature profile and pyrolysis takes place in the whole particle domain at the same rate. Large particles are usually pyrolyzed in the "*thermally thick regime*" (0.2 <Bi_T< 10). In this regime, a temperature gradient appears and both the kinetics and the heat transfer may control the

pyrolysis. The last regime corresponds to the *thermal wave regime* (Bi_T> 10): a well-defined pyrolysis front (1–3 mm size) is developed as a result of the thermal wave, which travels from the surface towards the interior of the pellet at a nearly constant velocity (Bryden et al. 2002).

Table 3.3 provides the estimated dimensionless numbers for different conditions used in this study. The P_y is always lower than 0.001 (at the lowest temperature studied), indicating that kinetics play a negligible role as a rate-controlling phenomenon. A similar trend is observed for Damköhler number (Da or external Pyrolysis number P_y'). Thus, the pyrolysis process can be considered to be limited by heat transfer. The Bi_T for both pellets ranges from 3.6 to 36.7 (**Table 3.3**). Therefore, the process is considered to be limited by the external/internal heat transfer at the lower limit of experimental condition and essentially controlled by internal heat transfer at the highest temperature (Bryden et al. 2002). In both cases, an internal temperature gradient will be developed. Moreover, at the highest temperature, a pyrolysis front induced by the thermal gradient inside the pellet is expected.

On this basis, both pellets behave non-isothermally and pyrolysis is controlled by the convection and conductive heat transfer at 1200°C for the 5 mm pellet. Further increase in the final temperature causes the pellet to be pyrolyzed under the thermal wave regime. These results are in agreement with the Computational Fluid Dynamics (CFD) calculations (Soria et al. 2017).

Table 3.3. Comparison of dimensionless numbers.

Dimensionless	800°C		1200°C		1600°C	
number	5 mm	10 mm	5 mm	10 mm	5 mm	10 mm
Py (50°C/s)	$3.4 \cdot 10^{-4}$	$8.5 \cdot 10^{-5}$	$4.8 \cdot 10^{-6}$	$1.2 \cdot 10^{-6}$	$4.2 \cdot 10^{-7}$	$1.1 \cdot 10^{-7}$
Da (50°C/s)	$1.8 \cdot 10^{-3}$	$9.2 \cdot 10^{-4}$	$6.3 \cdot 10^{-5}$	$3.2 \cdot 10^{-5}$	$7.7 \cdot 10^{-6}$	$3.8 \cdot 10^{-6}$
Bi_T (10°C/s)	3.6	7.2	8.8	17.5	12.2	24.5
Bi_T (50°C/s)	5.4	10.7	13.2	26.3	18.3	36.7

3.3.3 Yields of pyrolysis products

Char, gas, and tar yields for pyrolysis in the temperatures range of 800-1600°C, two heating rates (10 and 50°C/s), and two pellet heights (5 and 10 mm) were measured and plotted in **Figures 3.8a-c**. The next three subsections show the analysis of the yields corresponding to the three phases produced during pyrolysis experimental runs.

3.3.3.1 Char yield

For each pellet and identical heating rate, the char yield diminishes as operating temperature increases (**Figures 3.8a**). This trend is in accordance with previous results (Demirbas 2004a). This behavior can be caused by the heavy hydrocarbon thermal cracking, which increases with temperature, yielding more volatiles at the expenses of char (Tripathi et al. 2016). In addition, higher temperatures favor heterogeneous secondary reactions, increasing tar and gas yield while decreasing the char yield. The influence of temperature on char yield tends to decrease as operating temperature increases.

On the other hand, for each pellet, the decrease in the heating rate at a given temperature causes the increase in the char yield (Okekunle et al. 2011; Iwasaki et al. 2014). Polymerization of cellulose towards volatile products is enhanced at high heating rates, thus diminishing the char yield (Demirbas 2004b). Furthermore, the influence of the heating rate on char yield is more important at the lowest temperatures, which is in good agreement with observations reported by Trubetskaya et al. (2015).

The char yield increases with pellet size (**Figures 3.8a**). The heating rate of the pellet decreases progressively as heat moves from the surface towards the interior of the pellet due to internal heat transfer resistance caused by the low effective thermal conductivity (Zeng et al. 2016; Soria et al. 2017). The non-uniform temperature profile inside the pellet cause a gradient of char yield in the pellet, where the lowest char yield will be produced at the surface of the pellet (corresponding to zone with the highest heating rate) and the highest char yield will occur at the bottom of the pellet (region of lowest heating rate). This

effect will be more important as pellet size increases. Therefore, the char yield is associated with the pellet height.

The char yield difference for both pellet sizes tends to decrease as temperature increases, i.e., 3.2% at 10°C/s and 800°C against -0.1% at 10°C/s and 1600°C. For heating rate 50°C/s, a similar difference in the char yield is obtained for both pellets at 800°C and 1200°C (1.7% and 1.8%, respectively), though the difference is reduced to only 1% at 1600°C. As temperature increases tar secondary reactions may produce more char. On the contrary, char may be consumed by gasification reactions. Then, at 1600°C and 50°C/s, a net consumption of char may occur that will lead to a similar value of char yield (**Figure 3.8a**).

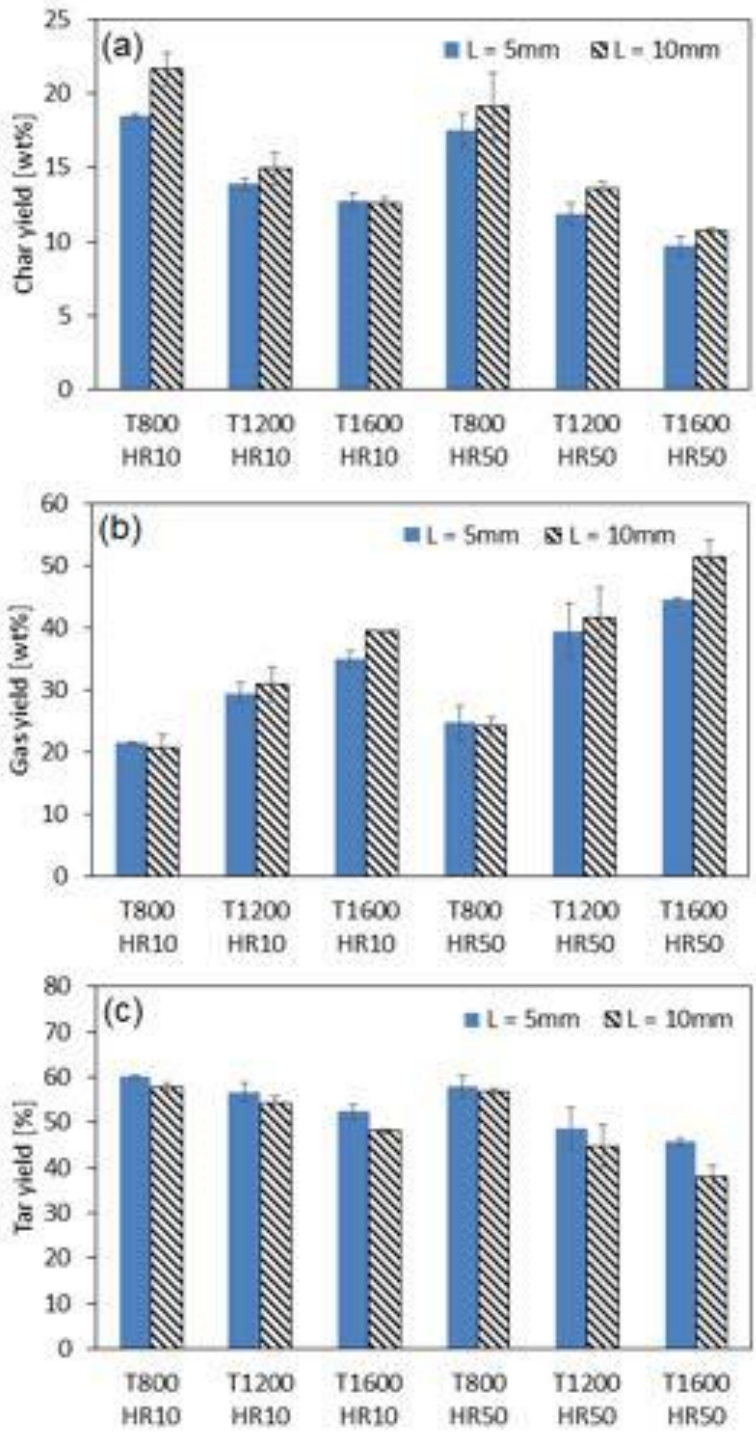

Figure 3.8. Product yields from solar pyrolysis. a: char; b: gas; and c: tar.

3.3.3.2 Gas yield

Regarding the gas yield, some observations can be derived from the results presented in **Figure 3.8b**. An increase in temperature results in more gas due to an enhancement in both

secondary cracking and gasification rates. This general trend of gas yield with temperature is in accordance with studies reported by Al Arni (2018). However, as temperature increases (above 1200°C), the gas yield still increases but at a lower rate, which may indicate that the influence of temperature could reach a plateau for higher temperatures.

Figure 3.8b also shows that an increase in the heating rate produces more gas. Moreover, the effect of the heating rate on the gas yield is more important as temperature increases. For both pellet sizes, the increment in gas yield, at 800°C and heating rate from 10°C/s to 50°C/s, is about 3%; while for the same heating rate change, the gas yield at 1200°C is around 10%. At 1600°C, the smaller pellet also presents a 10% increase from 10 to 50°C/s. The highest gas yield increase with heating rate is 12%, which is observed for the 10 mm pellet at 1600°C.

The influence of the pellet height can be analyzed when comparing the gas yield for both pellets (5 and 10 mm in height) at the same level of heating rate and temperature conditions. At the lowest surface temperature, smaller pellet yields more gas, although the differences are within the error bars. At 1200°C and 1600°C, the 10 mm pellet produces more gas than the 5 mm pellet, at both heating rates. At higher temperature, both homogeneous and heterogeneous secondary reaction and gasification reaction rates promote production of more non-condensable gas. Moreover, as the pellet height increases so does the thickness of the hot char layer as pyrolysis progresses together with the effectiveness of the heterogeneous reactions (Uddin et al. 2014). This description may also explain the fact that the maximum gas yield difference (6.8%) occurs at the highest surface temperature.

3.3.3.3 Tar yield

The total tar yield decreases with increasing temperature (**Figure 3.8c**). High temperature favors tar decomposition rate, yielding less tar. Besides, the influence of the temperature is more important at low temperature than at high temperature. At 50°C/s the tar cracking rate seems to decrease with temperature. This observation is not seen for the

case of 10°C/s, where the rate of decrease of tar yield with temperature remains constant at about 3%/°C for the 5 mm pellet.

It can also be seen that an increase in the heating rate reduces the tar yield. This observation is in agreement with results obtained by Okekunle et al. (2011). The lowest tar yield is measured at both the highest heating rate and temperature. This observation can be explained by the fact that the tar formed in the pellet must pass through the hot char layer formed at the top region of pellet, which has reached the final operating temperature rapidly due to the fast heating rate. Thus, the catalytic effect of char along with its thermal level causes the tar decomposition rate to increase, although intra-particle tar residence time diminishes with heating rate. Therefore, the tar yield will result from two competitive effects: (1) the lower residence time of tar given by the heating rate, and (2) the operating temperature that influences directly the intrinsic kinetics of tar reactions.

An increase in the pellet length may also reduce tar yield by secondary tar reactions. For similar operating conditions (heating rate 30°C/s and temperature 700°C) and particle size as used in this work, Okekunle et al. (2012) reported that tar yield decreases as the length increases, but a further length increase (above 5 mm) resulted in a tar yield plateau. Nonetheless, our results indicate that as temperature increases, the influence of pellet size on tar yield becomes more significant. It should also be pointed out that the pyrolysis experiments in that study were conducted at temperature <700°C, which is lower than that of the present work at temperature up to 1600°C at a higher heating rate (50°C/s).

3.3.4. Gas composition

The gas released during the biomass pyrolysis is composed of a mixture of H_2, CO, CO_2, and CH_4 and light hydrocarbons. The majority of gas is produced by thermal degradation of biomass components, i.e., cellulose, hemicellulose, and lignin. Gas yield can be increased by secondary tar reaction at high temperatures (both homogeneous and heterogeneous). In fact, secondary tar reactions involve many complex reactions which become significant at temperature levels above 600°C (Abnisa and Wan Daud 2014). In this context, the main

secondary reactions can be simplified by the set of reactions listed in **Table 3.4** (Soria et al. 2017).

Table 3.4. Main secondary tar reactions and gasification reactions (Soria et al. 2017).

Nº	Reaction name	Reaction	ΔH^0_{298K} (kJ/mol)
1	Primary pyrolysis	Biomass → Char + tar + CO + H_2 + CO_2 + CH_4 + H_2O	> 0
2	Tar cracking	Tar → $C_xH_yO_z$ + Char + CO + H_2 + CO_2 + CH_4 + H_2O + C_nH_m	> 0
3	Water-gas shift (secondary reaction)	CO + H_2O ↔ H_2 + CO_2	-41.2
4	Steam reforming: CH_4	CH_4 + H_2O ↔ $3H_2$ + CO	206.2
5	CO_2 reforming: CH_4	CH_4 + CO_2 ↔ 2CO + $2H_2$	258
6	Tar gasification	Tar + CO_2/H_2O → $C_xH_yO_z$ + Char + CO + H_2 + CO_2 + CH_4 + H_2O	> 0
7	Thermal cracking	C_nH_m ↔ $C_{n-x}H_{m-y}$ + H_2 + CH_4 + Char	> 0
8	Water gas (primary reaction)	C + H_2O ↔ CO + H_2	175
9	Boudouard	C + CO_2 ↔ 2CO	168
10	Hydrogenation	C + $2H_2$ ↔ CH_4	-74.9

Figure 3.9a and **b** depict the yields of main gaseous products (i.e., CO, H_2, CO_2, CH_4, and C_2H_6) for both 5 mm and 10 mm pellets, respectively, and compare the influence of temperature and heating rate on gas composition. Temperature significantly influences the gas composition, mostly through primary pyrolysis, char gasification, and secondary tar reactions (Luo et al. 2017), since these reactions are enhanced as temperature increases. Indeed, high final surface temperature favors considerably H_2 and CO generation, while the opposite tendency is observed for CO_2 where an increase in the surface temperature

reduces its molar yield. Demirbas (2009) reported the same trend for the pyrolysis of hazelnut shell, tea waste, and spruce wood.

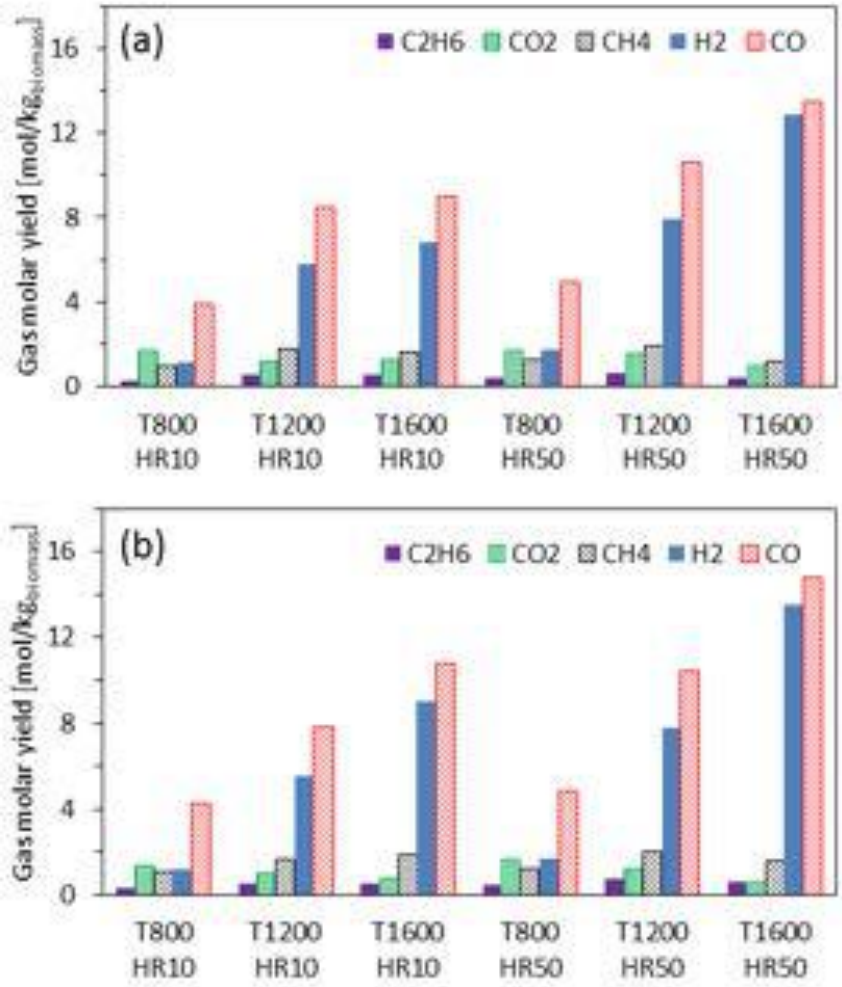

Figure 3.9. Gas product distribution from solar pyrolysis, influence of temperature and heating rate. a: 5 mm pellet; and b: 10 mm pellet.

When analyzing the influence of pellet size on gas composition, the H_2 and CO yields are very similar for both pellets at the two heating rates and temperatures of 800 and 1200°C (**Figure 3.10a** and **b**). Thus, pellet height seems to have no effect on the yields of H_2 and CO. However, at 1600°C the 10 mm pellet produces more H_2 than the 5 mm pellet at both heating rates. Thus, the influence of the pellet height on secondary tar reactions may increase with temperature. The effect of pellet size on CO_2 composition is more clearly

evidenced, an increase in the pellet height reduces the CO_2 yield, at all the operation conditions analyzed. In the case of the highest pellet, as the pyrolysis front moves towards the interior of the pellet, the CO_2 produced at the bottom of the pellet (due to primary pyrolysis reactions) flows through a more extensive char layer than in the case of the smallest pellet. Consequently, more CO_2 is consumed mainly by the Boudouard reaction. The influence of pellet height on C_2H_6 yield is more important at higher heating rates, as well as for CH_4.

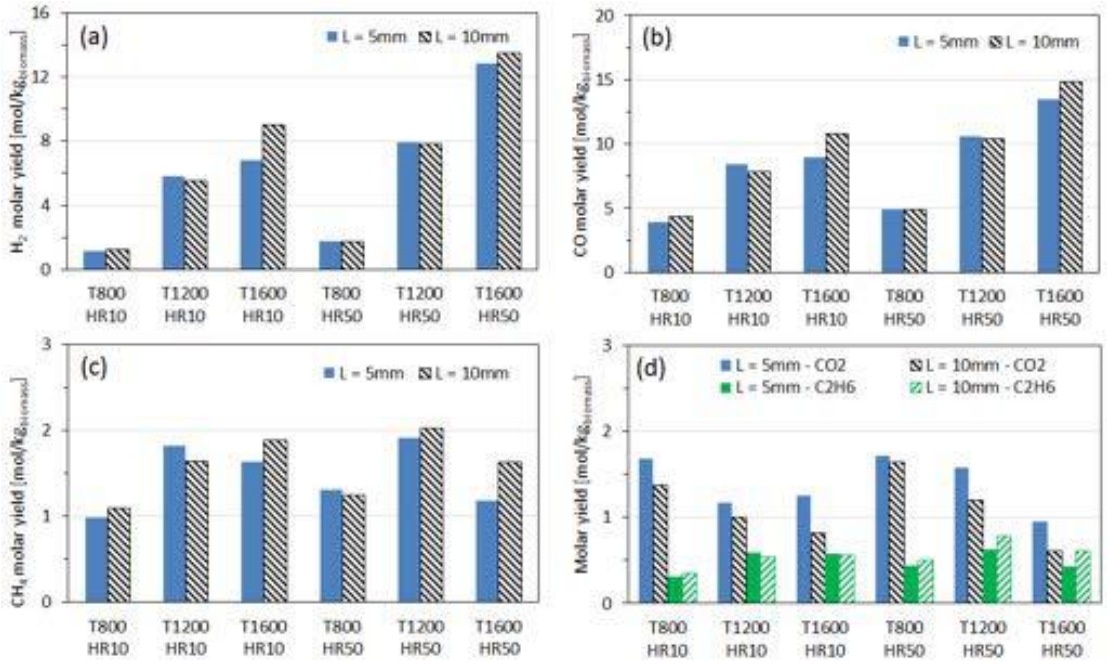

Figure 3.10. Gas product distribution, influence of pellet height. a: H_2; b: CO; c: CH_4; and d: CO_2 and C_2H_6.

3.3.5. Syngas quality analysis

Characterization of syngas quality is performed based on the parameters, such as syngas composition, H_2/CO ratio, CH_4/H_2 ratio, carbon conversion (X_C), and mechanical gas efficiency (MGE). Importantly, both H_2 and CO yields can be considered as an indicator of tar conversion degree (Morf et al. 2002). **Figure 3.11** shows the syngas molar composition in the gas phase for the three final surface temperatures, two heating rates, and two pellet heights. A comparative assessment demonstrates syngas fraction increases with both temperature

and heating rate. At a fixed heating rate and pellet size, raising temperature results in increase in the syngas composition (H_2 and CO), due to both primary pyrolysis and secondary tar reactions. Nonetheless, the syngas composition increases but at a lower rate for temperatures above 1200°C. For the high pellet samples, the syngas composition also decreases but at a higher rate.

Also, heating rate appears to affect significantly the syngas composition, especially at 1600°C. In fact, the optimal syngas composition is achieved at 50°C/s and 1600°C, with 91.1% and 90.8% at 5 mm and 10 mm pellet sizes, respectively. The effect of pellet size seems to be relevant at 10°C/s for which the increase in syngas composition is 3, 2.5, and 3.7% at 800, 1200, and 1600°C, respectively. However, results indicate that at 50°C/s, there is a negligible difference in the gas composition produced by both pellets.

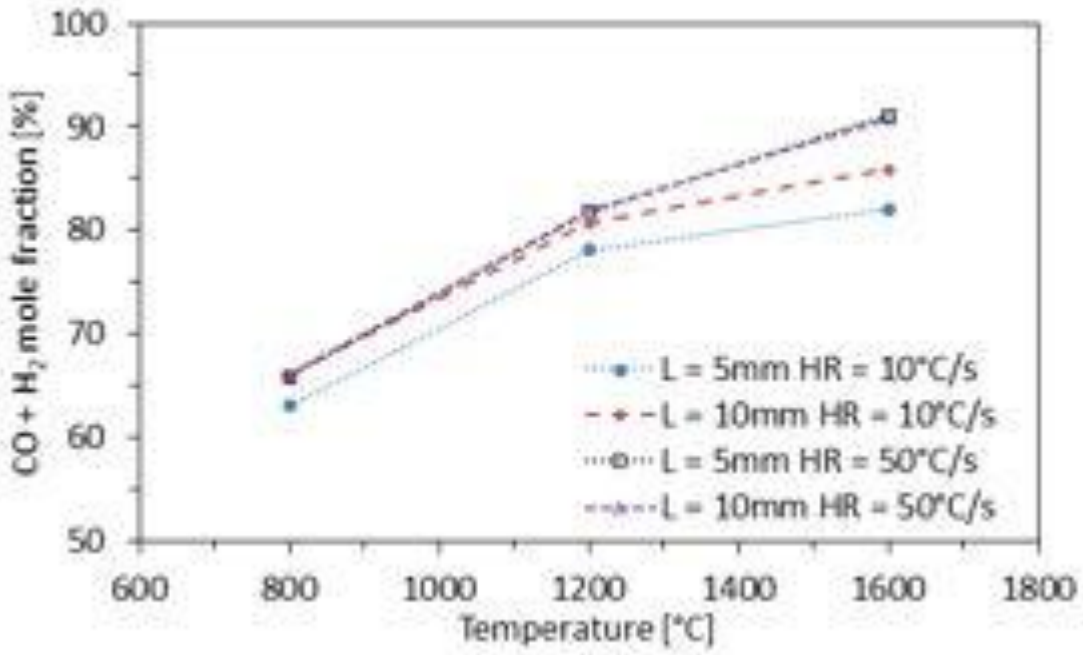

Figure 3.11. Molar composition of syngas (CO + H_2) in the gas product

The ratio of molar concentration between H_2 and CO is also analyzed as an indicator of syngas quality (**Figure 3.12a**). The lowest values of molar ratio range from 0.28 to 0.36 at the lowest temperature (800°C), while at 1600°C the range of ratio reaches 0.76-0.95. At each

final temperature, the lower values of H_2/CO ratio are obtained at 10°C/s, while the higher values correspond to 50°C/s. Therefore, the heating rate is associated with the syngas quality. At 10°C/s, the pellet height has a negligible influence at 800°C. At 1200°C and 10°C/s, the 10 mm pellet presents a higher H_2/CO ratio than the 5 mm pellet (0.71 vs 0.65). This difference remains similar with a rise in temperature (0.84 vs 0.76). At 50°C/s and 1200°C, the molar ratio is comparable for both pellets (0.75). At the same heating rate but with an increase in the final temperature, the highest pellet presents a lower value of H_2/CO ratio (0.88) in comparison with the 5 mm pellet (0.95).

Figure 3.12b depicts the molar ratio between CH_4 and H_2 in the syngas generated, where the general trend indicates the negative correlation between the temperature and this ratio. In fact, CH_4 production is favored at low temperature while hydrogen production increases at higher temperature. This result is in agreement with Al Arni (2018). The decrease in the concentration of CH_4 in the syngas can be explained on the basis of Le Chatelier's principle. With an increase in temperature, both endothermic reaction methane steam reforming and methane CO_2 reforming will shift the equilibrium towards the product generation, while the exothermic hydrogenation reaction will shift to the reactant side, thus reducing the composition of CH_4 in the syngas (Yao et al. 2017). Heating rate seems to have a considerable effect on the CH_4/H_2 ratio. An increase in the heating rate reduces the ratio. However, the molar ratio seems to be quite insensitive to the pellet size at the operating conditions adopted in this study. A slight difference can be seen at 10°C/s and 1200°C, whereas the highest pellet produces the lowest molar ratio.

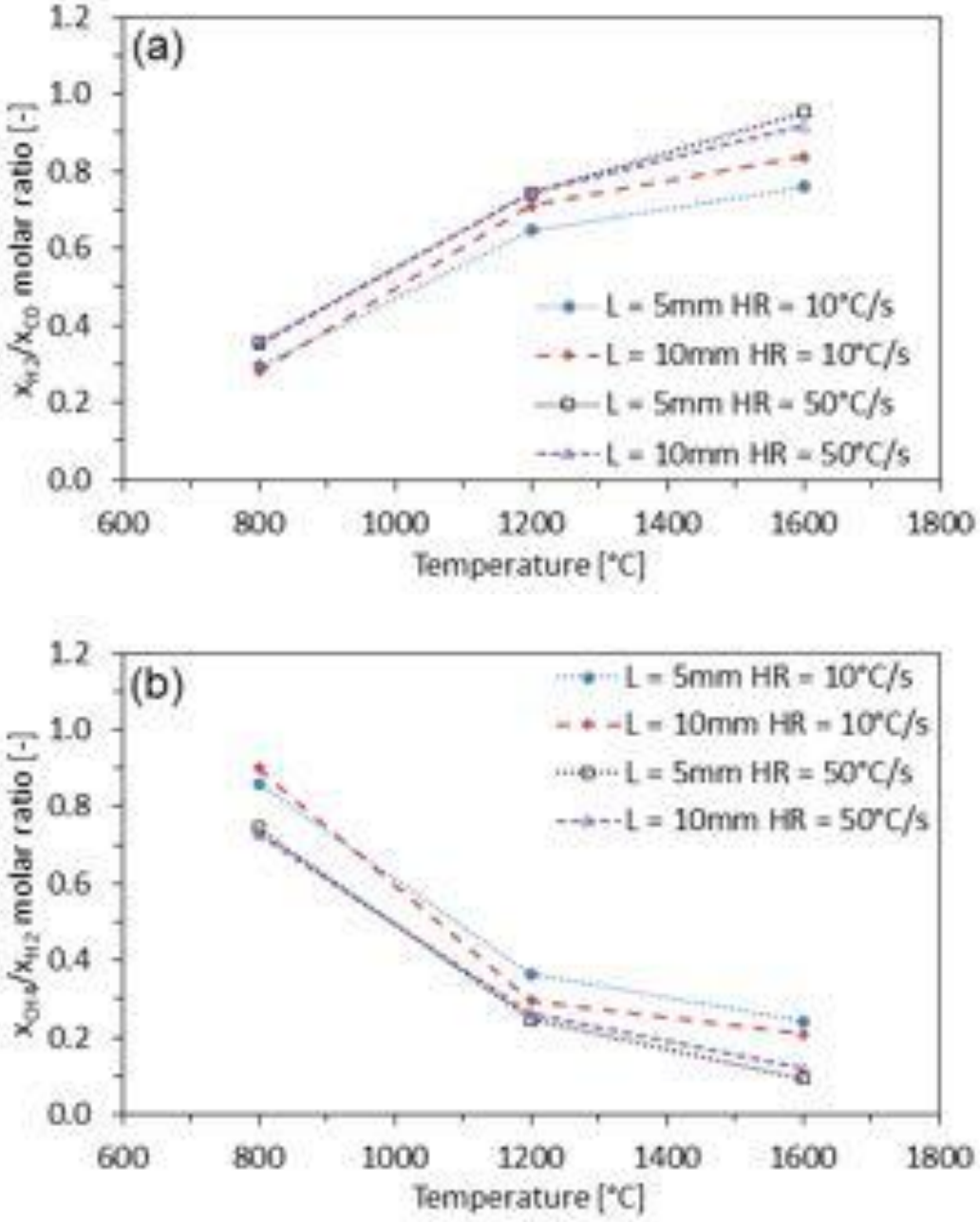

Figure 3.12. Influence of operating conditions and pellet size on H_2/CO (a) and CH_4/H_2 ratios (b) in syngas

3.3.6. Pyrolysis gas energy performance

The Mechanical Gas Efficiency (MGE) is defined as the ratio of the produced syngas LHV ($MJ/kg_{biomass}$) over the heating value of the biomass feedstock (pine sawdust pellet). Thus, the MGE can be written as follows:

$$MGE = \frac{LHV_{gas}}{LHV_{biomass}} \times 100\% \quad (3.1)$$

Where, the LHV of the produced syngas is estimated based on the following equation:

$$LHV_{gas} = \left(x_{CO} \times 126.36 + x_{H_2} \times 107.98 + x_{CH_4} \times 358.8 + x_{C_2H_6} \times 629.09\right) \times 10^{-3} \times V_{syngas}/m_{biomass} \quad (3.2)$$

Therefore, the resulting values of MGE will follow the behavior of LHV. Additionally, the carbon conversion efficiency (X_C) is calculated based on the mass percentage of carbon in ultimate analysis of the sample (C%), the molar percentages of the main gas species (CO, CO_2, CH_4, and C_2H_6), and the gas product yield ($V_{syngas}/m_{biomass}$). The expression can be written as follows:

$$X_C = \left[\frac{12 \times (V_{syngas}/m_{biomass}) \times (x_{CO} + x_{CO_2} + x_{CH_4} + 2x_{C_2H_6})}{22.4 \times C\%}\right] \times 100\% \quad (3.3)$$

The main results regarding these three parameters are presented in **Table 3.5**.

Table 3.5. Influence of operating condition and pellet height on LHV, MGE, and X_C.

HR	T	LHV (MJ/kg)			MGE (%)			X_C (%)		
(°C/s)	(°C)	5 mm*	10 mm	ΔL	5 mm	10 mm	ΔL	5 mm	10 mm	ΔL
10	800	2.65	2.81	0.16	14.37	15.26	0.89	17.19	17.23	0.04
10	1200	5.34	5.52	0.18	28.92	29.91	0.99	26.25	26.63	0.37
10	1600	6.08	7.39	1.31	32.95	40.03	7.09	29.48	33.72	4.24
50	800	3.41	3.42	0.01	18.48	18.56	0.08	20.35	20.15	-0.20
50	1200	6.72	7.61	0.89	36.41	41.23	4.82	33.09	36.06	2.97
50	1600	7.91	9.69	1.78	42.89	52.52	9.63	36.24	43.27	7.02

3.3.6.1 Effect of temperature on LHV and carbon conversion efficiency

A significant variation in the LHV with temperature is clearly evidenced, which follows the change in the gas composition. The LHV of the gas product increases with temperature (Neves et al. 2011). The increase of LHV is the consequence of the rapid increase in CO and H_2 concentrations. Even though the CH_4 molar fraction decreases with temperature, which may cause the LHV to diminish, its amount does not influence the LHV of syngas. The lowest LHV of the gas product was obtained at the lowest temperature (2.7-2.8 MJ/kg of biomass, for the 5 mm and 10 mm pellets, respectively), while the highest LHV for the gas was achieved at 1600°C (7.9-10.0 MJ/kg of biomass).

The carbon conversion efficiency reflects also directly the increase in the gas yield with temperature (**Table 3.5**). In the case of the 5 mm pellet, the rate of increase in the X_C with temperature is slower than for the 10 mm pellet. This is because the secondary tar reactions that leads to CO are favored as temperature increases.

3.3.6.2. Effect of heating rate on LHV and carbon conversion efficiency

Table 3.5 shows that the LHV of gas increases with heating rate. This can be explained by the significant influence of rapid heating rate on intra-particle secondary cellulose tar cracking to H_2 and CO yields (Uddin et al. 2014). Moreover, the influence of the heating rate is more evident at higher temperature. Thus, at 1600°C and 50°C/s the maximum value of LHV, for each pellet size, is achieved (7.9 and 9.7 KJ/kg of wood).

When comparing X_C at different heating rates (**Table 3.5**), with a fixed temperature and pellet height, it can be seen that heating rate has a considerable effect on the carbon conversion. In fact, at the lowest temperature, an increase in the heating rate from 10 to 50°C/s increases the X_C from 17 to 20%. For the case of the 5 mm pellet, the increase in the carbon conversion efficiency is around 7% at 1200°C and 1600°C; while for the pyrolysis of the 10 mm pellet, an increase of around 10% is observed as the heating rate shifts from 10 to 50°C/s. Thus, it can be suggested that the influence of the rise in the heating rate is more

significant at temperatures above 1200°C, and higher heating rates may lead to higher values of carbon conversion.

3.3.6.3. Effect of pellet size on LHV, MGE, and carbon conversion efficiency

Table 3.5 indicates that the LHV is relatively independent on the pellet size at the lowest surface temperature, with a difference of 0.16 and 0.01 MJ/kg for 10°C/s and 50°C/s, respectively. At 1200°C and 10°C/s, the LHV is insensitive to the pellet size, while at 1200°C and 50°C/s the influence of the pellet size becomes significant. As the temperature increases, the influence of the pellet size is evidenced. Indeed, at 1600°C, the increment in the gas LHV produced by the higher pellet is 1.31 MJ/kg of wood and 1.78 MJ/kg of wood at 10 and 50°C/s, respectively. These results are considered to be linked to the combined effect of high temperature, high heating rate, and high pellet size that favors simultaneously generation of tar cracking, and H_2, and CO.

The influence of the pellet height on carbon conversion can be analyzed from **Table 3.5**. At 10°C/s, carbon conversion efficiency is very similar for both pellets, except at the highest temperature level, where the 10 mm pellet presents an X_C higher (33.7%) than the 5 mm pellet (29.5%). However, at 50°C/s, the influence of the pellet size becomes significant at lower temperature (1200°C). Moreover, the highest values of X_C for the 5 mm and 10 mm pellets are obtained at 1600°C and 50°C/s, corresponding to 36.2% and 43.3%, respectively. Consequently, it can be concluded that 10 mm pellet along with high surface temperature and rapid heating rates are desirable to achieve secondary tar cracking and increase both yield and quality of syngas.

3.3.7 Conclusion

We carried out experimental tests regarding the combined influence of pellet size, temperature, and heating rate during solar fast pyrogasification (high temperature fast

pyrolysis). Firstly, a characteristic time analysis, as well as a dimensionless number analysis, was performed in order to estimate the controlling mechanisms during the solar pyrolysis of sawdust biomass pellets. Results indicate that for temperatures lower than 1200°C, the pyrolysis rate is controlled by heat transfer (thermally thick regime), while the thermal wave regime occurs for temperatures above 1200°C.

Secondly, product yields (gas, tar, and char), as well as main permanent gas product composition (H_2, CO, CO_2, CH_4, and C_2H_6), were studied based on the influence of both primary and secondary reactions during the pyrolysis process. Results evidenced that product yields result from the competition between both main operating variables, temperature, and heating rate. A higher heating rate causes the gas product to form rapidly, which increases the intra-particle pressure gradient and expels the gas out of the surface, diminishing the gas intra-particle residence time and, therefore, reducing tar cracking. The char layer formed at the particle surface is at a higher temperature than the interior, thus favoring tar cracking. The influence of the pellet size on the gas yield and gas species yield is more important when operating at the highest temperature.

Additionally, the syngas quality was analyzed by considering several parameters, such as H_2/CO, CH_4/H_2, LHV, and X_C. The influence of pellet height on H_2/CO molar ratio seems to be more important at 10°C/s. A further increase in the heating rate reduces the effect of pellet size. Similarly, the LHV increases with temperature and heating rate, as well as with pellet size, although the influence of the latter is more relevant at the highest operating conditions. A similar observation can be carried out when analyzing the carbon conversion efficiency. Finally, it can be considered that, in order to improve the quality of the syngas, the fast pyrogasification (high temperature fast pyrolysis) of large particles is convenient.

3.4 Pyrolysis of chicken-litter and rice husk

This work investigates the effects of different heating rates (10 to 500°C/s) (**Section 3.4.1**), temperature in the range from 800 to 1600°C (**Section 3.4.2**), and biomass type and

particle size (**Section 3.4.3**) on the product distribution and gas composition during the solar pyrolysis process. Chicken-litter and rice husk were used as the materials in the pyrolysis experiments. Product yield, gas composition, and the higher heating value (HHV) of the gases produced are thoroughly studied with respect to each pyrolysis parameters.

3.4.1 Influence of heating rate on product distribution and gas composition

Figure 3.13 shows the product distribution obtained from the pyrolysis of chicken-litter waste (280 μm particle size) at final temperature of 1200°C and heating rates of 10, 50, 200, and 500°C/s. When the heating rate increases from 10 to 50°C/s, the bio-oil and char yields slightly decrease from 52.7 and 29.2 wt.% to 47.0 and 28.1 wt.%, respectively, while the gas yield increases significantly from 18.1 to 25.3 wt.%. This is possibly explained by the enhancement of the secondary cracking reactions and the increase of the depolymerization rate of char and bio-oil to primary volatiles resulting from the increasing heating rates (Chen et al. 1997). Rising the heating rate to 200°C/s slightly reduces the char and bio-oil yields to 45.4 and 27.5 wt.%, respectively, while the gas yield increases to 27.1 wt.%. Further increase in the heating rate to 500°C/s slowly decreases the liquid yield to 39.7 wt.% and increases the gas yield to 34.2 wt.%. These changes could be attributed to the reduced heat and mass transfer limitation caused by the fast heating rates (Uzun et al. 2010).

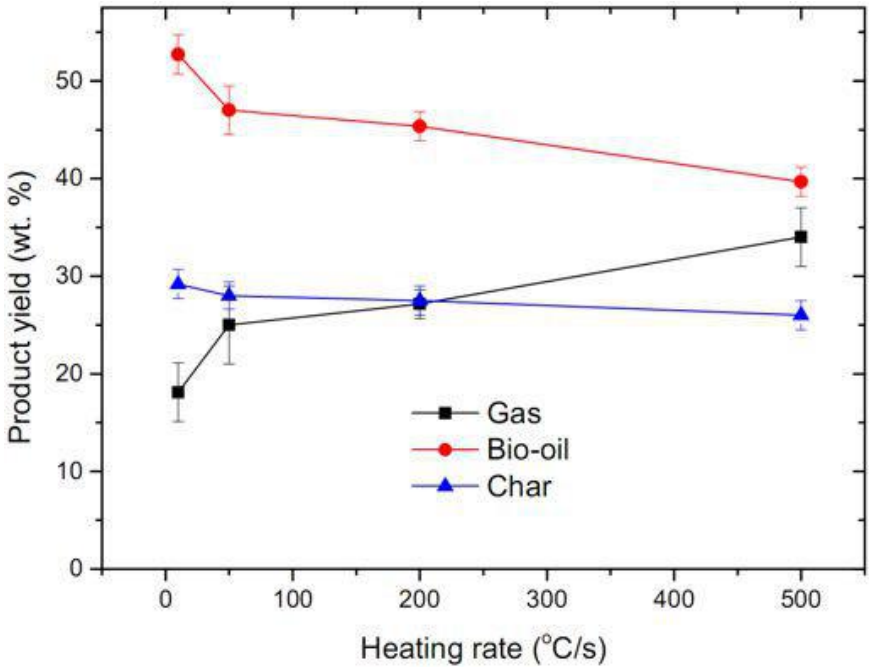

Figure 3.13. Product yields of chicken-litter waste pyrolysis formed at different heating rates to final temperature of 1200°C

The pyrolysis gas composition of the chicken-litter waste at different heating rates is depicted in **Figure 3.14**. The results demonstrate that CO, H_2, and CH_4 are the main gas components throughout the process. It is observed that the CO and H_2 contents substantially increase from 31.5 to 42.3%, and from 29.0 to 37.6%, respectively, when the heating rate increases from 10 to 50°C/s (**Figure 3.14**). On the contrary, the CH_4 production remarkably decreases from 23.6 to 9.1%. Meanwhile, the CO_2 and C_2H_6 contents are observed to slightly decrease from 11.4 to 10.2% and from 4.5 to 1.5%, respectively. The substantial increase in CO and H_2 with rise in the heating rate suggests that a rapid heating during the pyrolysis process enhances the secondary cracking of oxygenates and promotes the decarbonylation reactions to release CO gas. High concentration of CH_4 at 10°C/s, which eventually decreases to its minimum value of 5.7% at 500°C/s, is caused by the water shift and steam reforming reactions. These types of reactions have been previously shown to be at equilibrium between 800 and 1200°C but at longer residence time or lower heating rates (Newalkar et al. 2014). A further increase in the heating rate to 200 and 500°C/s does not bring significant difference to the gas composition.

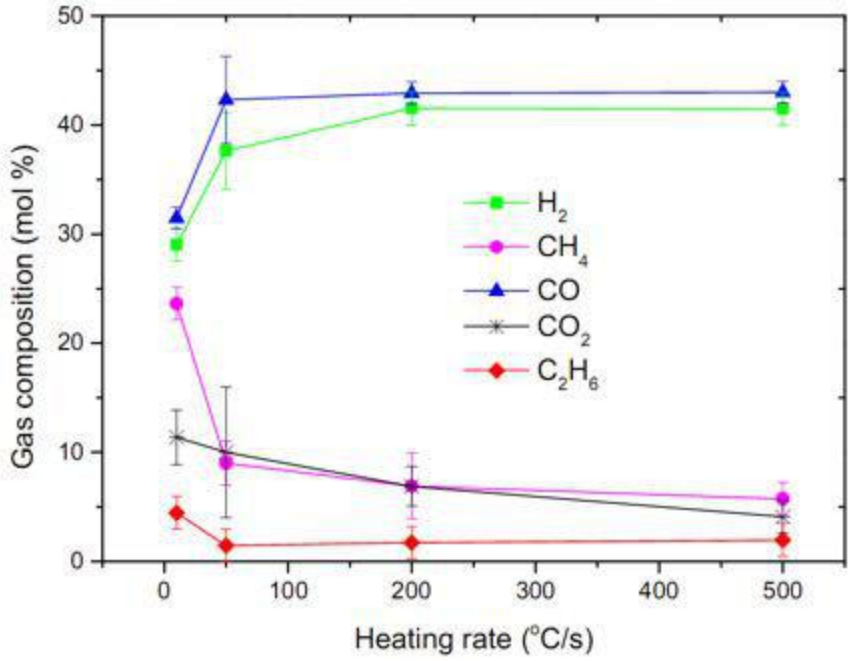

Figure 3.14. Gas composition of chicken-litter waste pyrolysis formed at different heating rates to final pyrolysis temperature 1200°C

Table 3.6 shows the higher heating values of the total and individual gas components. The HHV of the individual gas is calculated with the gas production (g/kg of sample) and the conversion factor (HHV) of the individual gas. It reveals remarkable change as the heating rate increases from 10 to 50°C/s. Specifically, the HHVs of H_2 and CO increase each by more than twice, from 764 ± 31 kJ/kg to 1641 ± 166 kJ/kg and from 827 ± 26 to 1840 ± 188 kJ/kg, respectively. This is due to the enhanced production of the H_2 and CO gases as the heating rate increases from 10 to 50°C/s. Whereas the HHVs of CH_4 and C_2H_6 substantially decrease from 1948 ± 97 to 742 ± 212 kJ/kg and from 644 ± 26 to 361 ± 52 kJ/kg as the heating rate increases from 10 to 50°C/s. However, a further increase in the heating rate slightly increases the HHVs but is not significant. The highest total gas HHV (6402 ± 810 kJ/kg) is achieved at 500°C/s. The H_2/CO ratio, which is almost unity for all heating rates, confirms that the pyrolysis gases produced in this form can have better performance in engines but at the expense of higher NOx emission (Sahoo et al. 2012).

Table 3.6. Higher heating values (kJ/kg) and H_2 to CO ratio of the pyrolysis gases at 1200°C final pyrolysis temperature, expressed based on the biomass weight.

Heating rates (°C/s)	H_2	CH_4	CO	C_2H_6	Total	H_2/CO
10	764 ± 31	1948 ± 97	827 ± 26	644 ± 161	4182 ± 315	0.9 ± 1
50	1641 ± 166	742 ± 212	1840 ± 188	361 ± 52	4585 ± 618	0.9 ± 0.9
200	1828 ± 52	953 ± 491	1885 ± 45	418 ± 104	5083 ± 692	1.0 ± 1.5
500	2328 ± 67	983 ± 218	2499 ± 58	592 ± 467	6402 ± 810	1.0 ± 1.5

3.4.2 Influence of final temperature on the product yield and gas composition

Figure 3.15 shows the measured product yields as a function of final pyrolysis temperatures at 50°C/s heating rate. Chicken litter waste with 280 μm particles size, packed into cylindrical pellets of 10 mm in diameter and 5 mm in thickness was used as the biomass feedstock. Heating at 800°C produces a maximum bio-oil yield of 48.4 wt.%, which continuously decreases with further increase in temperature, producing a minimum yield of 41 wt.% at 1600°C (**Figure 3.15**). Similarly, the char yield is sharply reduced from 42.1 wt.% at 800°C to 17.9 wt.% at 1600°C. This is due to the greater primary decomposition of the biomass or secondary decomposition of the char residue with increasing temperatures. On the other hand, the gas yield is constantly increased from its minimum yield of 9.5 wt.% at 800°C to its maximum yield of 38.6 wt.% at 1600°C. The trend is consistent with the results obtained from the solar pyrolysis of beech wood pellets in the same range of temperatures (Zeng et al. 2015b). Upon increasing the temperature, the reaction between the vapor and char phase is dominant. Moreover, secondary reaction of heavy molecular weight compounds is high, which can cause the char and bio-oil yields to decrease, while increasing the gas yield (Salehi et al. 2011).

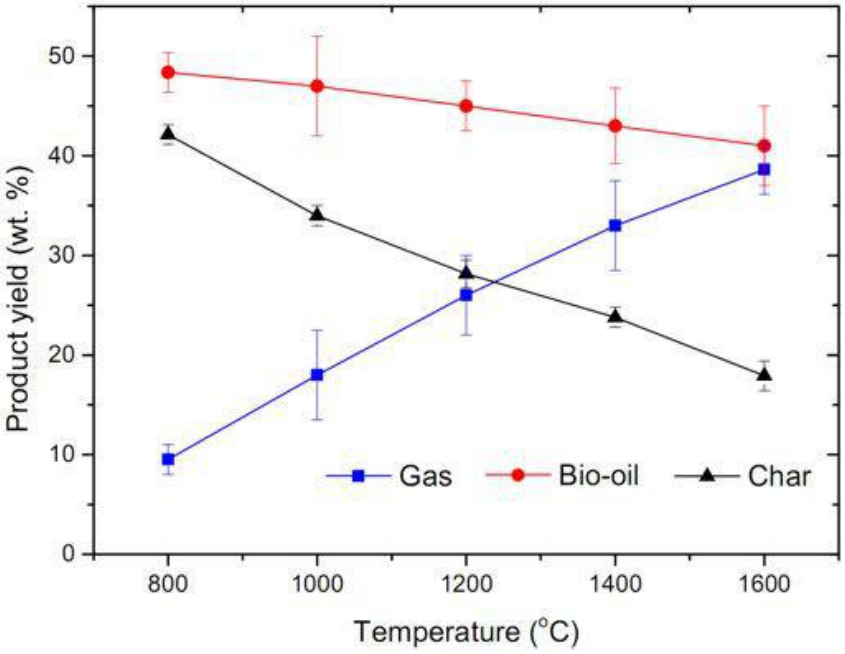

Figure 3.15. Product yield of chicken-litter waste pyrolysis formed at different final temperatures and 50°C/s heating rate

Gas composition of the chicken litter waste pyrolysis at a temperature range from 800 to 1600°C and heating rate of 50°C/s is shown in **Figure 3.16**. The effect of temperature is mainly observed in the evolution of CO, H_2, and CO_2. The dominant products are CO and H_2 with maximum molar yields of 46.3% and 48.1% at 1600°C, respectively. The increase of H_2 with temperatures can be associated with the cracking of all condensable and non-condensable products at higher temperatures, while the increase in CO content is due to the reverse Boudouard reaction at higher temperatures (Becidan et al. 2007), which is also responsible for substantially depleting CO_2 content from 38% to 2.2% (**Figure 3.16**). There are no appreciable changes to the contents of CH_4 and C_2H_6.

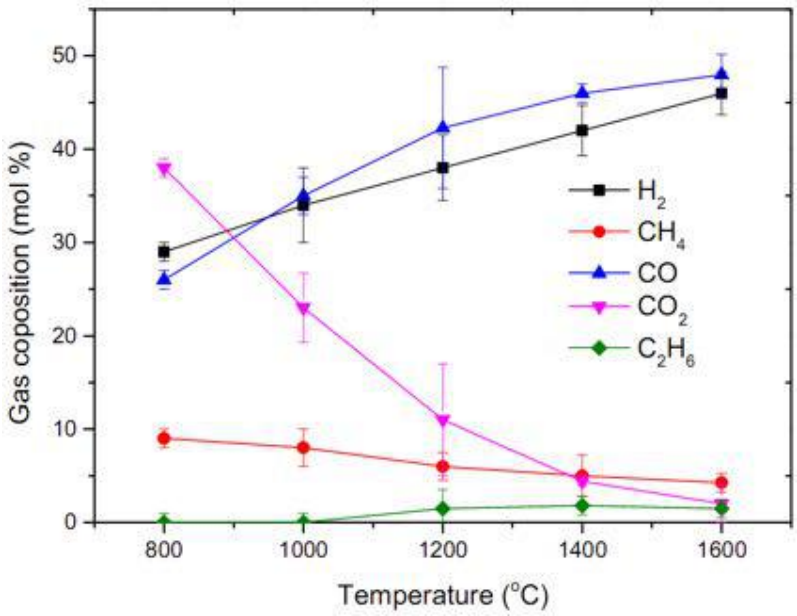

Figure 3.16. Gas composition of chicken-litter waste pyrolysis produced at different final temperatures and 50°C/s

Table 3.7 shows the HHVs, expressed based on the biomass weight, and H_2 to CO ratio of the pyrolysis gases obtained from chicken litter waster at temperatures ranging from 800 to 1600°C and 50°C/s heating rate. The HHVs of most gases and hence the total gas heating values increase with rise in temperature. The higher heating values of H_2 and CO at the lowest temperature (800°C) are 305 ± 11 and 262 ± 102 kJ/kg and continuously increase with temperature to the maximum values of 2798 ± 140 and 3066 ± 153 kJ/kg at 1600°C. Similarly, the highest HHV of the total gas increases linearly from 838 ± 48 at 800°C to 7255 ± 566 kJ/kg at 1600°C, due to the increased yield of H_2 and CO with temperature. The highest HHV of CH_4 (916 ± 458 kJ/kg) is obtained at 1400°C and decreases to 865 ± 247 kJ/kg at 1600°C, which is attributed to the cracking of CH_4 to H_2 and CO gases. The H_2/CO ratio is also affected with temperature. Except at 1200 and 1400°C, this ratio is either 1 or greater than 1 (1.1).

Table 3.7. Higher heating values (kJ/kg) and H_2/CO ratio of the pyrolysis gases formed from chicken litter at different final pyrolysis temperatures and 50°C/s, expressed based on the biomass weight.

Temperature (°c)	H_2	H	CO	C_2H_6	Total	H_2/CO
800	305 ± 11	271 ± 27	262 ± 10	0	838 ± 48	1.1 ± 1
1000	852 ± 95	698 ± 174	840 ± 49	0	2390 ± 318	1.0 ± 2
1200	1641 ± 149	742 ± 247	1841 ± 263	361 ± 5	4585 ± 665	0.9 ± 0.1
1400	2283 ± 126	916 ± 458	2561 ± 100	511 ± 26	6272 ± 611	0.9 ± 2
1600	2798 ± 140	865 ± 247	3066 ± 153	526 ± 26	7255 ± 566	1.0 ± 1

3.4.3 Influence of biomass type on the yield and gas composition

Chicken litter waste and rice husk with 280 μm particle sizes are pyrolysed in the temperature range of 800 to 1600°C at 50°C/s to determine the influence of biomass type on the yield and composition of the evolved volatiles. The product yields of pyrolysis of these two biomass samples under the concentrated solar radiation are shown in **Figure 3.17**. Variations in the product yields with respect to biomass type are not significant for gas but significant for char, in particular at high temperature. It can be seen that the lowest gas yields, 12 wt.% for chicken litter and 9.5 wt.% for rice husk, are obtained at 800°C and increase to 38.6 and 38.5 wt.%, respectively, at 1600°C. However, a remarkable difference is observed in the char and bio-oil yields, especially at the higher ranges of pyrolysis temperatures. It is further noticed that bio-oil yields produced from the chicken litter sample are higher than those of the rice husk at all pyrolysis temperatures (maximum difference being 5.3 wt.% at 1400°C). Contrary to the bio-oil, the char yields from the rice husk are higher than the chars from the chicken litter in almost all pyrolysis temperatures. The highest variation between the char yields produced from rice husk and chicken litter is 7.2 wt.%, recorded at 1400°C.

The opposite trends of the bio-oil and char yields from the two samples can be related to the volatile content of the feedstock, which is 62.6% in the chicken litter sample and 54.5%

in the rice husk (**Table 2.2**). Feedstock with high volatile contents have higher volatility and reactivity advantages which favor bio-oil production. Higher char yield from the rice husk indicates higher lignin content of the rice husk compared to the chicken litter waste. A high lignin content contributes to production of higher char yields (Guedes et al. 2018).

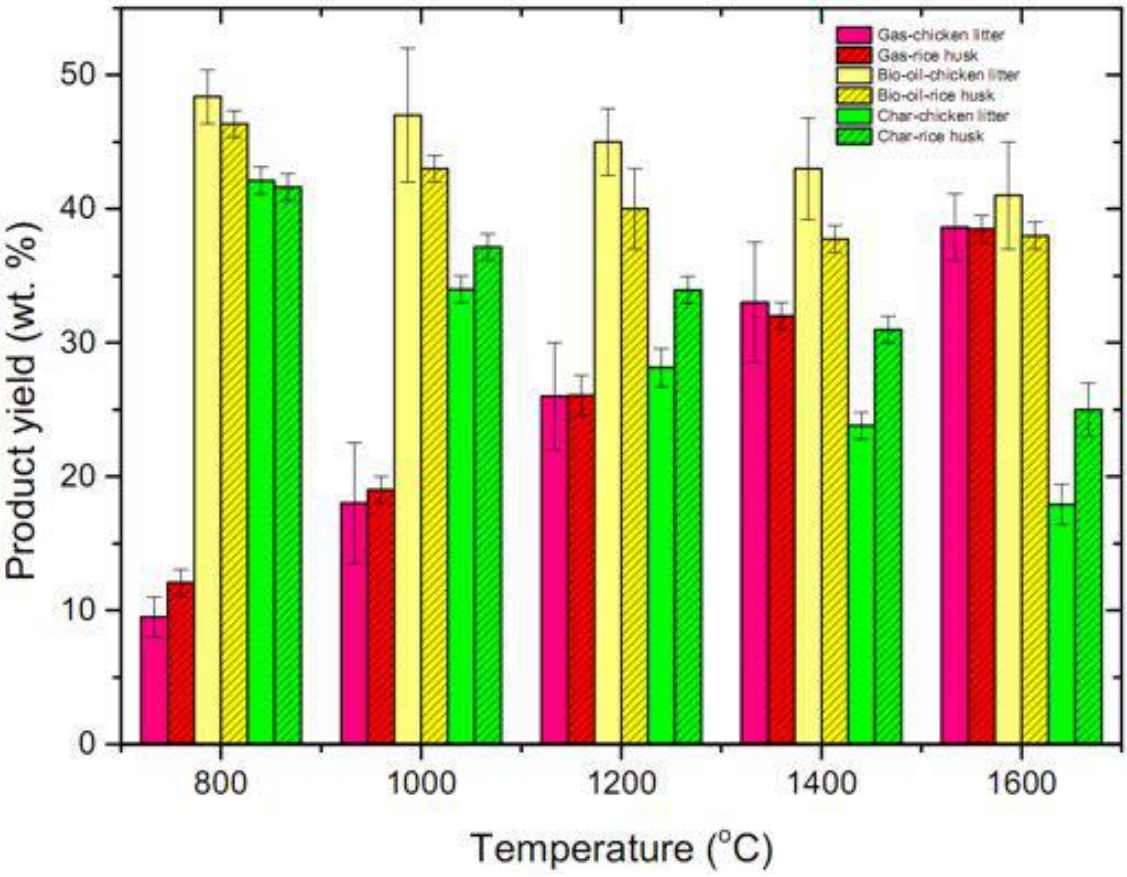

Figure 3.17. Product distribution from the pyrolysis of chicken litter and rice husk (280 µm sizes) at 50°C/s and different temperatures

Table 3.8 shows the composition of pyrolysis gases obtained from the 280 µm particle size of rice husk and chicken litter. There is a significant difference in H_2, CO, and CO_2 production at the lower ranges of pyrolysis temperatures (800 and 1000°C) with differences decreasing as the temperature increases and there are almost the same molar yields at 1600°C for both biomass samples. The H_2, CO, and CO_2 productions from the rice husk sample at 800°C are 13.2 ± 1.5%, 49 ± 1.5%, and 25.4 ± 1.5%, respectively. The H_2 and CO_2 productions from chicken litter sample are 29 ± 1% and 38 ± 1, respectively, while the CO production (26 ± 1 wt.%) was smaller than the rice husk. As the temperature increases to

1000°C, these differences are observed to reduce, and with further increase in the pyrolysis temperature the gas compositions are almost the same for both biomass samples. The difference in the gas composition could arise from the proteins, fats, and carbohydrates components of the biomasses. It is known that chicken litter has higher content of proteins and fats. Pyrolysis of these materials can produce significant amount of CO_2 as compared to the pyrolysis of rice husk which has higher lignin content than chicken litter (Azargohar et al. 2013). The higher H_2 production from the rice husk at 800 and 1000°C pyrolysis temperatures could also be explained by the higher lignin content of the biomass.

Table 3.8. Gas composition (mol%) from rice husk and chicken litter pyrolysis at 800 to 1600°C and 50°/s heating rate.

Temper-ature (°c)	H_2		CH_4		CO		CO_2		C_2H_6	
	Rice husk	Chicken litter	Rice husk	Chicken litter	Rice husk	Chicken litter	Rice husk	Chicken litter	Rice husk	Chicken litter
800	13.2±1.5	29.0±1.0	12.4±1.5	9.0±1.0	49.0±1.5	26.0±1.0	25.4±1.5	38.0±1.0	0	0
1000	23.5±1.5	34.0±4.0	10.0±1.5	8.0±2.0	44.0±1.5	35.0±2.0	15.0±1.5	23.0±3.7	0	0
1200	33.0±1.5	38.0±3.5	8.2±1.5	6.0±1.5	43.5±1.5	42.3±3.5	8.0±2.0	11.0±3.0	1.0±1.0	1.5±1.5
1400	42.0±2.5	42.0±2.7	6.4±1.5	5.0±2.2	45.6±1.5	46.0±1.0	5.6±1.6	4.4±0.5	1.0±1.0	1.8±1.0
1600	50.0±2.0	46.0±2.3	4.6±1.5	4.3±1.0	49.4±1.5	48.0±2.1	3.7±1.5	2.0±2.0	1.5±0.5	1.5±1.0

Table 3.9 shows the HHV and H_2 to CO ratio of the pyrolysis gases formed from the pyrolysis of rice husk at 800 to 1600°C and 50°C/s heating rate. Compared to the HHVs of the pyrolysis gases from chicken litter waste under similar operating parameters, the total gas HHVs slowly increase with temperature (**Table 3.6**). For example, the total gas HHV from rice husk at 800°C is 1271 ± 140 kJ/kg and slightly increases to its highest value of 7198 ± 531 kJ/kg at 1600°C; whereas the total gas HHV from chicken litter at 800°C is 838 ± 48 kJ/kg and sharply increases to 7255 ± 566 kJ/kg at 1600°C. The changes in CO production from rice husk at higher ranges of temperature are not considerable (**Table 3.7**); hence, the changes in the HHVs of the gas from rice husk are also not as significant as the HHVs of the gas obtained from chicken litter. The H_2/CO ratio shows significant variation with temperature from 0.3 at 800°C to 1 at 1600°C. This is due to the higher rate of H_2 production with temperature.

Table 3.9. Higher heating values (kJ/kg) and H_2 to CO ratio of the pyrolysis gases formed from rice husk at different final pyrolysis temperatures and 50°C/s heating rate, expressed based on the biomass weight.

Temperature (°c)	H_2	CH_4	CO	C_2H_6	C_2H_6	H_2/CO ratio
800	166 ± 18	490 ± 54	615 ± 15	0	1271 ± 140	0.3 ± 0.1
1000	768 ± 38	927 ± 116	1109 ± 28	0	2805 ± 183	0.5 ± 0.1
1200	1628 ± 54	1065 ± 213	1797 ± 47	597 ± 52	5087 ± 366	0.8 ± 0.1
1400	2107 ± 105	1018 ± 255	2325 ± 58	298 ± 50	5748 ± 423	0.9 ± 0.17
1600	2602 ± 104	916 ± 305	3150 ± 75	531 ± 47	7198 ± 531	1.0 ± 0.13

3.4.4 Influence of particle size on the yield and composition of pyrolysis products

Table 3.10 shows the product yields for the pyrolysis of rice husk with particle sizes of 280 and 500 μm at the final temperatures of 800, 1200, and 1600°C, respectively, at a heating rate of 50°C/s. Smaller biomass particles exhibit higher surface to volume ratio than the larger particles, which favors the fast rate of heat transfer. Higher gas and bio-oil yields can be expected from the biomass with smaller particle sizes in fast pyrolysis processes (Sensoz et al. 2006). The bio-oil yield slightly increases from 43.5 to 46.3 wt.% with decreasing the particle size. In contrast, **Table 3.10** also shows an increasing trend of gaseous yields from 12 to 19.9 wt.%, and a decreasing char yield from 41.6 to 36.59 wt.% as the particle size increases from 280 to 500 μm. These changes could be explained by the low bulk density and wider intra particle voids of the larger particles and associated heat transfer advantages, which could facilitate the diffusion of gaseous products and thermal cracking of the chars into small molecule gases. Pyrolysis of both biomass samples at 1200 and 1600°C does not bring any significant difference to the gas, bio-oil, and char yields. This observation is in a broad agreement with the findings reported in literature (Kersten et al. 2005; Kang et al. 2006; Shen et al. 2009).

Table 3.10. Product yields (%) from the pyrolysis of rice husk with 280 and 500 µm particle sizes at 800-1600°C pyrolysis temperatures and 50°C/s heating rate (error was less than 5%).

Product yields	Particle size (µm)	Temperature (°C)		
		800	1200	1600
Gas	280	12	26	39
	500	20	26	37
Char	280	42	34	25
	500	37	32	25
Bio-oil	280	46	40	38
	500	44	41	38

Table 3.11 presents the influence of rice husk particle size on the distribution of pyrolysis gases. The experiment was conducted at three temperatures (800, 1200, and 1600°C) and a heating rate of 50°C/s with 280 and 500 µm particle sizes. It is shown that the biomass particle size has little effect on the distribution of the pyrolysis gases. The highest effect is observed on the H_2 content at 1600°C. The 280 and 500 µm rice husks produce about 50% and 41% H_2, respectively. Similarly, with increasing the particle size from 280 to 500 µm, the CO_2 content decreases from 25.4% to 16.9%, but H_2 is observed to increase from 13.2% to 19.4% at 800°C.

Table 3.11. Influence of particle sizes on the pyrolysis gas composition (mol%).

Gas	Particle size (µm)	Temperature (°C)		
		800	1000	1600
H_2	280	13.2 ±1.5	33 ±1.5	50 ±2
	500	19.4 ±1.5	27.5 ±1.5	41 ±1.5
CH_4	280	12.4 ±1.5	8.2 ±1.5	4.6 ±1.5
	500	14.1 ±1.5	11.5 ±1.5	3.8 ±1.5
CO	280	50 ±1.5	43.5 ±1.5	49.4 ±1.5
	500	49.6 ±1	43.2 ±0.5	45.8 ±1
CO_2	280	25.4 ±1.5	8 ±2	3.7 ±1.5
	500	16.9 ±1.5	14.3 ±1.5	5.7 ±1.5
C_2H_6	280	0	1 ±0.5	1.5 ±0.5
	500	0	3.4 ±1	1.4 ±1.5

Table 3.12 shows the HHVs and the H_2 to CO ratio of the pyrolysis gases from the 280 and 500 µm sizes of rice husk sample. There is relatively sharp rise with temperature in the HHVs of individual and the total gases from the pyrolysis of the 280 µm size sample as compared to the HHVs of the gases from the rice husk with 500 µm size. The highest total gas heating value for the 280 µm particles substantially increases from 1271 ± 140 kJ/kg at 800°C to 7198 ± 531 at 1600°C. Whereas the lowest and highest HHVs of total gas produced at the same pyrolysis conditions for the 500 µm sample are 2663 ± 141 and 6617 ± 656, respectively. These differences are due to the combined effects of H_2 and CO from the pyrolysis of the 280 µm particle size which have higher production rate at each of the pyrolysis temperatures. The H_2/CO ratio of the gases from both particle sizes is almost identical in all pyrolysis temperatures. Overall, the effect of the feedstock size difference could not affect the HHVs and H_2/CO ratio of the gas.

Table 3.12. Higher heating values (kJ/kg) and H_2/CO ratio of the pyrolysis gases formed from rice husk at different final pyrolysis temperatures and 50°C/s heating rate.

Gas	Particle sizes (µm)	Temperature (°C)		
		800	1000	1600
H_2	280	166 ± 18	1628 ± 54	2602 ± 104
	500	457 ± 30	852 ± 34	2640 ± 76
CH_4	280	490 ± 54	1065 ± 213	916 ± 305
	500	1041 ± 87	1118 ± 140	721 ± 288
CO	280	615 ± 15	1797 ± 47	3150 ± 75
	500	1165 ± 24	1336 ± 17	2788 ± 62
C_2H_6	280	0	597 ± 52	531 ± 47
	500	0	577 ± 115	460 ± 230
Total	280	1271 ± 140	5087 ± 366	7198 ± 531
	500	2663 ± 141	3883 ± 306	6617 ± 656
H_2/CO	280	0.3 ± 1	0.8 ± 1	1.0 ± 1.3
	500	0.4 ± 1.5	0.6 ± 3	0.9 ± 1.5

3.4.5 Conclusion

Solar pyrolysis of chicken litter waste and rice husk of different particle sizes is performed at different heating rates and temperatures. Temperature and lower ranges of heating rates (10 to 50°C/s) are found to have significant influence on the yield and composition of pyrolysis products. The highest bio-oil yield of 53 wt.% is achieved for the pyrolysis of 280 µm particle size chicken litter waste at 1200°C and at a heating rate of 10°C/s; whereas maximum yields of bio-oil (38.6 wt.%) and char (42.1 wt.%) are obtained at 1600°C and 800°C, respectively, at 50°C/s heating rate. It is further noticed that the contents of CO and H_2 increase with rise in temperatures for both biomass types and particle sizes. Similarly, the HHVs of the total gases increase with temperature in all pyrolysis conditions. Bio-oil yield produced from chicken litter is greater than that from rice husk throughout the pyrolysis temperature; whereas char yields obtained from rice husk are greater than the chicken litter by a maximum of 7.2 wt.%. Variations in gas yield and composition with respect to particle size are insignificant. The highest H_2/CO ratio of most gases produced is around 1, which confirms that the pyrolysis gases produced can be utilized to run engines or power plants.

3.5 Bibliography

Abnisa F, Wan Daud WMA. A review on co-pyrolysis of biomass: An optional technique to obtain a high-grade pyrolysis oil. Energy Conversion and Management, 2014, 87: 71–85.

Akhtar J, Saidina Amin N. A review on operating parameters for optimum liquid oil yield in biomass pyrolysis. Renewable and Sustainable Energy Reviews, 2012, 16: 5101–5109.

Al Arni S. Comparison of slow and fast pyrolysis for converting biomass into fuel. Renewable Energy, 2018, 124: 197–201.

Authier O, Ferrer M, Mauviel G, Khalfi A.E, Lédé J. Wood fast pyrolysis: Comparison of Lagrangian and Eulerian modeling approaches with experimental measurements. Industrial & Engineering Chemistry Research, 2009, 48: 4796–4809.

Azargohar R, Jacobson KL, Powell EE, Dalai AK. Evaluation of properties of fast pyrolysis products obtained, from Canadian waste biomass. Journal of Analytical and Applied Pyrolysis, 2013, 104: 330–340.

Becidan M, Skreiberg Ø, Hustad JE. Products distribution and gas release in pyrolysis of thermally thick biomass residues samples. Journal of Analytical and Applied Pyrolysis, 2007, 78: 207–213.

Blondeau J, Jeanmart H. Biomass pyrolysis at high temperatures: Prediction of gaseous species yields from an anisotropic particle. Biomass Bioenergy, 2012, 41: 107–121.

Brigewater AV. Fast pyrolysis of biomass: A handbook 2005. CPL Press, Newbury (UK), 3: 121–146.

Bryden KM, Ragland KW, Rutland CJ. Modeling thermally thick pyrolysis of wood. Biomass and Bioenergy, 2002, 22: 41–53.

Chan W-CR, Kelbon M, Krieger BB. Modelling and experimental verification of physical and chemical processes during pyrolysis of a large biomass particle. Fuel, 1985, 64: 1505–1513.

Chen G, Yu Q, Sjöström K. Reactivity of char from pyrolysis of birch wood. Journal of Analytical and Applied Pyrolysis, 1997, 40-41: 491–499.

Chhiti Y, Salvador S, Commandré J-M, Broust F. Thermal decomposition of bio-oil: Focus on the products yields under different pyrolysis conditions. Fuel, 2012, 102: 274–281.

Christodoulou M, Mauviel G, Lédé J, Beaurain P, Weber M, Legall H, Billaud F. Novel vertical image furnace for fast pyrolysis studies. Journal of Analytical and Applied Pyrolysis, 2013, 103: 255–260.

Demirbas A. Effects of temperature and particle size on bio-char yield from pyrolysis of agricultural residues. Journal of Analytical and Applied Pyrolysis, 2004a, 72: 243–248.

Demirbas A. Determination of calorific values of bio-chars and pyro-oils from pyrolysis of beech trunkbarks. Journal of Analytical and Applied Pyrolysis, 2004b, 72: 215–219.

Demirbas A. Hydrogen-rich gases from biomass via pyrolysis and air-steam gasification.

Energy Sources, Part A: Recovery Utilization, Environmental Effects, 2009, 31: 1728–1736.

Fahmi R, Bridgwater A, Donnison I, Yates N, Jones JM. The effect of lignin and inorganic species in biomass on pyrolysis oil yields, quality and stability. Fuel, 2008, 87: 1230–1240.

Garcia-Perez M, Wang XS, Shen J, Rhodes MJ, Tian F, Lee W-J, Wu HW, Li CZ. Fast pyrolysis of oil mallee woody biomass: Effect of temperature on the yield and quality of products. Industrial and Engineering Chemistry Research, 2008, 47: 1846–1854.

Gibbins-Mathame J, Kandiyoti R. Coal pyrolysis yields from fast and slow heating in a wire-mesh apparatus with a gas sweep. Energy & Fuels, 1988, 2: 505–511.

Guedes RE, Luna AS, Torres AR. Operating parameters for bio-oil production in biomass pyrolysis: A review. Journal of Analytical and Applied Pyrolysis, 2018, 129: 134–149.

Horne P, Williams P. Influence of temperature on the products from the flash pyrolysis of biomass. Fuel, 1996, 75: 9: 1051–1059.

Iwasaki T, Suzuki S, Kojima T. Influence of biomass pyrolysis temperature, heating rate and type of biomass on produced char in a fluidized bed reactor. Energy and Environment Research, 2014, 4: 64–72.

Kang B-S, Lee KH, Park HJ, Park Y-K, Kim J-S. Fast pyrolysis of radiata pine in a bench scale plant with a fluidized bed: Influence of a char separation system and reaction conditions on the production of bio-oil. Journal of Analytical and Applied Pyrolysis, 2006, 76: 32–37.

Kersten SRA, Wang X, Prins W, Van Swaaij WPM. Biomass pyrolysis in a fluidized bed reactor. Part 1: Literature review and model simulations. Industrial & Engineering Chemistry, Research 2005, 44: 8773–8785.

Khan M, Crynes B. Survey of recent methane pyrolysis literature. Industrial & Engineering Chemistry, 1970, 62: 54–59.

Luo S, Guo J, Feng Y. Hydrogen-rich gas production from pyrolysis of wet sludge *in situ* steam agent. International Journal of Hydrogen Energy, 2017,42: 18309–18314.

Morf P, Hasler P, Nussbaumer T. Mechanisms and kinetics of homogeneous secondary reactions of tar from continuous pyrolysis of wood chips. Fuel, 2002, 81: 843–853.

Neves D, Thunman H, Matos A, Tarelho L, Gómez-Barea A. Characterization and prediction of biomass pyrolysis products. Progress in Energy Combustion Science, 2011, 37: 611–630.

Newalkar G, Lisa K, D'amico AD, Sievers C, Agrawal P. Effect of temperature, pressure, and residence time on pyrolysis of pine in an entrained flow reactor. Energy & Fuels, 2014, 28: 5144–5157.

Onay O. Influence of pyrolysis temperature and heating rate on the production of bio-oil and char from safflower seed by pyrolysis, using a well-swept fixed-bed reactor. Fuel Processing Technology, 2007, 88: 523–531.

Okekunle PO, Pattanotai T, Watanabe H, Okazaki K. Numerical and experimental investigation of intra-particle heat transfer and tar decomposition during pyrolysis of wood biomass. Journal of Thermal Science and Technology, 2011, 6: 360–375.

Okekunle PO, Watanabe H, Pattanotai T, Okazaki K. Effect of biomass size and aspect ratio on intra-particle tar decomposition during wood cylinder pyrolysis. Journal of Thermal Science and Technology, 2012, 7: 1–15.

Pütün AE, Özbay N, Apaydin Varol E, Uzun BB, Ates F. Rapid and slow pyrolysis of pistachio shell: Effect of pyrolysis conditions on the product yields and characterization of the liquid product. International Journal of Energy Research, 2007, 31: 506–514.

Pozzobon V, Salvador S, Bézian J.J, El-Hafi M, Le Maoult Y, Flamant G. Radiative pyrolysis of wet wood under intermediate heat flux: experiments and modeling. Fuel Processing Technology, 2014, 128: 319–330.

Pozzobon V, Salvador S, Bézian JJ. Biomass gasification under high solar heat flux: Advanced modeling. Fuel, 2018, 214: 300–313.

Sahoo BB, Sahoo N, Saha UK. Effect of H_2:CO ratio in syngas on the performance of a dual fuel diesel engine operation. Applied Thermal Engineering, 2012, 49: 139–146.

Salehi E, Abedi J, Harding T. Bio-oil from sawdust: Pyrolysis of sawdust in a fixed-bed system. Energy & Fuels, 2009, 23: 3767–3772.

Salehi E, Abedi J, Harding T. Bio-oil from sawdust: Effect of operating parameters on the yield and quality of pyrolysis products. Energy & Fuels, 2011, 25: 4145–4154.

Sensoz S, Demiral I, Ferdi Gercel H. Olive bagasse (*Olea europea* L.) pyrolysis. Bioresource

Technology, 2006, 97: 429–436.

Septien S, Valin S, Dupont C, Peyrot M, Salvador S. Effect of particle size and temperature on woody biomass fast pyrolysis at high temperature (1000–1400°C). Fuel, 2012, 97: 202–210.

Shen J, Wang X-S, Garcia-Perez M, Mourant D, Rhodes MJ, Li C-Z. Effects of particle size on the fast pyrolysis of oil mallee woody biomass. Fuel, 2009, 88: 1810–1817.

Shi X, Ronsse F, Pieters JG. Finite element modeling of intraparticle heterogeneous tar conversion during pyrolysis of woody biomass particles. Fuel Processing Technology, 2016, 148: 302–316.

Soltes EJ, Elder TJ. Pyrolysis. In Organic Chemicals from Biomass (IS Goldstein, ed.). CRC Press Inc., Boca Raton, FL, pp. 63–95 (1981).

Soria J, Zeng K, Asensio D, Gauthier D, Flamant G, Mazza GG. Comprehensive CFD modelling of solar fast pyrolysis of beech wood pellets. Fuel Processing Technology, 2017, 158: 226–237.

Tripathi M, Sahu JN, Ganesan P. Effect of process parameters on production of biochar from biomass waste through pyrolysis: A review. Renewable Sustainable Energy Review, 2016, 55: 467–481.

Trubetskaya A, Jensen PA, Jensen AD, Steibel M, Spliethoff H, Glarborg P Influence of fast pyrolysis conditions on yield and structural transformation of biomass chars. Fuel Processing Technology, 2015, 140: 205–214.

Uddin MN, Wan Daud WMA, Abbas HF. Effects of pyrolysis parameters on hydrogen formations from biomass: A review. RSC Advances, 2014, 4: 10467–10490.

Uzun BB, Apaydin-Varol E, Ateş F, Özbay N, Pütün AE. Synthetic fuel production from tea waste: Characterisation of bio-oil and bio-char. Fuel, 2010, 89: 176–184.

Williams P, Besler S. The influence of temperature and heating rate on the slow pyrolysis of biomass. Renewable Energy, 1996, 7: 3: 233–250.

Yao X, Yu Q, Xie H, Duan W, Han Z, Liu S, Qin Q. Syngas production through biomass/CO_2 gasification using granulated blast furnace slag as heat carrier. Journal of Renewable and Sustainable Energy, 2017, 9: 053101.

Zeng K, Flamant G, Gauthier D, Guillot E. Solar pyrolysis of wood in a labscale solar reactor:

Influence of temperature and sweep gas flow rate on products distribution. Energy Procedia, 2015a, 69: 1849–1858.

Zeng K, Gauthier D, Li R, Flamant G. Solar pyrolysis of beech wood: Effects of pyrolysis parameters on the product distribution and gas product composition. Energy, 2015b, 93: 1648–1657.

Zeng K, Soria J, Gauthier D, Mazza G, Flamant G. Modeling of beech wood pellet pyrolysis under concentrated solar radiation. Renewable Energy, 2016, 99: 721–729.

Chapter 4

Pyrolysis of Metal Polluted Biomass

4.1 Introduction

Phytoextraction is effective to contribute to solve the problem of HM pollution of soils, and pyrolysis is an effective and economical technology for converting HM contaminated biomass into char, gas, and oil. This chapter discusses the influence and combined effects of heavy metals (with temperature and heating rate) on products of solar pyrolysis reaction. A special attention ascribes to analyze the resulting contaminated chars. In this regard, copper and nickel were chosen for impregnating willow wood to simulate the hyperaccumulators, as these HMs are commonly detected in the contaminated plants. Moreover, both metals could act as *in situ* catalysts in contaminated biomass pyrolysis reactions (Nzihou et al. 2019). Copper and nickel represent a volatile and a non-volatile HM contents during the temperature range of solar pyrolysis reactions. Solar pyrolysis of HM contaminated biomass for disposal and improvement of pyrolysis product properties has not been studied. Therefore, there is a need to understand the role and behavior of HMs during solar pyrolysis reactions. The structure of this chapter is organized in the following two sections.

- **Section 4.2** reports pyrolysis of the raw and HM polluted willow woods. The combined

effects of HM and heating parameters (i.e., temperature and heating rate) on solar pyrolysis products are investigated.

- **Section 4.3** investigates the effects of temperature and HM contamination on the chemical composition, structure, and morphology of char generated from solar pyrolysis of the HM polluted willow woods.

4.2 Pyrolysis of heavy metal contaminated biomass: Product yield and gas composition

In **Section 4.2**, willow wood (virgin and HM impregnated) was used to study the effects of HMs, in combination with temperature (**Section 4.2.1**) and heating rate (**Section 4.2.1**), on pyrolysis products. Each section includes two parts: one devoted to the final product distribution and the other to pyrolysis gas composition and LHVs.

Reference of the corresponding paper:

Zeng K, **Li R**, Doan PM, Elsa W, Nzihou A, Xiao H, Flamant G. Solar pyrolysis of heavy metal contaminated biomass for gas fuel production. Energy, 2019, 187: 116016.

4.2.1 Combined effects of temperature and HM

4.2.1.1 Final product distribution at different temperatures

Product yields from the raw and impregnated willow pyrolysis under different temperatures are presented in **Figure 4.1**. For the raw willow pyrolysis, the char yield significantly decreases from 25.8% to 10.3% when temperature increases from 600 to 1600°C (**Figure 4.1a**), and the liquid yield noticeably decreases from 63.4% to 42.7% (**Figure 4.1b**), while the gas yield increases from 10.8% to 47.0% (**Figure 4.1c**). As the temperature rises from 600 to 800°C, the increase in the gas yield is mainly compensated by the decrease

in the char yield. It is due to volatile formation reactions becoming more favorable during the competition with char formation reactions with increasing temperature (Di Blasi 2008). The gas yield increases from 18.2% to 28.3% when temperature increases from 800 to 1000°C. In accordance, the char and liquid yields decrease by 4.1% and 5.9% with temperature, respectively. It proves that the increase in gas yield is caused by inhibited char primary formation and enhanced by secondary degradation of tar vapors in this temperature range (Di Blasi 2009). Then, the gas yield slightly increases (with small decrease of char and liquid yield) at higher temperatures (1000, 1200, and 1400°C). We assume that heat transfer resistance through the pellet willow reduces the actual degradation temperature of the sample due to the resulting internal thermal gradient (Di Blasi 2009). However, enhanced secondary reactions (such as cracking and polymerization) of tar vapors caused a rapid increase of gas yield and a decrease of liquid yield when temperature rises from 1400 to 1600°C (Morf et al. 2002). The char yield slightly decreases, because the decreasing formation of primary char is compensated by the enhanced formation of secondary char from tar, which is also reported by Neves et al. (2011).

The changing trend of pyrolysis product distribution with temperature was almost the same from the raw willow and the metal-impregnated willow. For the impregnated willow pyrolysis, the char and liquid yields also decrease with increasing gas yield when temperature increases from 600 to 1600°C. However, the presence of heavy metals (copper and nickel) leads to a decrease of the char yield compared to that of the raw willow (**Figure 4.1a**), which is consistent with the results of Said et al. (2018). Copper restricts the final degradation of lignin into char, causing a slight decrease of char yield obtained from the copper impregnated willow (Xing et al. 2016). For the nickel impregnated willow pyrolysis, the char yield decreases from 21.0% to 9.9% with temperature rising from 600 to 1600°C. It was reported that nickel could promote C-H and C-O bonds cleavage of char at high temperatures, thereby reducing the yield of char (Nzihou et al. 2019). The impact of heavy metal on pyrolysis liquid yield has two steps. The copper and nickel firstly promote the depolymerization of cellulose and hemicellulose resulting in more levoglucosan formation (Nzihou et al. 2019). Furthermore, they substantially catalyze the secondary reactions of

levoglucosan when the pyrolysis temperature is high enough. It results in higher liquid yields from the impregnated willow than from the raw willow when the pyrolysis temperature is not higher than 1000°C (**Figure 4.1b**). At temperature above 1000°C, the high activity of copper and nickel catalysts promotes the cracking and reforming reactions of tar, which causes the decrease of liquid yield (Yuan et al. 2015). It then leads to the increase of gas yield by 14.8% and 34.5% for the copper- and nickel-impregnated willow pyrolysis at 1200°C, respectively, compared to the raw willow (**Figure 4.1c**).

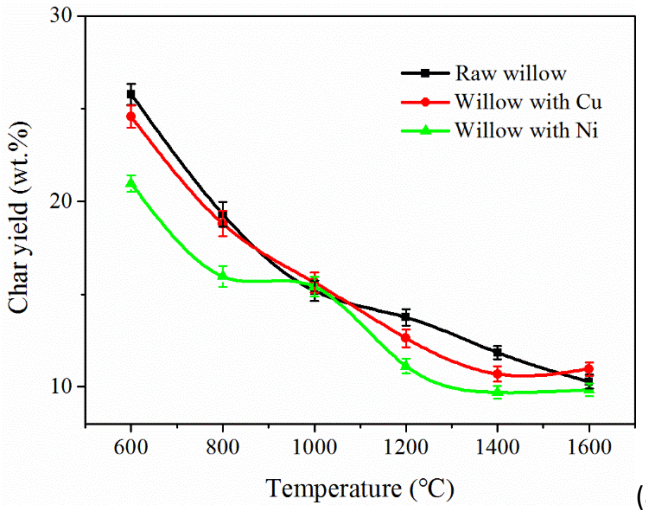

(a)

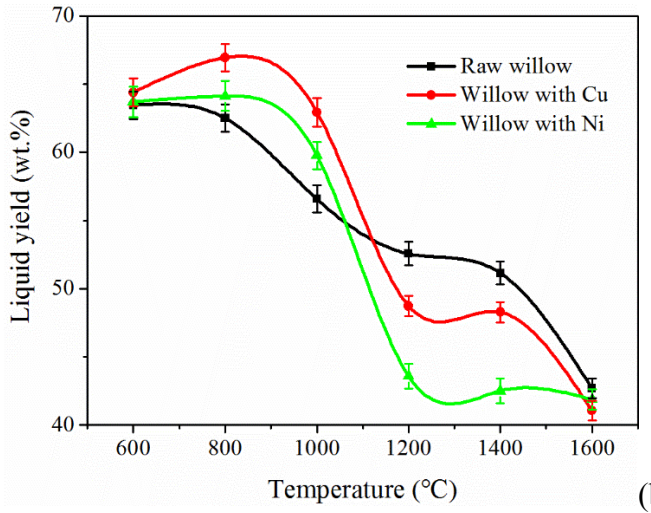

(b)

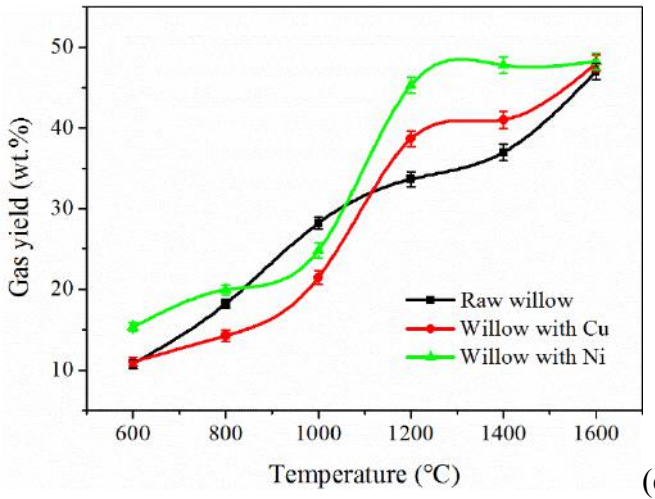

(c)

Figure 4.1. Combined effects of temperature and heavy metal on solar pyrolysis product distribution. a: char yield; b: liquid yield; and c: gas yield.

4.2.1.2 Pyrolysis gas composition and LHVs at different temperatures

The solar pyrolysis gas mainly consists of H_2, CO, and lower amounts of CH_4, CO_2, and C_2 hydrocarbons, and the distribution of these gases is different from the conventional pyrolysis gas compositions (Aysu and Kucuk 2014). Content of C_2H_6 mainly comes from tar decomposition (**Figure 4.2**), and it is not detected at 600°C, consistent with the previous study (Zeng et al. 2015a). Increasing temperature to 1600°C leads to increase in H_2 (**Figure 4.3**) and CO (**Figure 4.4**) yields from 0.16 to 12.1 mol/kg of wood and from 1.9 to 12.9 mol/kg of wood, respectively. In particular, their yields display a linear increase with temperature, which can be interpreted as an indicator for tar secondary reactions (Morf et al. 2002). A large part of their production comes from the intra-particle tar cracking reaction (Zeng et al. 2017a). Formation of CO was found to explain 50-70% of tar secondary reactions (Boroson et al. 1989). While, CO_2 yield firstly decreases from 1.1 to 0.7 mol/kg of wood as temperature increases from 600 to 1400°C (**Figure 4.5**). This result is attributed to the enhanced reverse Boudouard reaction (Septien et al. 2012). The maximum CO_2 yield of 1.15 mol/kg of wood is attained at 1600°C. Increase of CO_2 yield arises from the tar secondary reactions as it could account for up to 14% of tar conversion (Morf et al. 2002; Aysu and Kucuk 2014). Yields of CH_4 (**Figure 4.6**) and C_2H_6 (**Figure 4.2**) increase from 0.2 to 1.7 mol/kg of wood and from 0 to 0.6 mol/kg of wood with temperature increasing from 600 to 1000°C,

respectively, resulting from the tar cracking reaction (Zeng et al. 2015b). However, they reduce to 1.4 and 0.3 mol/kg of wood, respectively. It is mainly due to the enhancement of their own cracking reaction and steam reforming reaction as temperature increase from 1000°C to 1600°C, which dominates their degradation mechanisms (Lopez-Gonzalez et al. 2014; Zeng et al. 2017b).

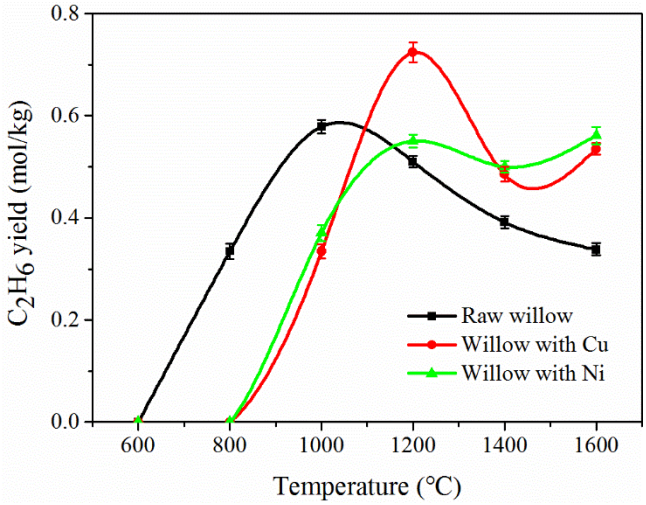

Figure 4.2. Combined effects of temperature and heavy metal on solar pyrolysis C_2H_6 yield

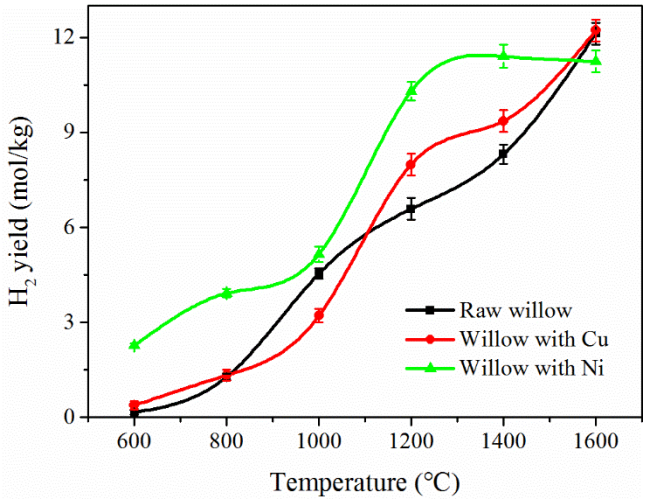

Figure 4.3. Combined effects of temperature and heavy metal on solar pyrolysis H_2 yield

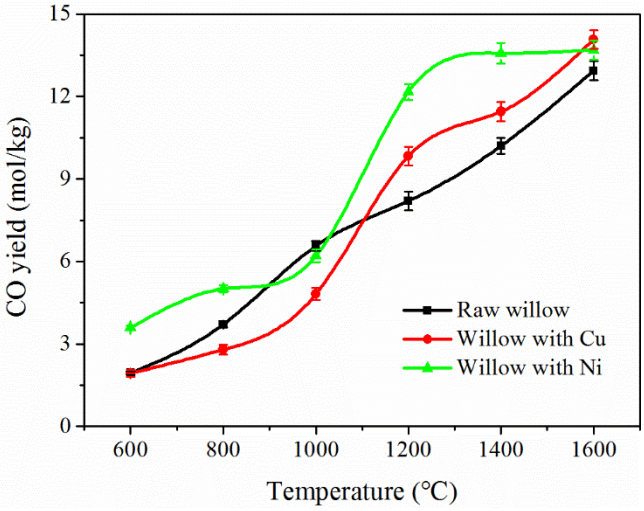

Figure 4.4. Combined effects of temperature and heavy metal on solar pyrolysis CO yield

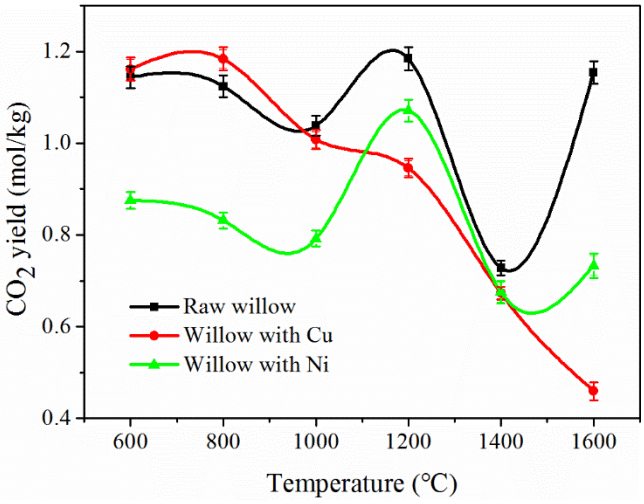

Figure 4.5. Combined effects of temperature and heavy metal on solar pyrolysis CO_2 yield

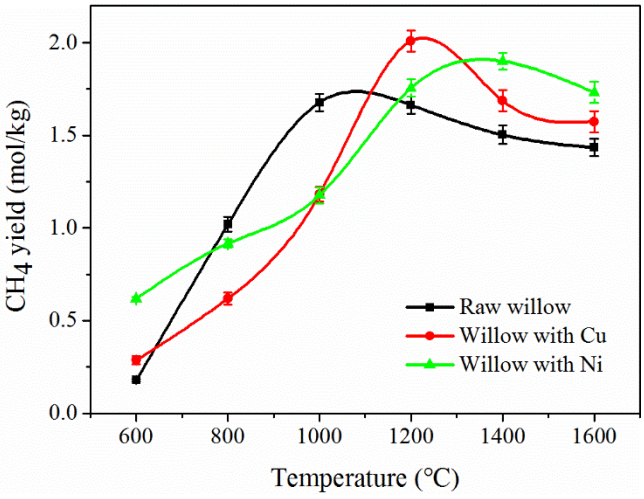

Figure 4.6. Combined effects of temperature and heavy metal on solar pyrolysis CH_4 yield

The variation trend of pyrolysis gas composition with temperature is almost the same from the raw and metal-impregnated willows. The presence of either copper or nickel increases the production of H_2, CO, CH_4, and C_2H_6, while it decreases the CO_2 yield when the pyrolysis temperature is higher than 1000°C. In particular, the H_2 yields for the copper- and nickel-impregnated willows increases from 8 and 10.3 mol/kg of wood to 12.2 and 11.2 mol/kg of wood with a temperature increase from 1200 to 1600°C, respectively (**Figure 4.3**). The increase of H_2 yield is correlated with the increase of CO yields. It increases from 9.8 and 12.2 mol/kg of wood to 14.0 and 13.7 mol/kg of wood (**Figure 4.4**). The increase of both H_2 and CO yields is assumed to be mainly due to the cracking and reforming reactions of tar (Zeng et al. 2017a). Indeed, copper and nickel are used as efficient catalysts for tar decomposition reactions for producing H_2 and CO (Richardson et al. 2010; Yuan et al. 2015). It was reported that copper and nickel must be in the metal forms (Cu^0 and Ni^0) resulting in a catalytic effect on biomass pyrolysis reactions (Nzihou et al. 2019). At low temperature, sulfur and oxygen have a high affinity with copper and nickel, respectively (Said et al. 2018). Therefore, a threshold temperature is required in biomass pyrolysis to induce the decomposition of nickel sulfide and copper oxide for enhancing their catalytic effect. The presence of copper slightly decreases H_2 and CO yields at pyrolysis temperature below 1000°C. It is mainly interpreted as the inhibition effects of copper oxide on pyrolysis of biomass main components (cellulose and lignin) (Yuan et al. 2015). Nickel and copper could catalyze reforming reactions of CH_4 and C_2H_6 and reduce their yields (Zhao et al. 2009; Li et al. 2019). The enhanced cracking reactions of tar by nickel and copper catalysts favor the formation of CH_4 and C_2H_6 (Liu et al. 2017a), as shown in **Figure 4.6** and **Figure 4.1**. The slight increase of CH_4 and C_2H_6 can be explained by the competition between formation reactions and reforming reactions that is dominated by the latter at temperature above 1000°C. As shown in **Figure 4.5**, the reduction of CO_2 yield is mainly due to Cu and Ni promoting the reverse Boudouard reaction (Zhao et al. 2009; Liu et al. 2012). The catalytic effect of both metals leads to almost the same tendency in solar pyrolysis gas composition with temperature. However, their influence is more obvious at temperature above 1000°C and the catalytic effect of nickel is more pronounced than copper.

The LHVs of the gas products significantly vary with temperature as a result of the gas composition change (**Table 4.1**). The LHVs of total gas product for the raw willow increase from 0.7 to 8.2 MJ/kg of wood, as the temperature increase from 600 to 1600°C. This variation mainly results from the variation in the LHVs of H_2 and CO. Lower heating values of total gas product for the copper- and nickel-impregnated willows increase from 0.9 to 8.9 MJ/kg of wood and 2.1 to 8.7 MJ/kg of wood, respectively, as the temperature increase from 600 to 1600°C. They significantly increase to 7.3 MJ/kg of wood and to 8.1 MJ/kg of wood as temperature increases to 1200°C, respectively. Then, there is no significant change in the total LHVs at higher temperatures. This result indicates that the presence of either copper or nickel could lower optimum temperature as 1200°C for obtaining valuable combustible gas products.

Table 4.1. Combined effects of temperature and heavy metal on LHVs (low heating values) of the total gas product.

Temperature (°C)	LHVs of total gas product (MJ/kg of wood)		
	Raw-willow	Cu-willow	Ni-willow
600	0.73	0.87	2.05
800	2.65	1.6	3.09
1000	5.11	3.55	4.45
1200	5.95	7.33	8.09
1400	6.63	7.51	8.7
1600	8.18	8.92	8.74

4.2.2 Combined effects of heating rate and HM

4.2.2.1 Final product distribution with different heating rate

Product yields from solar pyrolysis of the raw and the impregnated willows at 1200°C under heating rates of 10°C/s and 50°C/s are presented in **Figure 4.7**. For the raw willow

pyrolysis, the gas yield ranges from 30.8% to 47.0% under heating rates of 10°C/s and 50°C/s, respectively. The liquid yield decreases from 54.5% to 42.7% as heating rate increases from 10°C/s to 50°C/s. Meanwhile, the char yield decreases from 14.7% to 10.3%. Fast heating rates favor the formation of volatiles versus char during biomass primary decomposition reactions (Sulaiman et al. 2011; Zeng et al. 2015c). Hence, the char yield decreases with a rise in heating rate. Furthermore, the pyrolysis temperature of 1200°C is much higher than the critical temperature of tar secondary reactions (about 500°C) (Aysu and Kucuk 2014; Boroson et al. 1989). Consequently, an increase in the gas yield is caused by the tar secondary reactions. The changing trend of pyrolysis product yields with heating rate is almost identical for the raw and impregnated willows (**Figure 4.7**). For the copper-impregnated willow pyrolysis, the gas yield increases from 31.8% to 48.0% when heating rate increases from 10 to 50°C/s. Meanwhile, the liquid and char yields decrease from 54.1% to 41.0% and from 14.0% to 11.0%, respectively. For the nickel-impregnated willow pyrolysis, the gas yield increases from 39.0% to 48.3% with the heating rate rising from 10°C/s to 50°C/s. The liquid and char yields decrease from 47.7% to 41.9% and 13.4% to 9.9%, respectively. There is almost no difference in the product distribution of raw and impregnated willows under different heating rates except for the nickel-impregnated willow at 10°C/s. It is noted that gas yield and liquid yield significantly increase and decrease with the increasing heating rates, respectively, for the nickel-impregnated willow in comparison with the raw willow. Heating rate of 10°C/s results in longer residence time of tar vapors (Zeng et al. 2015a). Furthermore, the nickel is an active catalyst for tar cracking reactions (Eibner et al. 2015). Indeed, since the nickel is bundled to the wood matrix, liquid should pass through the nickel layer before evolving out of the wood (Said et al. 2018). During the process, the time of tar contact with nickel is enough for enhancing the activity of tar secondary reactions into gas products.

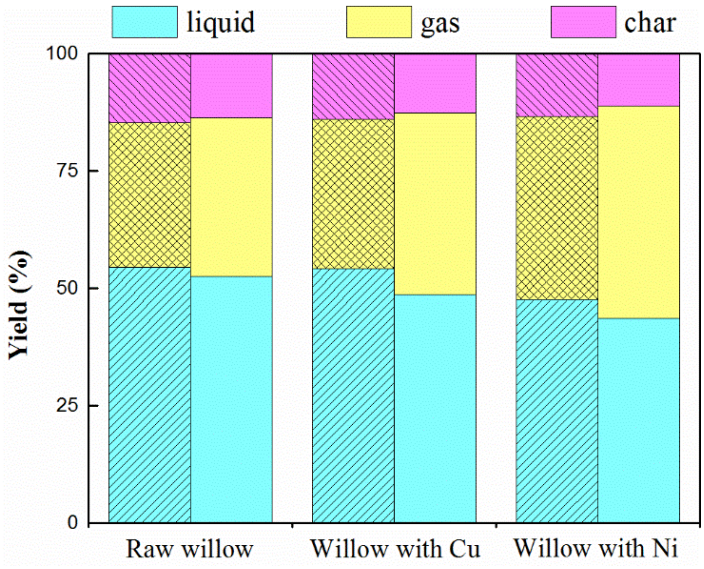

Figure 4.7. Combined effects of heating rate and heavy metal on solar pyrolysis product distribution at final temperature of 1200°C. Shaded area for 10°C/s and solid area for 50°C/s.

4.2.2.2 Pyrolysis gas composition and LHVs with different heating rates

The gas composition obtained from solar pyrolysis of raw and impregnated willows under different heating rates at 1200°C is illustrated in **Figure 4.8**. For the raw willow pyrolysis, the H_2, CO, and CO_2 yields remarkably increase from 6.3 to 12.1 mol/kg of wood, from 8.0 to 12.9 mol/kg of wood and from 0.7 to 1.2 mol/kg of wood, respectively, as the heating rate increases from 10 to 50°C/s. Simultaneously, the CH_4 and C_2H_6 yields slightly decrease from 1.7 to 1.4 mol/kg of wood and 0.5 to 0.3 mol/kg of wood, respectively. High heating rates favor the formation of primary volatiles, which tend to crack into H_2 and CO at 1200°C (Williams et al. 1996). The CO_2 increase is partly due to the inhibited reverse Boudouard reaction as its residence time inside the char reduced under higher heating rate (Beattie et al. 1983). Although some CH_4 and C_2H_6 are produced from the enhanced tar secondary reactions under high heating rates, their own cracking reaction is remarkably enhanced. The heavy metals change the trend of pyrolysis gas composition with heating rate (**Figure 4.8**).

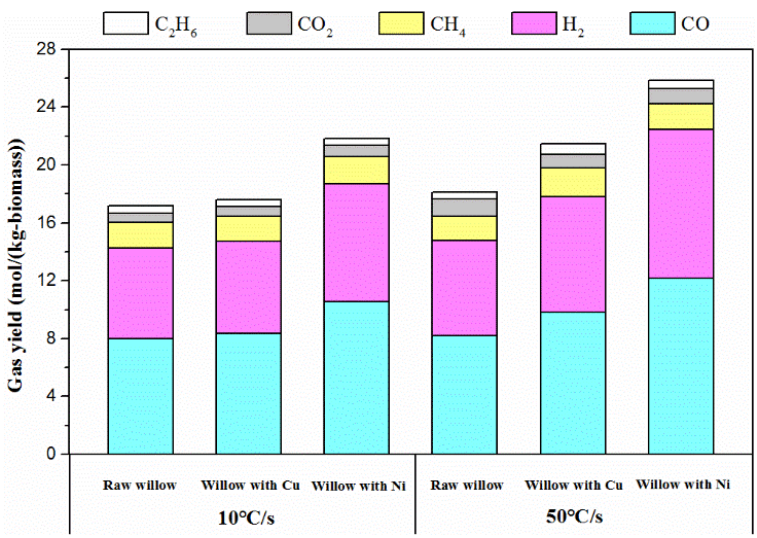

Figure 4.8. Combined effects of heating rate and heavy metal on solar pyrolysis gas composition at final temperature of 1200°C

Among them, CO_2 yields for pyrolysis of the copper- and nickel-impregnated willows decrease from 0.7 to 0.5 mol/kg of wood and 0.8 to 0.7 mol/kg of wood with increasing heating rate, respectively. Under a heating rate of 10°C/s, the gas composition is almost the same for the raw and copper-impregnated willows. While for the nickel-impregnated willow pyrolysis, the H_2 and CO yields increase to 8.2 and 10.5 mol/kg of wood in comparison with the raw willow, respectively. This finding agrees well with the nickel effect on product distribution indicated above. It also fits well with previous results indicating that nickel favored syngas production during cellulose pyrolysis (Li et al. 2019). Nickel can act as catalyst in pyrolysis and promote the dehydrogenation of benzene rings and cracking of carboxyl groups for H_2 and CO formation (Bru et al. 2007; Collard et al. 2012). Under a heating rate of 50°C/s, the presence of copper and nickel significantly decreases CO_2 yields. It is mainly due to the higher reactivity of char obtained at a heating rate of 50°C/s (Zeng et al. 2015c). In addition, the impregnated metals catalyze the gasification reactions with CO_2, which leads to the reduction of CO_2 yield (Said et al. 2017). The catalytic effect of both copper and nickel leads to the same tendency in the solar pyrolysis gas product yields with heating rate. However, the catalytic effect of nickel is more obvious: a 60% decrease in CO_2 production with nickel versus a 36% decrease with copper is observed.

The total gas product LHVs of the raw willow slightly increases from 5.9 to 6.0 MJ/kg of wood as the heating rate increases from 10 to 50°C/s. The total gas product LHVs of the copper- and nickel-impregnated willows increases from 5.9 to 7.3 MJ/kg of wood and 7.1 to 8.1 MJ/kg of wood, respectively. This increase is primarily due to variations in LHVs of CO, H_2, and CH_4. This result indicates that the heating rate effect on obtaining valuable combustible gas products is enhanced by the presence of either copper or nickel.

4.2.3 Conclusion

The experimental results on solar pyrolysis of metal-impregnated biomass indicate that the yields of char and liquid decrease with pyrolysis temperature and heating rate, while the gas yield significantly increases for the raw willow pyrolysis. A threshold temperature of 1000°C is required with the impregnated willow pyrolysis to make sure copper and nickel catalytic effects on promoting the cracking and reforming reactions of tar. Then, at 1200°C the gas yields from the copper- and nickel-impregnated willow pyrolysis increase by 14.8% and 34.5%, respectively, compared to the raw willow. In particular, the H_2 and CO production resulting from the nickel-impregnated willow solar pyrolysis is higher than from the raw willow (10.3 and 12.2 mol/kg of wood versus 6.6 and 8.2 mol/kg of wood) in case of fast pyrolysis (50°C/s). Under a heating rate of 10°C/s, the gas composition is almost the same for the raw and the copper-impregnated willows. While for the nickel-impregnated willow pyrolysis, the H_2 and CO yields increase from 6.3 and 8.0 to 8.2 and 10.5 mol/kg of wood in comparison with the raw willow, respectively. Both metals' catalytic effect leads to almost the same tendency in gas composition and LHVs with temperature or heating rate during solar pyrolysis. However, their influence is more obvious at temperature above 1000°C and a heating rate of 50°C/s. In addition, the catalytic effect of nickel is more pronounced than copper.

4.3 Pyrolysis of heavy metal contaminated biomass: Characterization of generated char

In this part, the char generated is characterized with various techniques. Characterizations address, the composition (**Section 4.3.1**), morphology and structure (**Section 4.3.2**), and mineral composition (**Section 4.3.3**). The char morphology and structure are characterized by Raman and BET analyses, and char mineral composition are studied by the ICP-OES and SEM-EDX methods.

Reference of the corresponding paper:

Zeng K, **Li R**, Doan PM, Elsa W, Nzihou A, Dian Z, Flamant G. Characterization of char generated from solar pyrolysis of heavy metal contaminated biomass. Energy, 2020, 206: 118128.

4.3.1 Char composition

Char yields obtained from solar pyrolysis of the heavy metal contaminated willow at different pyrolysis temperatures have already been indicated in our previous paragraph. It varied from 27, 24, and 22% to about 10% for the raw, Cu-impregnated and Ni-impregnated willow, respectively, for a temperature increasing from 600°C to 1600°C. **Figure 4.9** presents the elemental composition of the chars of the raw and impregnated willows under different pyrolysis temperatures and with heating rate of 50°C/s.

Regardless of the type of pyrolysis feedstock, the carbon mainly remains in char. This means that it becomes more aromatic (Hervy et al. 217). For the raw willow pyrolysis, carbon content increases from 70.0% to 88.4%, while the hydrogen and oxygen contents sharply decreases from 3.6% to 0.4% and 25.7% to 11.2%, respectively, with temperature increasing from 600 to 1600°C (**Figure 4.9a**). For the impregnated willow pyrolysis, the carbon contents also increases with declining hydrogen and oxygen contents. Carbon content increases from 71.0% to 87.7%, while hydrogen and oxygen contents decrease from

3.3% to 0.2% and 25.0% to 10.2% for the copper-contaminated willow pyrolysis char, respectively (**Figure 4.9b** and **c**). These results are consistent with the chemical composition of solar pyrolysis char explained by enhanced breaking of weak chemical bonds with increasing temperatures (Zeng et al. 2015b; 2017b).

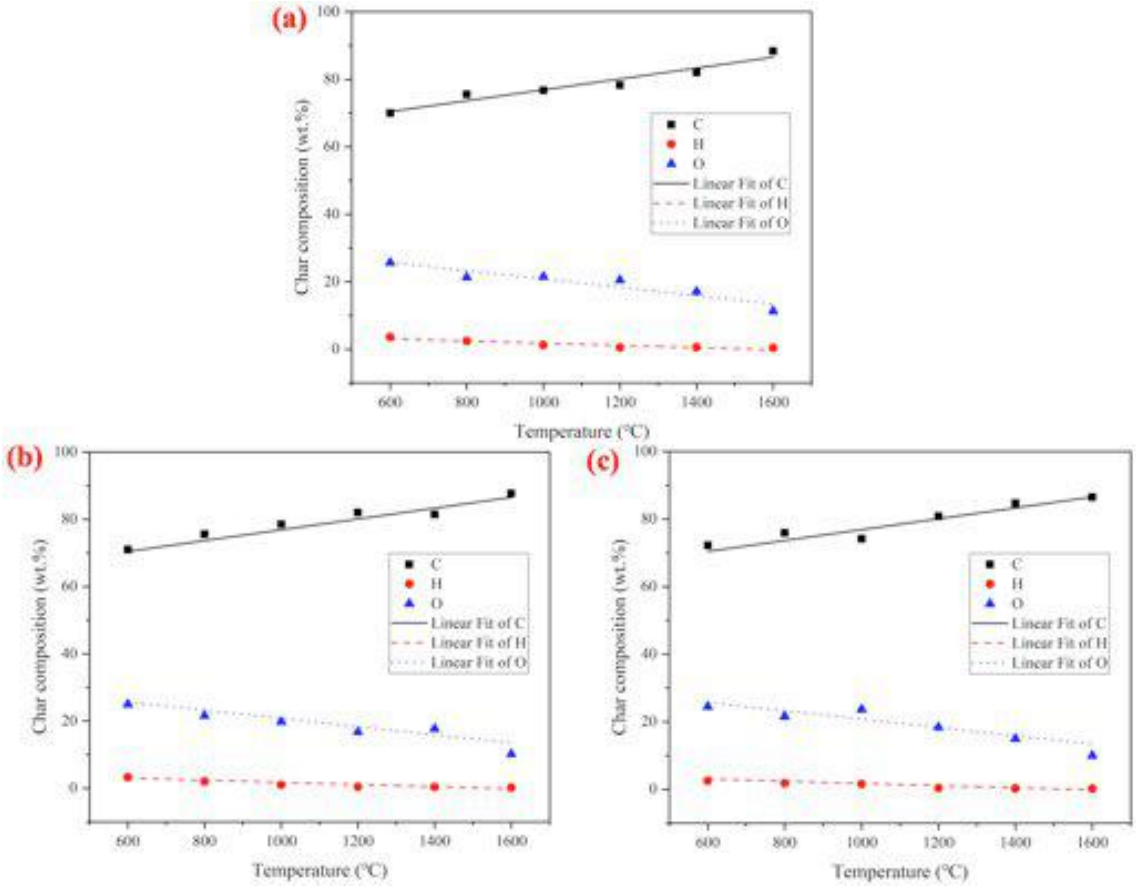

Figure 4.9. Effects of temperature and heavy metal contamination on solar pyrolysis char composition with heating rate of 50°C/s. a: raw willow; b: willow with Cu; and c: willow with Ni.

The presence of heavy metals (Cu or Ni) leads to a significant decrease of char hydrogen and oxygen contents compared to the raw willow char. In the temperature ranging from 600 to 1600°C, hydrogen and oxygen contents of the nickel-impregnated willow pyrolysis char decrease from 2.6% to 0.2% and 24.5% to 10.0%, respectively, compared to decrease from 3.6% to 0.4% and 25.7% to 11.2% for the raw willow (**Figure 4.9c**). It is assumed that copper or nickel could promotes depolymerization of cellulose and hemicellulose especially C-H and

C-O bonds cleavage (Nzihou et al. 2019). Besides, copper and nickel have noticeable catalytic activity with respect to tar cracking and reforming into H_2 and CO, which could further decrease hydrogen and oxygen contents in char (Said et al. 2018).

4.3.2 Char morphology and structure

4.3.2.1 Raman analysis

Initial data were fitted into Lorentzian profile, for the bands G (1580 cm^{-1}), D1 (1350 cm^{-1}), D2 (1620 cm^{-1}), and D4 (1150 cm^{-1}), and Gaussian profile, for the band D3 (1530 cm^{-1}) (Liu et al. 2015). Band G was used to study graphitic lattice, as an indicator of the char graphitic order. Bands D1 and D2 originate from disordered graphitic lattices vibration mode. Bands D3 and D4 are attributed to the amorphous carbon and mixed sp2-sp3 bonds, respectively (Xu et al. 2018). **Figure 4.10** shows the band area ratios, such as those of the defect bands to the band G denoted as I_{D1}/I_G, I_{D2}/I_G, I_{D3}/I_G, and I_{D4}/I_G, and that of the band G to the integrated area under the spectrum denoted as I_G/I_{All} for all chars.

The ratios I_{D1}/I_G, I_{D2}/I_G, and I_G/I_{All} correspond to microcrystalline planar size, graphitic domains thickness, and graphitic lattice proportion, respectively (Sheng 2007). The band area ratios of I_{D1}/I_G, I_{D2}/I_G, I_{D3}/I_G, and I_{D4}/I_G decrease along with the elevation of the pyrolysis temperature for all chars, while I_G/I_{All} increases (**Figure 4.10**). Different forms of structural and carbon crystallite defects are gradually eliminated during a severe heat treatment, as indicated by the downward trend of band area ratios (He et al. 2019). The correlation between the ratio I_{D1}/I_G and the crystallite size shows an inverse proportional behavior (Guizani et al. 2017). The decrease in I_{D1}/I_G means an increase in the average planar size of the graphite microcrystals. The decrease in I_{D3}/I_G and I_{D4}/I_G indicates that the amorphous phase of char is converted into a crystalline form. As a result, a more organized char structure is formed as the temperature increases, which leads to an increase in I_G/I_{All}.

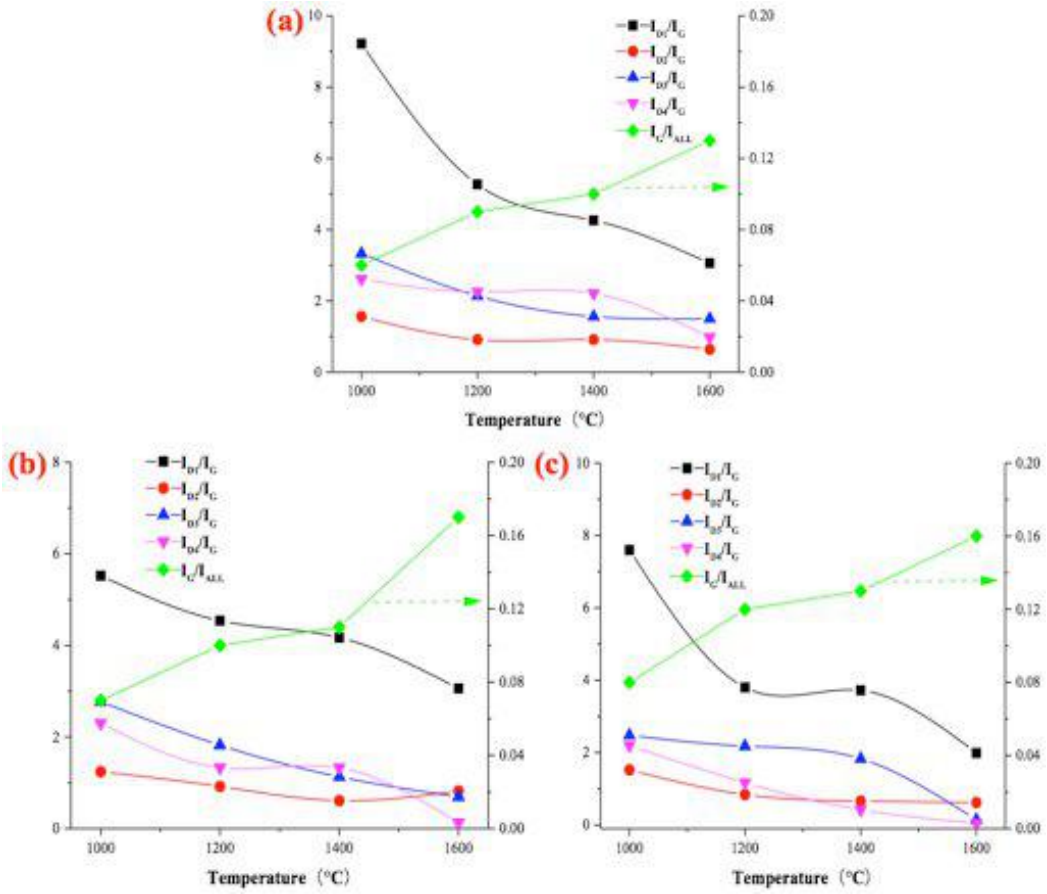

Figure 4.10. Effects of temperature and heavy metal contamination on Raman band area ratios of solar pyrolysis char. a: raw willow; b: willow with Cu; and c: willow with Ni.

For the impregnated willow pyrolysis chars, a similar trend of the band area ratios as a function of temperature is observed (**Figure 4.10b** and **c**). Generally, the Cu chars and Ni chars are found to have a higher I_G/I_{All} ratio and lower I_{D1}/I_G, I_{D2}/I_G, I_{D3}/I_G, and I_{D4}/I_G ratios than the raw willow, implying to be more ordered and aromatic than the raw chars generated at the same temperature in the range of 1000-1600°C. Besides, the presence of heavy metals (Cu or Ni) during willow pyrolysis increases large proportion of aromatic rings as indicated by the lower I_{D1}/I_G ratio compared to the raw willow. Tay et al. (2014) found that the presence of minerals favored the formation of large aromatic ring systems in reducing atmosphere. The I_{D3}/I_G and $I_{D4}/_{IG}$ ratios were regarded as indicators for char active sites (Xu et al. 2018). Chars derived from the metal-impregnated willow pyrolysis exhibit a lower $I_{(D3+D4)}/I_G$ than the raw willow char, which denotes a lower reactivity. It is mainly due to amorphous carbon and mixed sp2-sp3 bonds disappearing with the catalytic effect of Cu and

Ni during pyrolysis.

4.3.2.2 BET analysis

Table 4.2 shows the effects of temperature and HM contamination on BET surface area. For both chars generated from the raw and impregnated willows, BET surface area exhibits a drastic variation with temperature with a sharp maximum at about 1000°C in the temperature range of 600-1600°C. These results are in agreement with the literature data showing that rice straw pyrolysis char total surface area firstly increased with temperature up to 900^{o}C and then decreased at higher temperatures (Fu et al. 2012). The increase could be attributed to the intensifying volatile release during pyrolysis, resulting in the formation of internal porous structure (Li et al. 2019). However, thermal deactivation of char might dominate during pyrolysis over 900^{o}C, which induced pore fuse, structure ordering and char melting (Lu et al. 2002).

Table 4.2. Effects of temperature and heavy metal contamination on solar pyrolysis char BET surface area.

Char samples	Temperature (^{o}C)	BET surface area (m^2/g)
Raw-willow	600	5.3
Raw-willow	1000	161.0
Raw-willow	1600	21.2
Cu-willow	600	7.8
Cu-willow	1000	320.0
Cu-willow	1600	41.5
Ni-willow	600	10.2
Ni-willow	1000	359.0
Ni-willow	1600	60.2

The BET surface area of raw willow char (161 m^2/g) obtained at 1000^{o}C is drastically lower than that of the Cu contaminated willow char (320 m^2/g) and the Ni contaminated

willow char (359 m^2/g), implying that the presence of heavy metal affects strongly the BET surface area. The heavy metals (Cu and Ni) promote C-H and C-O bonds cleavage from char with enhancing gas release, which favors micropore formation (Stals et al. 2010). However, there is almost no difference of BET surface area for chars of the raw and contaminated willows at 600^{o}C. This result agrees with the literature data explaining that, at this temperature, some micropores are blocked by heavy metal nanoparticles even considering their catalytic effect on gas formation (Shen et al. 2015; Liu et al. 2017b).

4.3.3 Char mineral composition

4.3.3.1 ICP-OES

Analysis of ICP-OES was carried out for the chars prepared with the raw and contaminated willows at different pyrolysis temperatures. The mineral elements shown in **Figure 4.11** are mainly categorized into Alkali and Alkaline Eearth Metals (A&AEMs) elements (Ca, K, Mg, and Na), Si and heavy metal elements (Cu and Ni) according to their abundant order. As can be seen, A&AEMs elements in the raw willow chars are majority, their amounts are about 300 times larger than the heavy metal elements. In addition, heavy metal element concentrations are very low indicating no risk (Azargohar et al. 2014). As temperature increases from 600 to 800^{o}C, pyrolysis causes enrichment of A&AEMs elements in the char. For instance, the concentration of Ca and K increases from 11,473 and 2457 mg/kg at 600^{o}C to 15,230 and 3573 mg/kg, respectively, at 800^{o}C. This finding agrees well with other similar study (Wang et al. 2017). This trend could be due to the combined effect of two processes: decomposition of organic compounds with volatile release and evaporation of inorganic elements (He et al. 2019). The first process causes strong loss of C, H, and O elements in solid matrix contributing to the increase of mineral element relative contents. The second process induces volatilization of mineral elements. Organic compound decomposition seems to be dominant over mineral element evaporation as their volatilization rates are small at this temperature range.

Contrarily, A&AEMs element contents decrease in the char with pyrolysis temperature further increasing from 800 to 1600°C. This result is consistent with the change of dominant process, metal vaporization becoming more and more intense with the temperature increase (Dong et al. 2015). In contrast, pyrolysis temperature from 600 to 1600°C has no influence on the volatilization of Cu and Ni (Bert et al. 2017). As a result, the Cu and Ni element contents increase in all of the char due to the enhanced organic compound decomposition. Besides, there is a small increase of A&AEMs elements content in the char from the willow wood impregnated with Cu or Ni compared to those of the raw willow char. This trend is assumed to be linked with the catalytic effects of Cu or Ni for promoting C-H and C-O bond cleavage from char (Stals et al. 2010).

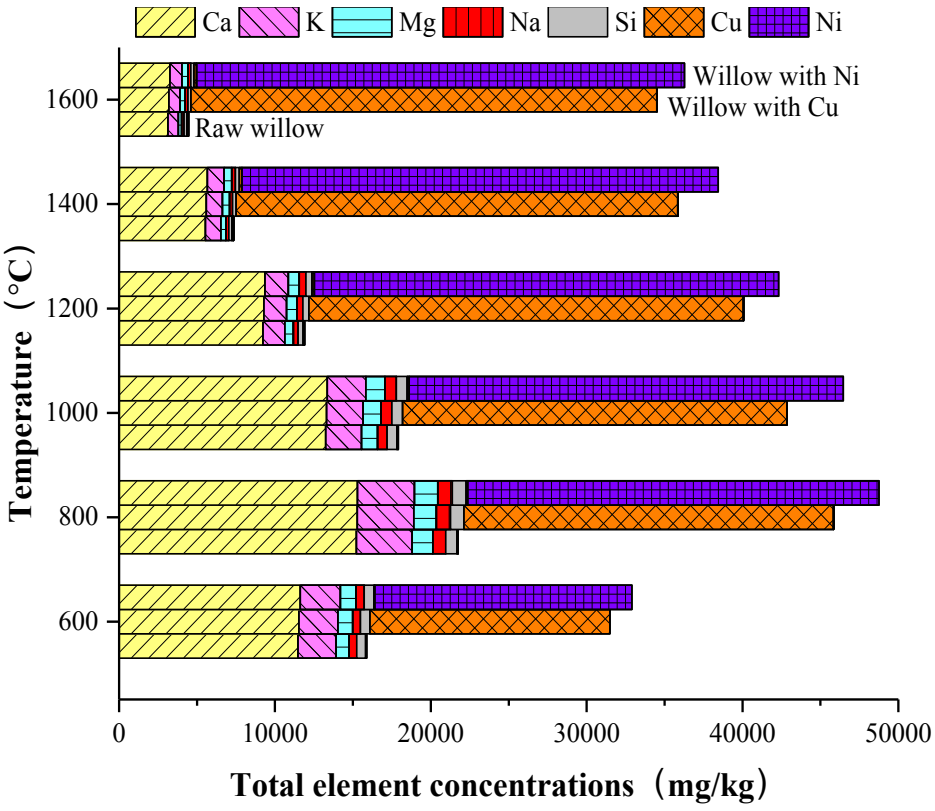

Figure 4.11. Effects of temperature and heavy metal contamination on solar pyrolysis char mineral element concentration.

4.3.3.2 SEM-EDX

Figure 4.12 presents SEM images of the raw willow char prepared at 600, 1000, 1600°C and heating rate of 50°C/s with EDX analysis of selected areas. As shown in **Figure 4.12a**, 600°C raw willow char contains mainly large fibrous texture nodules with some spherical shape and cavities. Char chemical composition is not uniform at micro-scale (Hervy et al. 2017). One white cubic grain can be clearly seen in the **Figure 4.12a**, as indicated by rectangle with an arrow. From this grain, high content of Ca with some carbon and oxygen is detected by EDX analysis. Besides, traces of Cu and Ni are also detected. One can assume that calcium carbonate is initially at this location and not moving on the surface. It is not possible to confirm the diffusion of minerals from the core to the surface at this stage.

As the pyrolysis temperature increases to 1000°C, more twisted and rough char is formed with some pore collapse (**Figure 4.12b**). It is due to the intensified volatile release with the temperature increase resulting in more cracks and pores formation (Jin et al. 2016). It indicates that increasing pyrolysis temperature to a certain extent benefits the char porosity increase as confirmed by previous BET analysis (Li et al. 2019). However, char partial melting is observed as indicated by the rectangle, at this location high concentrations of Si, K, and Ca are detected by EDX analysis. During pyrolysis at 1000°C, K vaporizes and migrates from biomass matrix to its surface. Potassium silicates might form when K vapour contacts with silica, whose melting temperature was about 600°C (Wornat et al. 1995). The widely distributed A&AEMs elements like Ca as oxides in biomass tend to react with molten potassium silicates to form K-Ca-silicates (Wang et al. 2015). Besides, alkaline elements amount in 1000°C char grains reduce compared to those in 600°C char. It indicates more intensive alkaline elements vaporization at higher temperature than 1000°C. Increasing pyrolysis temperature promotes A&AEMs species vaporization, mainly M_XCO3 and M_XO, leaving cavities on char surfaces (Wornat et al. 1995).

When pyrolysis temperature increases to 1600°C, the char experiences plastic deformation (**Figure 4.12c**). A smooth and compact structure of char surface is developed due to sintering effect, in agreement with our previous study (Zeng et al. 2015b). At severe

devolatilization condition like high temperature, char plastic transformation may occur due to solid matrix softening and cell structure melting, which leads to pore closing (Wang et al. 2013). EDX analyses of small grains on char surfaces reveal that most of A&AEMs elements migrate and coalesce during vaporization. Meanwhile, small part of A&AEMs is retained and stays incorporated into char matrix. The 1600°C char particles have significantly higher content of Cu and Ni in the small grains on char surface than those of 600 and 1000°C char because almost no volatilization of Cu and Ni occurs (Bert et al. 2017).

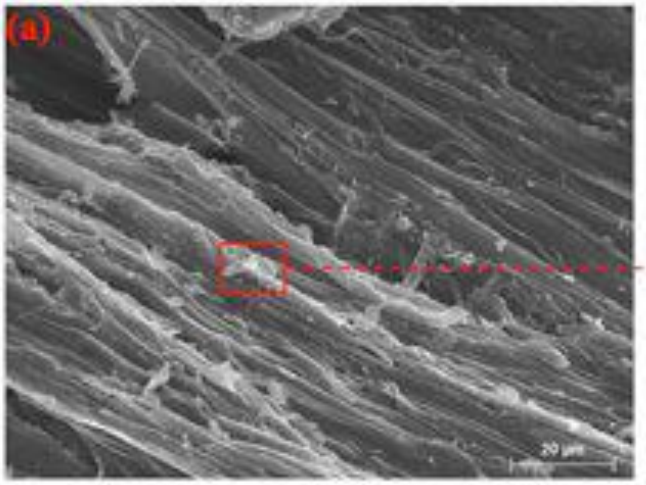

Elem	wt. %
C	70.5
O	13.7
Ca	14.7
Cu	0.8
Ni	0.3

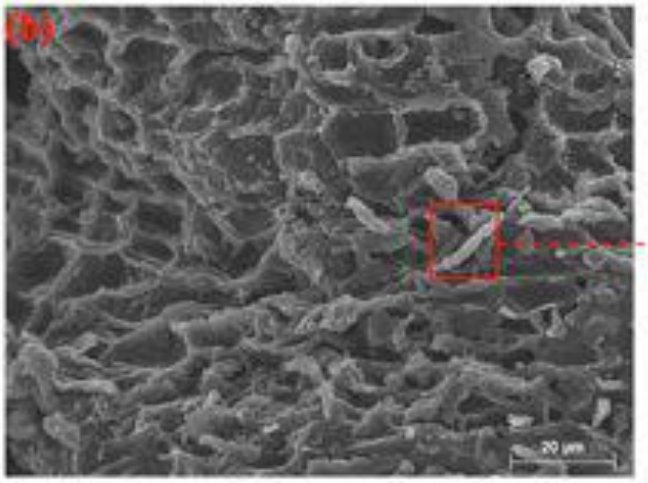

Elem	wt. %
C	74.5
O	7.2
Ca	9.2
Si	3.2
K	4.2
Cu	1.1
Ni	0.6

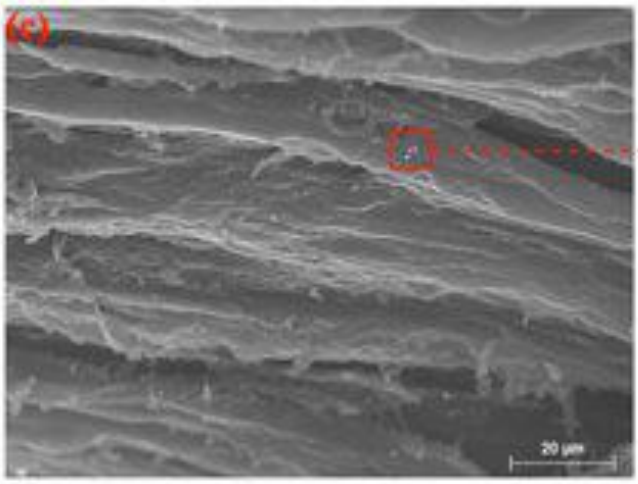

Elem	wt. %
C	87.5
O	1.5
Ca	4.2
K	1.0
Cu	4.1
Ni	1.7

Figure 4.12. SEM-EDX analysis of solar pyrolysis raw willow char prepared with heating rate of 50°C/s. a: 600°C; b: 1000°C; and c: 1600°C.

The changing trend of char morphology with temperature was almost the same for the raw and the heavy metal impregnated willows. Images obtained by SEM with corresponding EDX of chars prepared with the Cu and Ni impregnated willows at 1600°C are presented in

Figure 4.13. There are few A&AEMs, such as Ca, on char surface grains. While the Cu content in the Cu-impregnated willow char (**Figure 4.13a**) and the Ni content in the Ni-impregnated willow char (**Figure 4.13b**) increase significantly compared to the raw willow char, indicating that the impregnated Cu or Ni has been embedded into carbon matrix. According to the EDX analysis, the Cu content in Cu-char grain and the Ni content in Ni-char grain increase to 15.6% and 14.3%, respectively. These results are in agreement with literature about Fe and Ni enrichment in their impregnated rice husk pyrolysis char (Liu et al. 2017).

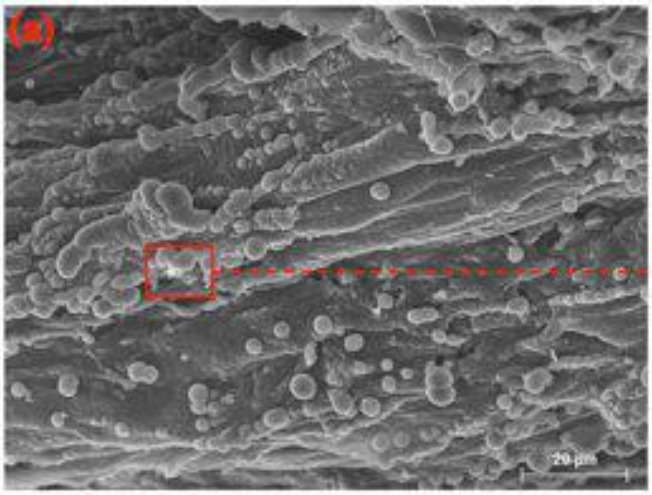

Elem	wt. %
C	78.5
O	1.8
Ca	2.2
Cu	15.6
Ni	1.9

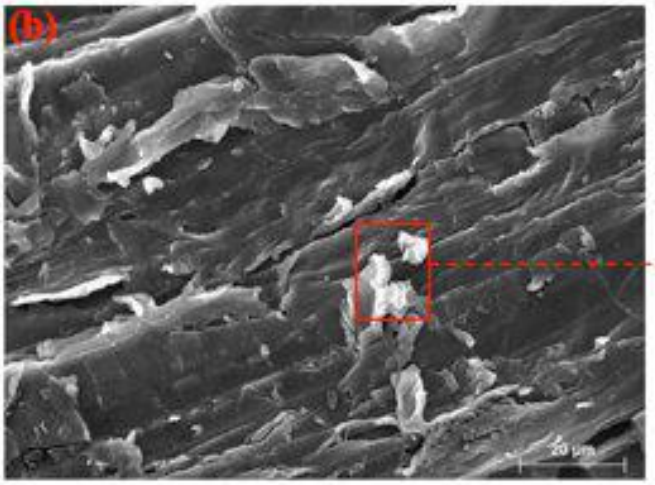

Elem	wt. %
C	80.2
O	1.1
Ca	1.7
Cu	2.7
Ni	14.3

Figure 4.13. SEM-EDX analysis of solar pyrolysis heavy metal contaminated willow char at 1600°C. a: with Cu; and b: with Ni.

4.3.4 Conclusion

Solar pyrolysis temperature and heavy metals affect the char properties. A more

ordered and aromatic char is formed with increasing pyrolysis temperature, in which carbon content increases while hydrogen and oxygen contents decline. Char BET surface area exhibits a maximum at approximately 1000°C, the decrease at higher temperature is due to plastic deformation. Besides, the BET surface area of raw willow char (161 m^2/g) obtained at 1000^oC is lower than that of the Cu contaminated willow char (320 m^2/g) and the Ni contaminated willow char (359 m^2/g). Pyrolysis causes enrichment of alkaline elements in the char as temperature increases from 600 to 800°C. At higher temperature, alkaline content decreases due to enhanced vaporization. The addition of Cu or Ni leads to the decrease of hydrogen and oxygen contents. Contrarily, the significant increase of Ni or Cu in char with temperature indicates that the vaporization of both metals is small by comparison with alkaline elements. The copper and nickel contaminated willow pyrolysis chars are found more organized in comparison with the raw willow char as confirmed by the Raman spectra showing a higher I_G/I_{All} ratio and lower I_{D1}/I_G, I_{D2}/I_G, and I_{D3}/I_G ratios.

4.4 Bibliography

Aysu T, Kucuk MM. Biomass pyrolysis in a fixed-bed reactor: Effects of pyrolysis parameters on product yields and characterization of products. Energy, 2014, 64: 1002–1025.

Azargohar R, Nanda S, Kozinski JA, Dalai AK, Sutarto R. Effects of temperature on the physicochemical characteristics of fast pyrolysis bio-chars derived from Canadian waste biomass. Fuel, 2014, 125: 90–100.

Beattie WH, Berjoan R, Coutures J-P. High-temperature solar pyrolysis of coal. Solar Energy, 1983, 31: 137–143.

Bert V, Allemon J, Sajet P, Dieu S, Papins A, Collet S, Gaucher R, Chalot M, Michiels B, Raventos C. Torrefaction and pyrolysis of metal-enriched poplars from

phytotechnologies: Effect of temperature and biomass chlorine content on metal distribution in end-products and valorization options. Biomass and Bioenergy, 2017, 96: 1–11.

Boroson ML, Howard JB, Longwell JP, Peters AW. Products yields and kinetics from the vapor phase cracking of wood pyrolysis tars. AIChE Journal, 1989, 35: 120–128.

Bru K, Blin J, Julbe A, Volle G. Pyrolysis of metal impregnated biomass: An innovative catalytic way to produce gas fuel. Journal of Analytical and Applied Pyrolysis, 2007, 78: 291–300.

Chhiti Y, Salvador S, Commandre J, Broust F. Thermal decomposition of bio-oil: Focus on the products yields under different pyrolysis conditions. Fuel, 2012, 102: 274–281.

Collard F, Blin J, Bensakhria A, Valette J. Influence of impregnated metal on the pyrolysis conversion of biomass constituents. Journal of Analytical and Applied Pyrolysis, 2012, 95: 213–226.

Di Blasi C. Modeling chemical and physical processes of wood and biomass pyrolysis. Progress in Energy and Combustion Science, 2008, 34: 47–90.

Di Blasi C. Combustion and gasification rates of lignocellulosic chars. Progress in Energy and Combustion Science, 2009, 35: 121–140.

Dong J, Chi Y, Tang YJ, Ni MJ, Nzihou A, Weiss-Hortala E, Huang QX. Partitioning of heavy metals in municipal solid waste pyrolysis, gasification, and incineration. Energy & Fuels, 2015, 29: 7516–7525

Eibner S, Broust F, Blin J, Julbe A. Catalytic effect of metal nitrate salts during pyrolysis of impregnated biomass. Journal of Analytical and Applied Pyrolysis, 2015, 113: 143–152.

Fu P, Hu S, Xiang J, Sun LS, Su S, Wang J. Evaluation of the porous structure development of chars from pyrolysis of rice straw: Effects of pyrolysis temperature and heating rate. Journal of Analytical and Applied Pyrolysis, 2012, 98: 177–183.

Guizani C, Haddad K, Limousy L, Jeguirim M. New insights on the structural evolution of biomass char upon pyrolysis as revealed by the Raman spectroscopy and elemental analysis. Carbon, 2017, 119: 519–521.

He J, Strezov V, Kan T, Weldekidan H, Asumadu-Sarkodie S, Kumar R. Effect of temperature on heavy metal(loid) deportment during pyrolysis of *Avicennia marina* biomass

obtained from phytoremediation. Bioresource Technology, 2019, 278: 214–222.

He X, Zeng K, Xie YP, Flamant G, Yang HP, Yang XY, Nzihou A, Zheng AQ, Ding Z, Chen HP. The effects of temperature and molten salt on solar pyrolysis of lignite. Energy, 2019, 181: 407–416.

Hervy M, Berhanu S, Weiss-Hortala E, Chesnaud A, Gérente C, Villot A, Pham Minh D, Thorel A, Coq LL, Nzihou A. Multi-scale characterisation of chars mineral species for tar cracking. Fuel, 2017, 189: 88–97.

Jin JW, Li YN, Zhang JY, Wu SC, Cao YC, Liang P, Zhang J, Wong MH, Wang MY, Shan SD, Christie P. Influence of pyrolysis temperature on properties and environmental safety of heavy metals in biochars derived from municipal sewage sludge. Journal of Hazardous Materials, 2016, 320: 417–426.

Li RH, Huang H, Wang JJ, Liang W, Gao PC, Zhang ZQ, Xiao R, Zhou BY, Zhang XF. Conversion of Cu(II)-polluted biomass into an environmentally benign Cu nanoparticles-embedded biochar composite and its potential use on cyanobacteria inhibition. Journal of Cleaner Production, 2019, 216: 25–32.

Liu W, Tian K, Jiang H, Zhang X, Ding H, Yu H. Selectively improving the bio-oil quality by catalytic fast pyrolysis of heavy-metal-polluted biomass: Take copper (Cu) as an example. Environmental Science & Technology, 2012, 46: 7849–7856.

Liu Y, Guo F, Li X, Li T, Peng K, Guo C, Chang J. Catalytic effect of iron and nickel on gas formation from fast biomass pyrolysis in a microfluidized bed reactor: A kinetic study. Energy Fuels, 2017b, 31: 12278–12287.

Liu W, Li W, Jiang H, Yu H. Fates of chemical elements in biomass during its pyrolysis. Chemical Reviews, 2017a, 117: 6367–6398.

Liu XH, ZhengY, Liu ZH, Ding HR, Huang XH, Zheng CG. Study on the evolution of the char structure during hydrogasification process using Raman spectroscopy. Fuel, 2015, 157: 97–106.

Lopez-Gonzalez D, Fernandez-Lopez M, Valverde JL, Sanchez-Silva L. Pyrolysis of three different types of microalgae: Kinetic and evolved gas analysis. Energy, 2014, 73: 33–43.

Lu LM, Kong CH, Sahajwalla V, Harris D. Char structural ordering during pyrolysis and

combustion and its influence on char reactivity. Fuel, 2002, 81: 1215–1225.

Morf P, Hasler P, Nussbaumer T. Mechanisms and kinetics of homogeneous secondary reactions of tar from continuous pyrolysis of wood chips. Fuel, 2002, 81: 843–853.

Neves D, Thunman H, Matos A, Tarelho L, Gomez-Barea A. Characterization and prediction of biomass pyrolysis products. Progress in Energy and Combustion Science, 2011, 37: 611–630.

Nzihou A, Stanmore B, Lyczko N, Minh DP. The catalytic effect of inherent and adsorbed metals on the fast/flash pyrolysis of biomass: A review. Energy, 2019, 170: 326–337.

Richardson Y, Blin J, Volle G, Motuzas J, Julbe A. *In situ* generation of Ni metal nanoparticles as catalyst for H_2-rich syngas production from biomass gasification. Applied Catalysis A: General, 2010, 382: 220–230.

Said M, Cassayre L, Dirion J, Joulia X, Nzihou A. Effect of nickel impregnation on wood gasification mechanism. Waste and Biomass Valorization, 2017, 8: 2843–2852.

Said M, Cassayre L, Dirion J, Nzihou A, Joulia X. Influence of nickel on biomass pyro-gasification: Coupled thermodynamic and experimental investigations. Industrial & Engineering Chemistry Research, 2018, 57: 9788–9797.

Septien S, Valin S, Dupont C, Peyrot M, Salvador S. Effect of particle size and temperature on woody biomass fast pyrolysis at high temperature (1000-1400°C). Fuel, 2012, 97: 202–210.

Shen YF, Chen MD, Sun TH, Jia JP. Catalytic reforming of pyrolysis tar over metallic nickel nanoparticles embedded in pyrochar. Fuel, 2015, 159: 570–579.

Sheng CD. Char structure characterised by Raman spectroscopy and its correlations with combustion reactivity. Fuel, 2007, 86: 2316–2324.

Stals M, Thijssen E, Vangronsveld J, Carleer R, Schreurs S, Yperman J. Flash pyrolysis of heavy metal contaminated biomass from phytoremediation: Influence of temperature, entrained flow and wood/leaves blended pyrolysis on the behavior of heavy metals. Journal of Analytical and Applied Pyrolysis, 2010, 87: 1–7.

Sulaiman F, Abdullah N. Optimum conditions for maximising pyrolysis liquids of oil palm empty fruit bunches. Energy, 2011, 36: 2352–2359.

Tay HL, Kajitani S, Wang S, Li CZ. A preliminary Raman spectroscopic perspective for the roles

of catalysts during char gasification. Fuel, 2014, 121: 165–172.

Wang L, Li T, Güell BM, Løvås T, Sandquist J. An SEM-EDX study of forest residue chars produced at high temperatures and high heating rate. Energy Procedia, 2015, 75: 226–231.

Wang L, Sandquist J, Varhegyi G, Güell BM. CO_2 gasification of chars prepared from wood and forest residue: A kinetic study. Energy & Fuels, 2013, 27: 6098–6107.

Wang SS, Gao G, Li TC, Ok YS, Shen CF, Xue SG. Biochar provides a safe and value-added solution for hyperaccumulating plant disposal: A case study of *Phytolacca acinosa* Roxb. (Phytolaccaceae). Chemosphere, 2017, 178: 59–64.

Williams PT, Besler S. The influence of temperature and heating rate on the slow pyrolysis of biomass. Renewable Energy, 1996, 7: 233–250.

Wornat MJ, Hurt RH, Yang NYC, Headley TJ. Structural and compositional transformations of biomass chars during combustion. Combustion and Flame, 1995, 100: 131–143.

Xing S, H Yuan, Huhetaoli, Qi Y, Lv P, Yuan Z, Chen Y. Characterization of the decomposition behaviors of catalytic pyrolysis of wood using copper and potassium over thermogravimetric and Py-GC/MS analysis. Energy, 2016, 114: 634–646.

Xu M, Hu HY, Yang YH, Huang YD, Xie K, Liu H, Li X, Yao H, Naruse I. A deep insight into carbon conversion during Zhundong coal molten salt gasification. Fuel, 2018, 220: 890–897.

Yuan H, Xing S, Huhetaoli, Lu T, Chen Y. Influences of copper on the pyrolysis process of demineralized wood dust through thermogravimetric and Py-GC/MS analysis. Journal of Analytical and Applied Pyrolysis, 2015, 112: 325–332.

Zeng K, Doan PM, Gauthier D, Weiss-Hortala E, Nzihou A, Flamant G. The effect of temperature and heating rate on char properties obtained from solar pyrolysis of beech wood. Bioresource Technology, 2015c, 182: 114–119.

Zeng K, Gauthier D, Doan PM, Weiss-Hortala E, Nzihou A, Flamant G. Characterization of solar fuels obtained from beech wood solar pyrolysis. Fuel, 2017b, 188: 285–293.

Zeng K, Gauthier D, Li R, Flamant G. Solar pyrolysis of beech wood: Effects of pyrolysis parameters on the product distribution and gas product composition. Energy, 2015a, 93: 1648-1657.

Zeng K, Gauthier D, Li R, Flamant G. Combined effects of initial water content and heating parameters on solar pyrolysis of beech wood. Energy, 2017a, 125: 552–561.

Zeng K, Gauthier D, Lu J, Flamant G. Parametric study and process optimization for solar pyrolysis of beech wood. Energy Conversion and Management, 2015b, 106: 987–998.

Zeng K, Pham Minh D, Gauthier D, Weiss-Hortala E, Nzihou A, Flamant G. The effect of temperature and heating rate on char properties obtained from solar pyrolysis of beech wood. Bioresource Technology, 2015b, 182: 114–119.

Zhao M, Florin NH, Harris AT. The influence of supported Ni catalysts on the product gas distribution and H_2 yield during cellulose pyrolysis. Applied Catalysis B: Environmental, 2009, 92: 185–193.

Chapter 5

Modeling of Solar Pyrolysis

5.1 Introduction

This modelling stage aims at predicting the temperature change according to the time and axial position during the first minutes of the solar pyrolysis of biomass pellets through simulation with the help of MATLAB and Excel.

A conduction model was developed to describe the temperature evolution inside the pellets. A kinetic scheme form literature involving the primary and the secondary reactions is adopted to carry out the simulations of temperature. A finite difference method is used for solving the heat transfer equation with an explicit scheme. An analytical equation taken from the kinetic scheme is used to evaluate the consumption of biomass.

This model is a first simple approach that needs to be improved in the future.

- **Section 5.2** introduces the model and the numerical approach.

- **Section 5.3** describes parameter settings, such as thermo-physical values, temperature profile, biomass consumption, power, and characteristic evolution, considered during the simulation of solar pyrolysis process using pine wood as a testing material.

- **Section 5.4** gives a conclusion and prospect of the simulation of solar pyrolysis. Biomass consumption and temperature distribution is associated with time and axial position. A simple model can describe the overall evolution of a complex set of pyrolysis process. Such a model can be used to predict the temperature and concentration of different biomass types. However, an experimental verification is needed.

5.2 Modeling of solar pyrolysis

5.2.1 Equations of the model

5.2.1.1 Kinetics

In order to describe the heat transfer during the pyrolysis process, a simple dynamic model was developed. Pyrolysis can be described by several reaction schemes, some of which are slightly more detailed than others. In fact, a choice can be made between multiple mechanisms. Here are three examples are illustrated (**Figure 5.1)**.

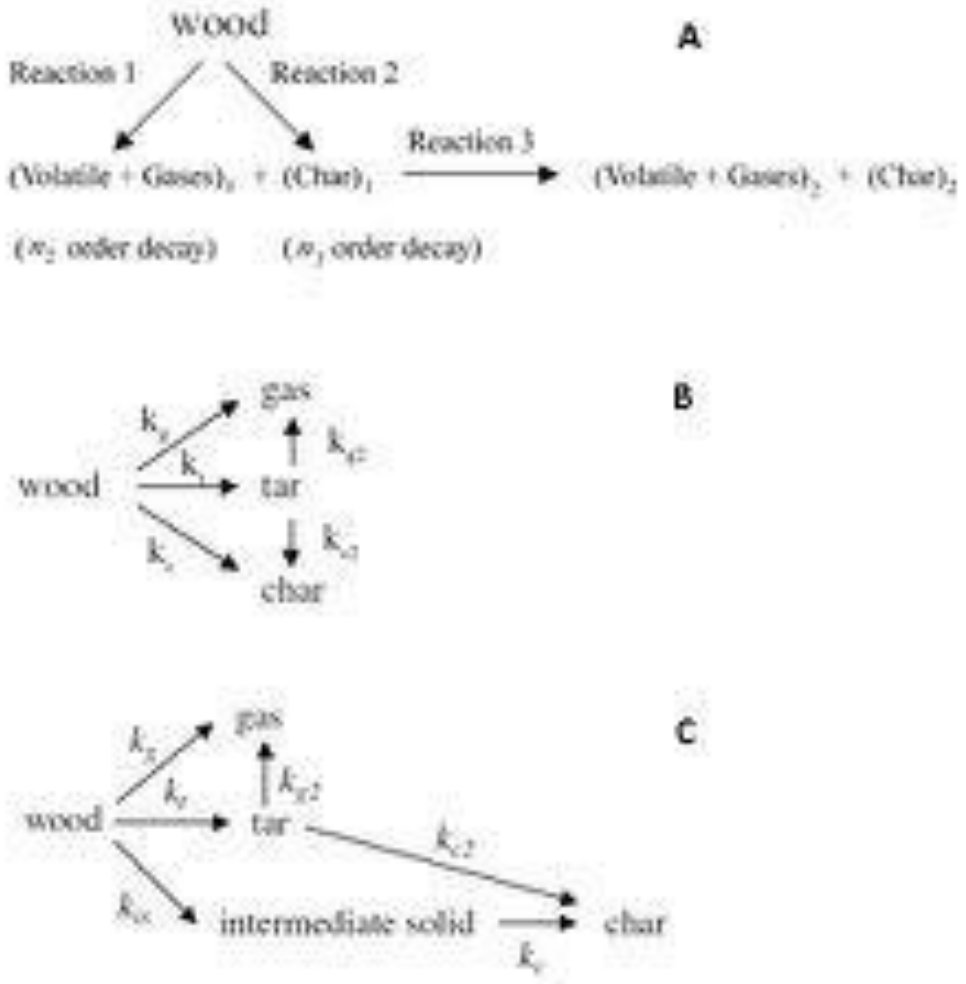

Figure 5.1 Reaction scheme Model 1 (A) (Babu and Chaurasia 2002), Model 2 (B) (Blasi 2002), and Model 3 (C) (Koufopanos et al. 1991)

In order to model, we use the first model proposed by Babu et al. (2002). This model is chosen for simplicity. During the reaction, the solid density changes with time, expressed as $\partial\rho/\partial t$, which is easy to operate when inserted into the conductive model. The biomass decomposed into gas, volatile ("including tar") and char after three reactions. The kinetic equation is shown below (Koufopanos et al. 1991).

$$\frac{\partial C_B}{\partial t} = -k_1 {C_B}^{n_1} - k_2 {C_B}^{n_1}$$

$$\frac{\partial C_{G_1}}{\partial t} = k_1 {C_B}^{n_1} - k_3 {C_{G_1}}^{n_2} {C_{C_1}}^{n_3}$$

$$\frac{\partial C_{C_1}}{\partial t} = k_2 {C_B}^{n_1} - k_3 {C_{G_1}}^{n_2} {C_{C_1}}^{n_3}$$

$$\frac{\partial C_{G_2}}{dt} = k_3 {C_{G_1}}^{n_2} {C_{C_1}}^{n_3}$$

$$\frac{\partial C_{C_2}}{\partial t} = k_3 {C_{G_1}}^{n_2} {C_{C_1}}^{n_3}$$

k_i is kinetic constant of the reaction, n_i is the order of reaction, and C_i is biomass, gas (volatile plus gas), and char concentration. For consistency, the concentration of each compound is always the same unit kg/m^3.

$$k_1 = A_1 \exp\left(\frac{D_1}{T} + \frac{L_1}{T^2}\right) \qquad k_2 = A_2 \exp\left(\frac{D_2}{T} + \frac{L_2}{T^2}\right) \qquad k_3 = A_3 \exp\left(\frac{E_3}{R_C T}\right)$$

Table 5.1. Adapted values for the kinetic constants (Koufopanos et al. 1991).

i	A_i	D_i	L_i	E_i
1	$9.973 * 10^{-5} \mathrm{s}^{-1}$	17254.4 K	-9061227 K²	-
2	$1.068 * 10^{-3} \mathrm{s}^{-1}$	10224.4 K	-6123081 K²	-
3	$5.7 * 10^{5} \mathrm{s}^{-1}$	-	-	81 kJ/mol

From these equations we can determine the variation of the density versus time (**Equation 5.1**) that serves for the heat transfer equation.

$$\frac{\partial \rho}{\partial t} = \frac{\partial C_B}{\partial t} + \frac{\partial C_{C_1}}{\partial t} + \frac{\partial C_{C_2}}{\partial t} = -k_1 {C_B}^{n_1} \qquad (5.1)$$

It is not necessary to find all concentrations of products and reagents related to the reaction. In fact, we only need the evolution of biomass concentration versus time. Since the consumption of biomass is easy to be integrated, an anaclitic solution of the first kinetic equation is used.

$$\frac{\partial C_B}{\partial t} = -k_1 {C_B}^{n_1} - k_2 {C_B}^{n_1} \rightarrow \frac{\partial C_B}{\partial t} = -(k_1 + k_2) {C_B}^{n_1} \rightarrow \frac{\partial C_B}{{C_B}^{n_1}} = -(k_1 + k_2) \partial T$$

$$n_1 = 0 \;\rightarrow\; C_B = -(k_1 + k_2) t + C_{B_0}$$

$$n_1 = 1 \;\rightarrow\; C_B = C_{B_0} \exp\left(-(k_1 + k_2) t\right)$$

After analyzing the two options, it is suitable for high temperature to apply the second condition, the order of $n_1 = 1$ to express C_B.

5.2.1.2 Geometry

A 1D geometry is assumed as illustrated in **Figure 5.2**.

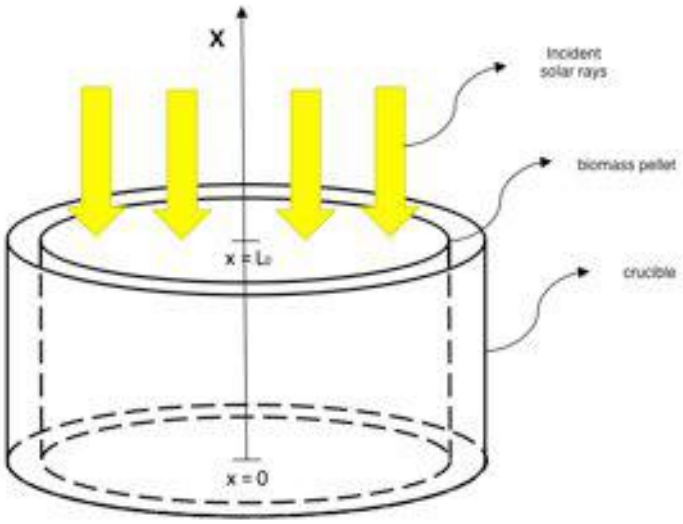

Figure 5.2. Biomass pellet geometry

In order to simplify the model and shorten the calculation time, a uniaxial geometry is selected with one single dimension. It goes from the bottom (x = 0) to the surface of the biomass pellet (x = Lo).

5.2.1.3 Energy conservation

When the solid pellet of biomaterial is exposed to sunlight, heat is transferred to the surface of the pellet by radiation and then by conduction and convection into the interior of particles. Thus, the temperature in the solid increases, which leads to the removal of initial moisture and then to the pyrolysis reaction. There is a nonlinear thermal gradient due to chemical reaction and phase change. In order to build our model, we have to identify the inputs, outputs, sources, and energy wells. There's one entrance:

- Concentrated solar radiation.

There are five outlets or wells:

- The energy consumed by the reaction, i.e., the energy stored in the product.
- Sensible heat in gas.
- Water evaporation.
- Reflected and emitted energy by the sample surface.
- Pellet surface convection.

In addition, heat is transferred by three mechanisms in the same solid pellet:

- Conduction inside the pellet.
- Convection inside the pores of the particles.
- Radiation on the pellet surface.

In order to simplify the model, we will consider only conduction in the solid particle. Based on the above, the heat transfer equation in rectangular coordinate is:

$$\frac{\partial(C_p \rho T)}{\partial t} = \frac{\partial}{\partial x}\left(k_x \frac{\partial T}{\partial x}\right) + \frac{\partial}{\partial y}\left(k_y \frac{\partial T}{\partial y}\right) + \frac{\partial}{\partial z}\left(k_z \frac{\partial T}{\partial z}\right) + q$$

The term on the left refers to enthalpy accumulation. The first three terms on the right describe heat conduction flux, and the last term refers to heat consumed/generated by pyrolysis reactions. k is a function of T, so it is also a function of t, but in order to simplify the solution of the equation, we will consider that it is independent of time. So only *x* and *k* (independent of *x*) are considered.

$$\frac{\partial(C_p \rho T)}{\partial t} = k\frac{\partial^2 T}{\partial x^2} + q$$

Where, C_p, ρ, and k are the specific heat capacity, density and heat conductivity of the solid. T is the local temperature, t is the time, and x is the coordinate of the axial position. The q expression is shown below, where ΔH is the heat of reaction, as ΔH>0, the reaction is endothermic.

$$q = (\Delta H)\left(-\frac{\partial \rho}{\partial t}\right)$$

C_p is a function of T, so it is also a function of t, but we have considered that it is independent of time. Therefore, the C_p value is obtained from the T.

$$C_p \frac{\partial(\rho T)}{\partial t} = k\frac{\partial^2 T}{\partial x^2} + (\Delta H)\left(-\frac{\partial \rho}{\partial t}\right)$$

ρ and T depend on time, so the model can be simplified.

$$\frac{\partial(\rho T)}{\partial t} = \rho\frac{\partial T}{\partial t} + T\frac{\partial \rho}{\partial t}$$

$$C_p\rho\frac{\partial T}{\partial t} = k\frac{\partial^2 T}{\partial x^2} + (\Delta H + C_p T)\left(-\frac{\partial \rho}{\partial t}\right)$$

If we introduce **Equation 5.1**, we can obtain **Equation 5.2**:

$$C_p\rho\frac{\partial T}{\partial t} = k\frac{\partial^2 T}{\partial x^2} + (\Delta H + C_p T)k_1 {C_B}^{n_1} \qquad (5.2)$$

In order to complete the heat transfer model, the initial conditions and limit conditions must be determined.

Initial conditions:

$$t = 0;\ \ T(x,0) = T_{amb} = T_0$$

Boundary conditions:

Symmetry is assumed at the bottom of the pellet.

$$t > 0;\ \ x = 0;\ \ \left(\frac{\partial T}{\partial x}\right)_{x=0} = 0$$

For the upper surface under solar radiation, convection and radiation loss can be considered as **Equation 5.3**:

$$t > 0;\ \ x = L_0;\ \ k\left(\frac{\partial T}{\partial x}\right)_{x=L_0} = \alpha_S FS_S - \varepsilon\sigma(T^4 - T_{ciel}) - h(T - T_{argon}) \qquad (5.3)$$

FS_S is the solar energy flux, α_S is the absorption coefficient of the pellet surface, ε is the emissivity of carbon surface, and h is the convective heat transfer coefficient between argon and solid surface.

5.2.2 Solution method

5.2.2.1 General treatment

A finite difference method is used to solve the differential equations. This approximation replaces the expression of the derivative and is a function evaluated at different points.

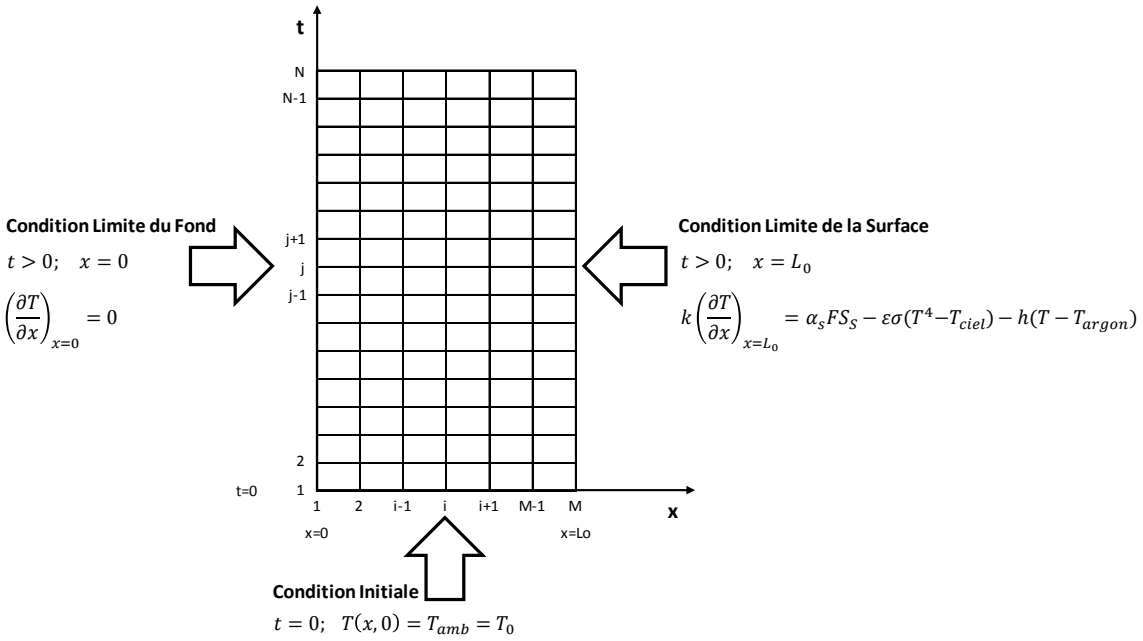

Figure 5.3. Computational domain

*Conduction equation (**Equation 5.2**):*

$$C_p\,\rho\left(\frac{T_{ij+1} - T_{ij}}{\Delta t}\right) = k\left(\frac{T_{i+1j} - 2T_{ij} + T_{i-1j}}{\Delta x^2}\right) + \left(\Delta H + C_p\,T\right)k_1 {C_B}^{n_1}$$

$$T_{ij+1} = \frac{k}{\Delta x^2}\frac{\Delta t}{C_p\,\rho}\left(T_{i+1j} + T_{i-1j}\right) + \left(1 - \frac{2k}{\Delta x^2}\frac{\Delta t}{C_p\,\rho}\right)T_{ij} + \frac{\Delta t}{C_p\,\rho}(\Delta H + Cp\,T)k_1 {C_B}^{n_1}$$

Initial conditions:

$$t = 0;\ j = 1, \qquad T_{i1} = T_0$$

Symmetry relative to the bottom:

$$j > 1, \qquad i = 1,\ T_{2j} = T_{1j}$$

*Surface equation (**Equation 5.3**):*

$$j > 1,\ i = M,\quad T_{Mj} = T_{M-1j} + \frac{\Delta x}{k}\left(\alpha_S F S_S - \varepsilon\sigma(T^4 - T_{ciel}) - h(T - T_{argon})\right)$$

5.2.2.2 Boundary condition at the surface

On the surface, the evolution of the solar flux with time is considered. So, to describe what happens on the surface, we have a system of equations (uniaxial).

$$\begin{cases} C_p\rho\dfrac{\partial T}{\partial t} = k\dfrac{\partial^2 T}{\partial x^2} + q \\ k\left(\dfrac{\partial T}{\partial x}\right)_{x=L_0} = \alpha_S FS_S - \varepsilon\sigma(T^4 - T_{ciel}) - h(T - T_{argon}) \end{cases}$$

The following equations are obtained by introducing the corresponding finite difference operators.

$$\begin{cases} C_p\rho\left(\dfrac{T_{Mj+1} - T_{ij}}{\Delta t}\right) = k\left(\dfrac{T_{Mj} - 2T_{M-1j} + T_{M-2j}}{\Delta x^2}\right) + q \\ k\left(\dfrac{T_{Mj} - T_{M-1j}}{\Delta x}\right) = \alpha_S FS_S - \varepsilon\sigma(T^4 - T_{ciel}) - h(T - T_{argon}) \end{cases}$$

Therefore, the reaction heat q (0.5 mm in depth, Δx) can be suppressed to simplify the resolution. After the mathematical processing, we can obtain the final equation for the simulation.

$$FS_S = \frac{C_p\rho V_C\dfrac{\Delta x}{2} + \left(T_{ij} - T_{i-2j}\right)\dfrac{k}{2\Delta x} + \varepsilon\sigma(T^4 - T_{ciel}) + h(T - T_{argon})}{\alpha_S}$$

Where, V_C is the heating rate, measured by pyrometer, and controlled by PID through the opening of the shutter.

$$T_{Mj+1} = T_{Mj}\left(1 - \frac{k\Delta t}{\Delta x^2 C_p\rho}\right) + \frac{2\Delta t}{\Delta x C_p\rho}\left(\alpha_S FS_S - \varepsilon\sigma(T^4 - T_{ciel}) - h(T - T_{argon})\right) + \frac{k\Delta t}{\Delta x^2 C_p\rho}T_{M-2j}$$

Where, T_{Mj+1} is an attempt to simulate the surface temperature of the experiments, i.e., heating rate of 50 K/s and final temperature of 1473.15K (1200°C), in the selected case.

Correct surface modeling is an important aspect of this work. The surface is the first contact between biomass pellet and concentrated solar energy for the posterior propagation of heat. On the other hand, this model will enable us to account for the solar flux, as well as the opening of the modulator.

5.2.2.3 Stability and convergence

The solution is explicit with possibility to have the problem of error propagation associated to this approach. For the final resolution of our problem, it is important that

errors (for example, due to the rounding) do not accumulate over time. This is a very important condition, which involves the restrictions of time. In addition, the conditions of convergence are difficult to verify. This condition indicates that the solution of the equation is close to the exact solution of the original partial differential equation. In other words, errors tend to zero.

For example, derivative approximations are obtained from the Taylor series.

$$u(x,t+\Delta t) = u(x,t) + \Delta t\frac{du(x,t)}{dt} + \cdots + \frac{\Delta t^n}{n!}\frac{d^n u(x,t)}{dt^n} + \cdots$$

Rewrite equation:

$$\frac{du(x,t)}{dt} = \frac{u(x,t+\Delta t) - u(x,t)}{\Delta t} + \Delta t\left(-\frac{1}{2!}\frac{d^2u(x,t)}{dt^2} - \cdots - \frac{\Delta t^{n-2}}{n!}\frac{d^n u(x,t)}{dt^n} - \cdots\right)$$

$$\frac{du(x,t)}{dt} = \frac{u(x,t+\Delta t) - u(x,t)}{\Delta t} + O(\Delta t)$$

Where, $O(\Delta t)$ is the approximate local truncation error,

$$O(\Delta t) = \frac{\Delta t}{2!}\frac{d^2u(x,t)}{dt^2}$$

If this type of error that is introduced to solve the original model tends to zero, there is a convergence to the original solution. After several attempts, we determined $\Delta t = 0.001\ s$ and $\Delta x = 0.05\ mm$. In this condition, the rounding error is not propagated.

5.3 Model parameters

The 5 mm cylindrical pellet was simulated with MATLAB for 300 seconds (5 minutes). The heating rate and the final surface temperature were set at 50 K/s and 1473.15 K (30×10^5 temperature data). The most important data to predict are:

- Absorbed solar flux.
- Temperature profile in the pellet.
- Consumption of biomass.
- Evolution of some properties

5.3.1 Thermophysical properties

Mathematical model equations can be easily solved by standard numerical methods. First, we worked with the Excel platform, but as the complexity increased, we used MATLAB.

Table 5.2. The main thermophysical values used in this model.

Apparent biomass density	$\boldsymbol{\rho_{B0}}$	**764**	$\boldsymbol{kg\ /\ m^3}$	**Soria et al. (2017)**
Intrinsic density of char	ρ_{C0}	2000	$kg\ /\ m^3$	Soria et al. (2017)
Porosity	P_o	0.365	-	Soria et al. (2017)
Thermal conductivity of biomass	k_B	$0.291 + 0.000836 * 0.33 * T$	W/mK	Soria et al. (2017)
Thermal conductivity of char	k_C	$1.47 + 0.0011 * T$	W/mK	Soria et al. (2017)
Specific heat of biomass	C_{PB}	$2300 - 1150\ exp(-0.0055 * T)$	J/kgK	Soria et al. (2017)
Specific heat of char	C_{PC}	$1430 + 0.355 * T - 7.32 * 10^7 * T^{-2}$	J/kgK	Soria et al. (2017)
Sample length	L_0	0.005	m	Measured
Luminosity	ε	0.95	-	Soria et al. (2017)
Heat of reaction	ΔH	225 000	J/kg	Babu and Chaurasia (2002)
Convective heat transfer coefficient	h	25	W/m^2K	Calculated
Order of reaction 1	n_1	1	-	Babu and Chaurasia (2002)
Initial temperature	T_0	303	K	Mesured
Direct Normal Irradiation	DNI	1 000	W/m^2	Mesured
Absorption coefficient	α_S	0.95	-	Soria et al. (2017)

Before the results, we present the numerical values used for the simulation. The density, thermal conductivity, and specific heat of biomass particles are calculated for the biomass pellet. Porosity and consumption of biomass are taken into account when calculating each attribute.

- Extent of reaction: $X_B = \frac{\rho_{B0} - \rho_B}{\rho_{B0}}$
- Solid properties: $\lambda_s = (1 - X_B)\lambda_B + X_B\lambda_C$
- Effective properties: $\lambda_{eff} = (1 - P_o)\lambda_s + P_o\lambda_{argon}$

Although porosity is changing, it is considered constant. A very thin layer of carbon is added to the surface of the pellet to achieve the emissivity of 0.95 to be consistent with the experiment. The convective heat transfer coefficient (h) between argon and particle surface is calculated together with the Pholhausen equation considering the Reynolds and Prandtl numbers (Soria et al. 2017).

5.3.2 Net solar power

The net solar power absorbed is the energy consumption index of the pyrolysis experiment. The net power profile according to time correlates the solar flux with the response of the modulator. **Figure 5.4** shows the net solar power required for the assigned surface temperature increase. To obtain 50 K/s and 1473.2 K as the final temperature of the pellet surface, this power is achieved by simulation. In the first second, a sharp increase in power can be seen due to the high temperature required and the energy consumption of the pyrolysis reaction. After the peak power, it declines until it stabilizes at about 24 W.

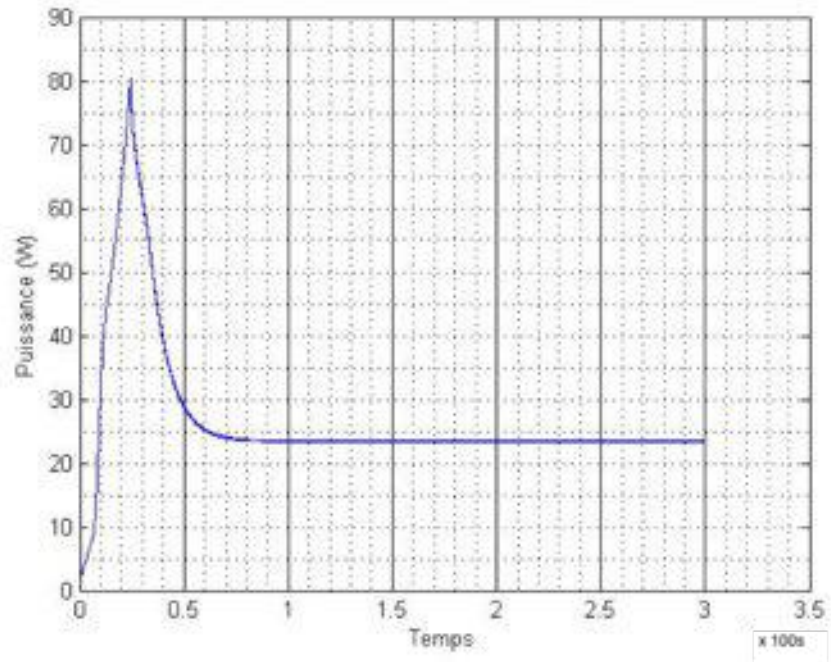

Figure 5.4. Change of power (W) over times

In order to clarify the results of power, there is an example next to the resulting chart showing the position of the solar flux modulator according to different power (**Figure 5.5**). The first point shows low power because the modulator is almost off. The second point is in medium power, so the modulator turns on a little bit. Finally, the last point shows that the opening rate of the blade is close to 100% to maintain the high heating rate. The total time of simulation is 300 s and the step is 0.001 s. According to the result, the power stabilized after around 60 to 100 s, which is in agreement with the observation during the experiment.

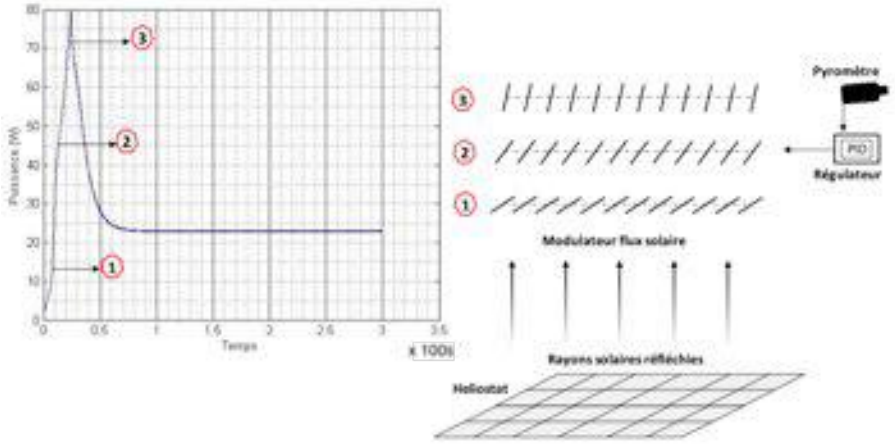

Figure 5.5. Qualitative comparison of the power obtained with the modulator (shutter) position

5.3.3 Temperature profile

Temperature profiles inside the pellet at different time and position are presented in **Figure 5.6**. On the other hand, **Figure 5.7** plots the heat propagation with time at different positions (every 0.5 mm, from the bottom to the surface). The surface shows a slope of 50 K/s to final temperature of 1473.15 K, indication that the working conditions set out in the code are being assessed. However, from zero to 300 seconds, the temperature propagation depends on the axial position at different times (every 3 seconds). After heating for about 20 s, the temperature is constant which agrees with the experiment.

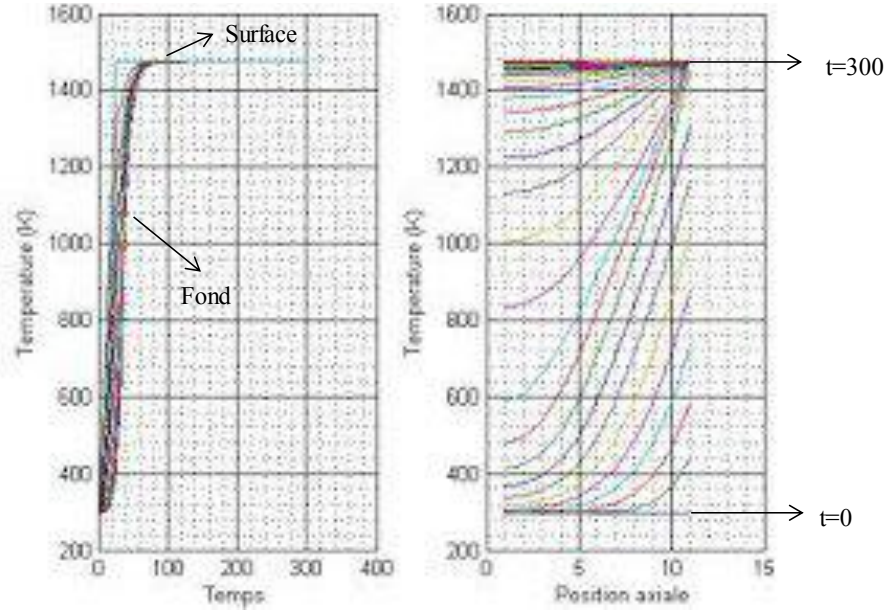

Figure 5.6. Temperature profile (K) based on time (s) and axial position, respectively

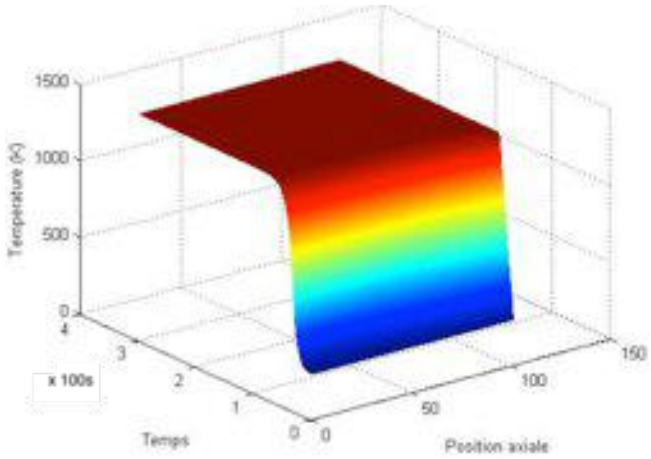

Figure 5.7. Temperature (K) change according to time (s) and axial position

5.3.4 Biomass consumption

The biomass consumption is calculated according to the equation obtained for integrating the kinetic model, i.e., the analysis equation of biomass concentration (**Figure 5.8**). This result is important because it enables us to balance the thermo-physical properties adopted for the pellet between the properties of biomass and char. At t = 0, the chart starts with the initial density of the pellet, 764 kg/m^3. Then, it is quickly consumed in the first part of the experiment, before 50 s.

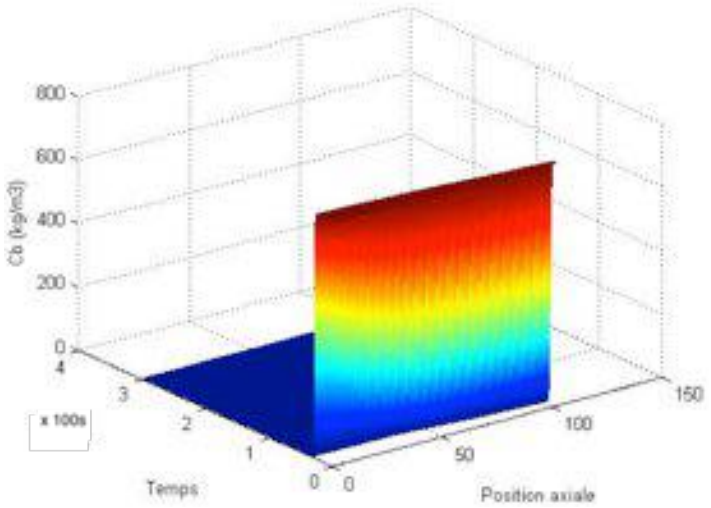

Figure 5.8. Change in biomass concentration (kg/m^3) based on time and axial position

5.3.5 Evolution of the solid properties

After analyzing the temperature and consumption distribution of biomass in solid particles, the change of each characteristic can be analyzed by the simulation process. **Figure 5.9** shows that at zero time (t = 0), the density is 764 kg/m^3 (initial density of biomass pellet), but over time, biomass is used for pyrolysis reaction, so it is converted into gas, tar, and char. At the end of biomass consumption, the density of pellet reaches the highest of 1270 kg/m^3, i.e., the density of char considering the porosity of pellet is constant.

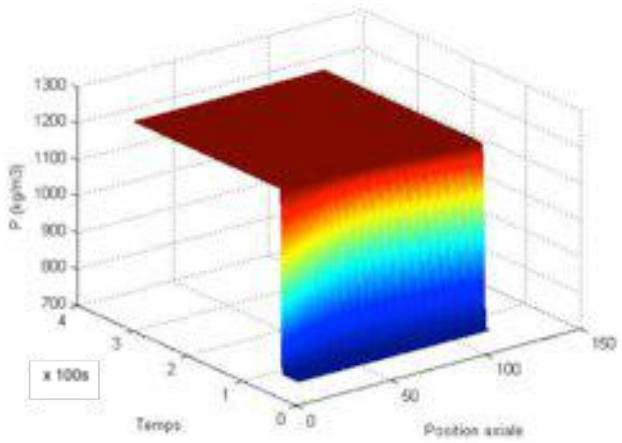

Figure 5.9. Change of solid particle density (kg/m^3) according to time and axial position

Figure 5.10 starts with the specific heat capacity of biomass particles, 1512 J/kg.K, at ambient temperature (300K). Because of biomass consumption and temperature distribution, the specific heat capacicaty varies significantly over time or axial position. Finally, the capacity reaches its final value of 1408 J/Kg.K, the specific heat capacity of char considering the porosity of the particle is constant.

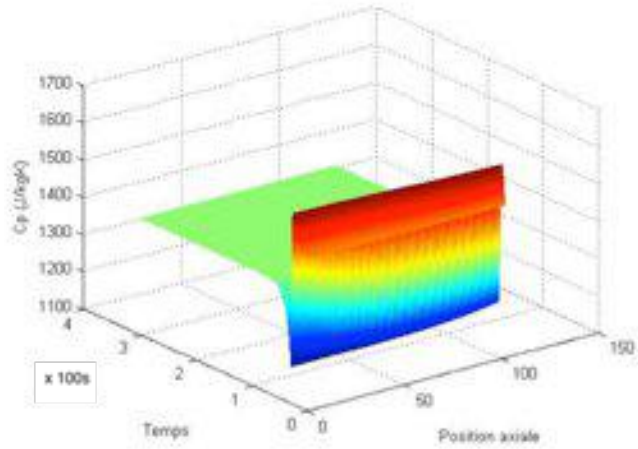

Figure 5.10. Specific heat capacity change of solid particles (J/kg.K) according to time and axial position

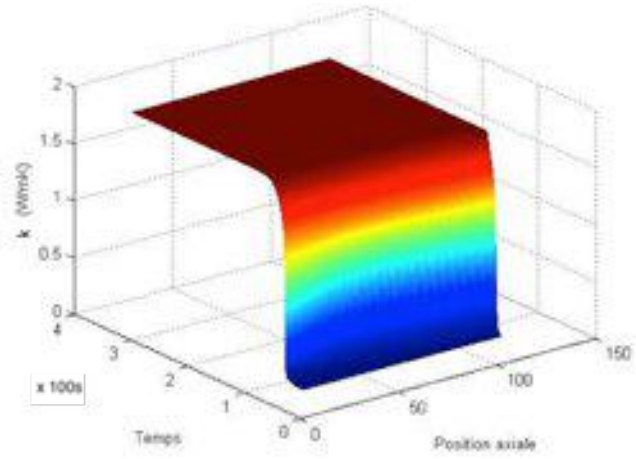

Figure 5.11. Thermal conductivity (W/mK) of solid particles changes according to the time and axial position

The thermal conductivity of the pellet is about 0.24 W/m.K at t = 0 and with ambient temperature. Its change is consistent with temperature distribution and pyrolysis reaction, which consumes biomass. So after some time, the thermal conductivity is coming to its final value. After the consumption of whole biomass and the stabilization of the temperature distribution, the value of thermal conductivity is about 2 (1.98) W/m.K.

5.4 Conclusion

The simple model presented in this chapter is a first step to link the temperature evolution of the pellet to the net absorbed solar power at the surface. This approach differs with the previous model (Soria et al., 2017) that assumed a given temperature variation of the pellet surface (given temperature versus given radiative flux). More efforts are necessary to propose a valuable comparison with experimental results. Only qualitative conclusions can be drawn.

1. Biomass consumption and temperature distribution versus time are qualitatively correct, their trends are the same as literature profiles.

2. A simple model, coupled with some restrictive but realistic assumptions can describe the overall evolution of a complex set of processes, such as pyrolysis.

3. After improvement, the developed model can be used to predict the temperature and concentration profile of different biomass types for a wide range of temperature and heating rate.

5.5 Bibliography

Babu BV, Chaurasia AS. Modeling for pyrolysis of solid particle: Kinetics and heat transfer effects. Energy Conversion and Management, 2002, 44: 2251–2275.

Di Blasi C. Modeling intra- and extra-particle processes of wood fast pyrolysis. AIChE Journal, 2002, 48: 2386–2397.

Koufopanos CA, Papayannakos N, Maschio G, Lucchesi A. Modelling of the pyrolysis of biomass particles. Studies on Kinetics, Thermal and Heat Transfer Effects. The Canadian Journal of Chemical Engineering, 1991, 69: 907.

Park WC, Atreya A, Baum HR. Experimental and theoretical investigation of heat and mass transfer processes during wood pyrolysis. Combustion and Flame, 2010, 157: 481–494.

Soria J, Zeng K, Asensio D, Gauthier D, Flamant G, Mazza G. Comprehensive CFD modelling of solar fast pyrolysis of beech wood pellets. Fuel Processing Technology, 2017, 158: 226–237.

Chapter 6

Conclusions and Perspectives

6.1 Conclusions

Biomass, including agricultural and forestry by-product wastes, represents a class of renewable energy source, an attractive solution for the substitution of fossil fuels. Solar pyrolysis is promising to convert biomass into applicable form of energy, such as syngas. The present work is a contribution to the definition of the solar pyrolysis operating parameters to release the energies stored in the agricultural and forestry wastes. We investigated the effects of solar pyrolysis operating conditions applied to the agricultural and forestry by-product biomass on the product yields and syngas composition. On the other hand, the effects of pellet size were studied using the model developed by our Argentine colleagues (PROBIEN, CONICET – UNCo.). Characterizations of char from the HM-polluted willow pyrolysis (RAPSODEE – IMT Mines d'Albi were made to investigate the effects of temperature and HM contamination on the char properties. A simple conduction model was developed to describe the temperature distribution inside the biomass pellet. Thus, results from this study approach the following six main conclusions:

(1) Products of pyrolysis are influenced by both operating conditions of the reactor and lignocellulose compositions of biomass

Solar pyrolysis of agricultural and forestry biomass is performed under adjustable parameters. So, the pyrolysis operating parameters impact on the quantity and property of biomass pyrolysis products. In the present study, the major studied parameters are the final temperature (in the range of 800-2000°C) and the heating rate (in the range of 10-150°C/s). Four types of agricultural and forestry biomass by-products, including pine sawdust, peach pit, grape stalk, and grape marc with varying levels of lignocellulose compositions, were pyrolyzed under a constant sweep gas flow rate of 6 NL/min. In general, gas yield increases with temperature and heating rate for different types of biomass residues and the highest gas yield (63.5 wt%) is obtained from pine sawdust pyrolyzed at a final temperature of 2000°C and heating rate of 50°C/s; whereas liquid yield progresses oppositely. Lignocellulose composition of biomasses affects not only the quantity but also the distribution of pyrolysis products. High lignin content enriches the char yield and H_2 content, whereas high cellulose and hemicellulose contents promote production of the gas, for example CO. High final temperature decreases CO_2, CH_4, and C_2H_6 contents. The H_2/CO ratio is always greater than one for both marc and stalk of grape.

(2) Pellet size of biomass affects the profile of pyrolysis products

Particle size affects the syngas quality because intra-particle secondary reactions occur. To provide an experimental evidence, pine sawdust in different pellet height (5 and 10 mm) on the product yields (tar, char, and gas), gas composition (H_2, CO, CO_2, and CH_4), and the secondary tar reactions under fast solar pyrolysis were investigated at temperatures of 800, 1200, and 1600°C and heating rates of 10 and 50°C/s. The parameters of H_2/CO, CH_4/H_2 ratios, mechanical gas efficiency, and carbon conversion efficiency were used to analyze the effect of pellet height on syngas quality. Results indicate that gas yield and composition do not differ significantly for the two pellet heights pyrolyzed at temperature below 1200°C. The effect of pellet height can be detected when temperature increases. Thus, fast pyrogasification of large particles is advisable to improve the yield and quality of the syngas.

(3) Pellet size, temperature, and heating rate jointly affects the profile of pyrolysis products

Three analyses were carried out to determine the combined influence of pellet size, temperature, and heating rate during solar fast pyrogasificaion (high temperature fast pyrolysis). Firstly, a characteristic time and a dimensionless number analysis of sawdust biomass pyrolysis demonstrates that the pyrolysis rate is controlled by heat transfer (thermally thick regime) under temperatures below 1200°C. It is performed to estimate the controlling mechanisms during the solar pyrolysis of sawdust, while the thermal wave regime occurs at temperatures above 1200°C.

Secondly, based on the influence of both primary and secondary reactions during the process, product yields result from the competition between both main operating variables, i.e., temperature and heating rate. On the other hand, a high heating rate causes rapid formation of gas product, which increases the intra-particle pressure gradient and expels the gas out of the surface. This diminishes the gas intra-particle residence time and, therefore, reducing tar cracking. At a high temperature, the char layer on the particle surface is formed faster than in the interior, favoring tar cracking. The influence of the pellet size on the gas yield and gas species yield is important when operating at the highest temperature (1600°C).

Thirdly, the syngas quality was analyzed by considering several parameters, such as H_2/CO, CH_4/H_2, LHV, and X_C. The influence of pellet height on H_2/CO molar ratio seems to be more important at 10°C/s than at 50°C/s. A further increase in the heating rate reduces the effect of pellet size. Similarly, the LHV increases with temperature and heating rate, as well as with pellet size, although the influence of the latter is more relevant at the highest operating conditions (1600°C, 50°C/s). It can be concluded that the fast pyrogasification (high temperature fast pyrolysis) of large particles is convenient in order to improve the quality of the syngas.

(4) Biomass types influence the products generated by the solar pyrolysis at different operating conditions

At all pyrolysis temperatures, chicken litter waste produces greater amount of bio-oil but less yields of char than rice husk. Yield and composition of pyrolysis products from these by-products are significantly influenced by pyrolysis temperature at lower heating rates (10 to 50°C/s). The optimal conditions to achieve the highest bio-oil yield (53 wt.%) from 280 μm particle size chicken litter waste are at temperature of 1200°C and heating rate of 10°C/s; and temperature of 1600°C and 800°C are the optimal temperatures to obtain highest yields of bio-oil and char at a heating rate of 50°C/s. Rise in temperature promotes the production of CO and H_2, as well as HHVs of total gas for both biomass types and particle sizes. Variation in gas yield and composition with respect to particle size was insignificant. The highest H_2/CO ratio of most gases produced is around 1, which confirms that the pyrolysis gases produced from chicken litter and rice husk can be used to run engines or power plants.

(5) Heavy metals affect the pyrolysis products in both quantity and property

Copper- and nickel-impregnated willows are pyrolyzed to study the effects of heavy metals on the pyrolysis products. Copper and nickel significantly decrease char and liquid yields with respect to virgin wood, but increase gas production with temperature and heating rate, compared to the raw willow pyrolysis. There is a threshold temperature, 1000°C, to initiate the catalytic effects of copper and nickel on cracking and reforming reactions of tar. Under fast pyrolysis (heating rate 10°C/s), copper and nickel promote production of gas, in particularly, H_2 and CO. However, at a lower heating rate of 10°C/s, copper impregnation does not impact on the gas composition, while nickel impregnation promotes the H_2 and CO yields in comparison with the raw willow. Both metals have the same catalytic effect on gas composition and LHVs with temperature or heating rate during solar pyrolysis. Such effect is more obvious at the temperature above the threshold during fast pyrolysis. The catalytic effect of nickel is more pronounced than copper.

Solar pyrolysis temperature and heavy metal affect the char properties. Increase of temperature facilitates the formation of more ordered and aromatic chars, in which carbon content increases, while hydrogen and oxygen content decreases. The maximum of BET surface area of char appears at approximately 1000°C. The copper and nickel contaminated

willow chars have very larger BET surface areas than the raw willow char. Copper and nickel reduce the hydrogen and oxygen contents. Vaporization of copper and nickel is small comparing to alkaline elements. Copper and nickel impregnated willows produce more organized pyrolysis chars compared to the raw willow char, as evidenced by the Raman spectra of higher I_G/I_{All} ratio and lower I_{D1}/I_G, I_{D2}/I_G, and I_{D3}/I_G ratios.

(6) Numerical modelling allows predicting the effect of the solar pyrolysis operation process parameters

Simulation can produce a set of theoretical results, while pyrolysis operation can produce a series experimental results. Based on a simulation analysis of pine wood sawdust, biomass consumption and temperature distribution versus time is calculated. A simple model, coupled with some restrictive but realistic assumptions can describe the overall evolution of a complex set of processes, such as pyrolysis. After improvement, the developed model can be used to predict the temperature and concentration profile of different biomass types for a wide range of temperature and heating rate.

6.2 Perspectives

The main conclusions of this study are shown in the previous section. The results obtained from the present study lay a foundation for future researches. The perspectives can be stated around four main aspects:

(1) Technical improvement of existing solar experimental system

Although the accuracy of the solar experiments has been largely improved since the beginning of this study, improvement of the experimental process or measurement technology is still needed in regards to the experimental issues that have not been totally solved. The measurement of sample surface temperature in the smoky atmosphere, by

optical pyrometry must be improved. Synchronization of the PID control system with shutter and timer must be also improved. Moreover, installation of a convenient tar collecting system is of particular interest. Analysis of the tar composition and measurement of the HM contamination can complete the characterization of the solar pyrolysis products.

(2) Validation of the simulation results and improvement of the model

The confrontation of the simulated and experimental is necessary to produce more profound analysis. Characterization of biomass properties, such as density, thermal conductivity, and specific heat, is necessary prior to initiation of pyrolysis modelling. Calorimetric measurements must be done to get the solar flux according to the opening of the shutters. The model has several simplifications, such as the assumption of a constant sample porosity during the reaction. In fact, the porosity of the sample evolves with temperature and reaction extent, which needs to be improved for producing more accurate results.

(3) Installation of the Laser-Induced Breakdown Spectroscopy (LIBS) system

As shown in **Figure.6.1**, in order to perform *in situ* measurement of metal evolution (such as Na, K, Ca, Cu, and Ni) during solar pyrolysis of biomass, it is necessary to incorporate a LIBS measurement with the existing solar reactors. Linkage of the LIBS measurements relating to metal vaporization at high temperatures with the syngas data and char properties is necessary to understand the behavior of the metals during the pyrolysis reactions.

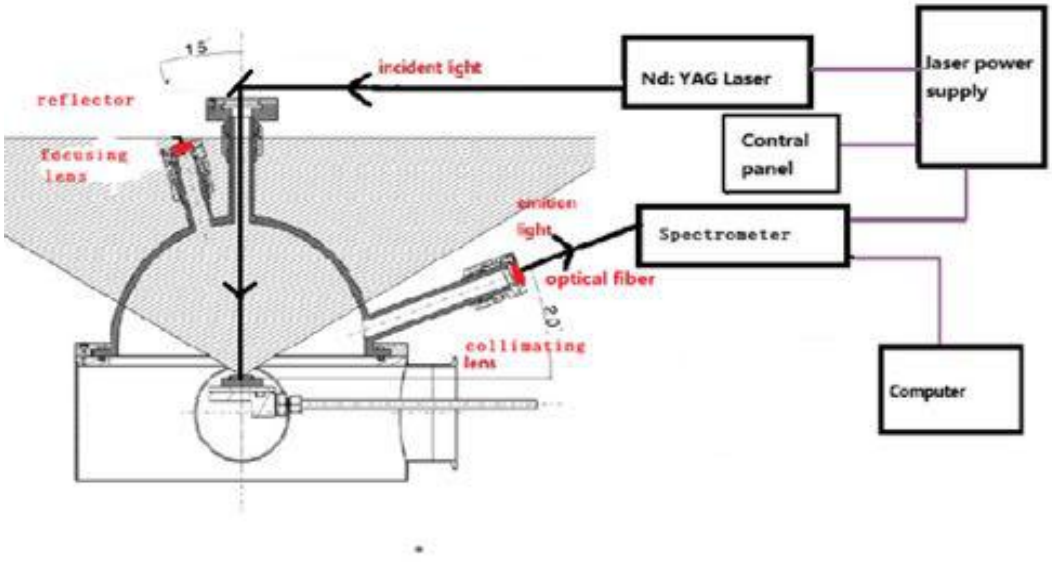

Figure 6.1. Schematic of the LIBS system

(4) Scale-up of the solar reactor from lab-scale measurement results

The goal of solar pyrolysis technology is to develop a MW-scale demonstration unit operating in a continuous mode. This unit can use either the moving reacting front concept (the reactant is pushed continuously at the focal point and the char separated by gravity), a fluidized bed or a molten salt reactor. Molten salt reactor allows the heat to be quickly transferred to raw materials and run stably even under solar energy transients, which can retract HMs from contaminated biomass and retain in molten salt. Unique features of solar reactor include the direct control of reactor temperature, heating rate, and solid residence time. The reactor is designed to operate over a range of biomass HM contents.

Appendix

Appendix I

List of Figures

Appendix II

List of Tables

Appendix III

Publications Related to This Work

1. **Li R**, Zeng K, Soria J, Mazza G, Gauthier D, Rodriguez R, Flamant G. 2016. Product distribution from solar pyrolysis of agricultural and forestry biomass residues. Renewable Energy, 89: 27-35.
2. Zeng K, Gauthier D, **Li R**, Flamant G. 2015. Solar pyrolysis of beech wood: Effects of pyrolysis parameters on the product distribution and gas product composition. Energy, 93: 1648-1657.
3. Zeng K, Gauthier D, **Li R**, Flamant G. 2017. Combined effects of initial water content and heating parameters on solar pyrolysis of beech wood. Energy, 125: 552-561.
4. Soria J, **Li R**, Flamant G, Mazza GD. 2019. Influence of pellet size on product yields and syngas composition during solar-driven high temperature fast pyrolysis of biomass. Journal of Analytical and Applied Pyrolysis, 140: 299-311.
5. Weldekidan H, Strezov V, **Li R**, Kan T, Town G, Kumar R, He J, Flamant G. 2020. Distribution of solar pyrolysis products and product gas composition produced from agricultural residues and animal wastes at different operating parameters. Renewable Energy, 151: 1102-1109.
6. Zeng K, **Li R**, Doan PM, Elsa W, Nzihou A, Xiao H, Flamant G. 2019. Solar pyrolysis of heavy metal contaminated biomass for gas fuel production. Energy, 187: 116016.
7. Zeng K, **Li R**, Doan PM, Elsa W, Nzihou A, Dian Z, Flamant G. 2020. Characterization of char generated from solar pyrolysis of heavy metal contaminated biomass. Energy, 206: 118128.